UNIVERSITY OF CALIFORNIA,
IRVINE

Pulvinar contributions to visual cortical processing in the rat

DISSERTATION

submitted in partial satisfaction of the requirements
for the degree of

DOCTOR OF PHILOSOPHY

in Psychology

by

Leo Russell Scholl

Dissertation Committee:
Associate Professor David C. Lyon, Chair
Professor Jeffrey L. Krichmar
Distinguished Professor George Sperling

2019

DEDICATION

To the rats.

TABLE OF CONTENTS

LIST OF FIGURES

Page

LIST OF TABLES

ACKNOWLEDGMENTS

Thank you to Alex Zhang and Andrzej Foik for teaching me so much. Thanks also to Georgina Lean and Yongjun Liu for keeping me company in the lab, and to David Lyon for your unlimited wisdom and guidance (and your hit album). Thank you to Alissa Ting for being a wonderful partner and friend.

This work was supported in part by the Whitehall Foundation and the National Eye Institute.

CURRICULUM VITAE

Leo Russell Scholl

EDUCATION

Doctor of Philosophy in Psychology **2019**
University of California, Irvine *Irvine, CA*

Master of Science in Cognitive Neuroscience **2017**
University of California, Irvine *Irvine, CA*

Bachelor of Science in Biological Sciences **2014**
Carnegie Mellon University *Pittsburgh, PA*

PUBLICATIONS

Projections between visual cortex and lateral posterior nucleus in the rat. Scholl LR, Foik A, and Lyon DC. *Journal of Comparative Neurology*, under review

Detailed visual cortical responses generated by retinal sheet transplants in rats with severe retinal degeneration. Foik A, Lean GA, Scholl LR, et al. *Journal of Neuroscience*, 2018.

Whole genome comparison of a large collection of mycobacteriophages reveals a continuum of phage genetic diversity. Pope WH, et al. *Elife*, 2015.

ABSTRACT OF THE DISSERTATION

Pulvinar contributions to visual cortical processing in the rat

By

Leo Russell Scholl

Doctor of Philosophy in Psychology

University of California, Irvine, 2019

Associate Professor David C. Lyon, Chair

The extrageniculate visual pathway, which carries visual information from the retina through the superficial layers of the superior colliculus and the pulvinar nucleus, is poorly understood. Several studies have implicated this pathway, in particular the pulvinar, in cognitive tasks such as selective attention, but no specific mechanism or circuit has been described that could support such a function. In order to better understand what role this secondary visual pathway serves, here we examine the basic anatomical and functional properties of cells in the pulvinar, and what driving or modulating effect these cells have on visual cortex.

In the first study, we made extracellular recordings in the pulvinar nucleus of lightly anesthetized rats. We identified visually responsive cells that have large receptive fields on the order of 80 degrees of visual field, fire selectively in response to low spatial frequencies, and can sometimes be selective to the direction or orientation of moving grating stimuli. We also determined that the anatomically-defined lateral subdivision encodes a greater diversity of temporal frequency stimuli than the more medial subdivision, which has better direction selectivity. In the second study, we used modified rabies viruses to retrogradely trace connections between rat pulvinar and visual cortex in order to better understand from where pulvinar receives its visual information and to which cortical areas it is best connected. We found a significantly weaker projection from pulvinar to primary visual cortex (V1) than

from pulvinar to higher visual cortex (V2). In the final study, we designed and tested a new modified rabies virus to optically excite and silence populations of the more numerous projections to V2 from the rat pulvinar. We found that pulvinar modulates cortical size tuning and suppresses flash responses, but doesn't drive activity in V2.

This dissertation builds a foundational understanding of the role of the pulvinar nucleus in rodents, illustrating how pulvinar integrates spatiotemporal information from visual cortex and the superior colliculus, and regulates firing rates in rodent V2. The new rabies virus variant described here is well suited to test theories of pulvinar function, in addition to its wide potential applications in non-transgenic animals such as cats or non-human primates, where models of pulvinar are already well developed.

1. Introduction

1.1 Background

Traditional models of visual processing assume a hierarchical relationship between areas starting with the lateral geniculate nucleus and primary visual cortex, then passing through dorsal and ventral stream cortical areas (Vermaercke et al., 2014; Nishio et al., 2018). However, the so-called higher-order thalamic relays have been shown to participate in cortico-thalamo-cortical transmission across multiple hierarchical areas, inconsistent with feedforward models of visual processing (Theyel et al., 2010; Cortes & Vreeswijk, 2012). Unlike first-order thalamic relays like the lateral geniculate nucleus (LGN), these higher-order nuclei receive most or all of their driving input from the cortex while also sending significant reciprocal projections to cortex, putting them in a position to process and relay information between cortical areas (Sherman and Guillery, 1998; Bickford, 2015). However, not much is known about what kind of information is relayed, nor what additional computations are performed en route through the thalamus.

The pulvinar nucleus of the thalamus is well connected to all of visual cortex (Benevento and Rezak, 1976; Trageser and Keller, 1995; Nakamura et al., 2015; Kamishina et al., 2009) and has been implicated in visual attention tasks including directing attention to different spatial locations, filtering of unwanted information, and shifts of attention across the visual field (Saalmann and Kastner, 2011, Bridge et al., 2016). Injury to the pulvinar leads to impairments of visually guided behavior and deficits in spatial attention (Sprague & Meikle, 1965; Cowey et al., 1984; Fabre-Thorpe et al., 1986). In stroke patients with damage to the thalamus encompassing the pulvinar but not the LGN, for example, visual discrimination was comprimised when salient distractors were present, but rescued when the stimulus con-

trast was increased (Snow et al., 2008), indicating that the pulvinar is involved in filtering irrelevant stimuli rather than driving conscious vision.

However, although the pulvinar is the locus of these behavioral deficits, its function cannot be explained by simply removing it. Deficits of the pulvinar have been associated with several clinical disorders, including schizophrenia (Byne et al. 2007), attention deficit disorders (Ivanov et al. 2010), autism spectrum disorder (Schuetze et al. 2016), and alzheimer's disease (Fredericks et al., 2019), so it is no surprise that experimental inactivation of the pulvinar leads to profound changes in cognitive tasks like attention. Instead, the underlying circuitry needs to be examined and functional connectivity between the pulvinar and other areas involved in vision and attention needs careful review at a finer scale. Some progress has recently been made with this approach, for example cortical axon terminals from pulvinar in mice have been shown to carry information about discrepancy between visual and motor inputs (Roth et al., 2016), and recent in vitro work has demonstrated that pulvino-recipient neurons in mouse visual cortex typically respond strongly to pulvinar activity only if they in turn project to areas that are involved in guiding visual movements (Zhou et al., 2017). But even so, detailed functional and structural properties of pulvinar neurons have not been well studied.

1.2 Open questions

Single unit recordings in the pulvinar nucleus of primates have identified basic receptive field properties and highlighted important differences between subregions of the nucleus. In monkeys, cells in the dorsomedial pulvinar (Pdm) have much larger receptive fields, longer response latencies, and are less retinotopically organized than cells in inferior (PI) and lateral (PL) pulvinar (Petersen et al., 1985), which have well-defined receptive fields selective to orientation or direction (Bender et al., 1982; Petersen et al., 1985; Gattass et al., 1979).

These differences could contribute to the respective role of each subdivision in guiding visual behavior, since receptive fields with faster response latencies are more suited for motion processing whereas cells with higher spatial acuity are more likely to process object vision (Shetht & Young, 2016). However, little is known about receptive field properties of LPrm and LPl neurons in mice (Roth et al., 2015; Ahmadlou et al., 2018; Bennett et al., 2019) and even less so in rats (Montero et al., 1968), making it difficult to predict what role these regions have in modulating cortical activity. This lack of basic knowledge also makes it unclear whether or not rodent LP would be a useful model of human and non-human primate pulvinar.

There is also a trend in the existing literature of denser and more numerous projections from pulvinar to higher visual cortex compared to projections from pulvinar to V1. In rats, anterograde injections in LP labeled both V1 and V2, but V1 labeling was much more sparse, with many more fibers being labeled in both medial and lateral V2 (Nakamura et al., 2015). In squirrels, dense pulvinar labeling was observed following retrograde tracer injections into the temporal posterior area and visual area 19, but very few cells were labeled following V1 (area 17) injection (Robson & Hall, 1977). Tree shrew, a close primate relative, exhibits a similar pattern of connectivity following retrograde tracer injections in V1 and V2; only sparse, topographic labeling was observed in caudal pulvinar following V1 injection, whereas V2 injection was followed by denser labeling spread across large regions of caudal and ventral pulvinar (Lyon et al., 2003). Similarly, in monkeys, retrograde injections in V1 of macaque labeled very few cells in pulvinar compared to injections in V2 in marmoset (Kaas & Lyon, 2007). Although this pattern seems to have gone largely unnoticed, it is present in all of the anatomical literature we have come across. However, how the density or number of neurons projecting from pulvinar to V1 compares to other thalamocortical projections or to pulvinar projections to other visual areas has not been formally tested.

Attempts to understand the functional role of pulvinar have focused in animal models on

brute force removal or inactivation of the pulvinar, and in humans and non-human primates on correlations between activity in pulvinar and other brain regions. For example, superior colliculus lesions in mice cause changes to speed tuning across multiple cortical areas (Tohmi et al., 2014), presumably because the pulvinar, which receives some input from the superior colliculus, relays speed information to the cortex. However, these changes are hard to attribute to the pulvinar since the superior colliculus also projects to other thalamic nuclei (Partlow, et al., 1977; Pasquier & Villar, 1982). Pulvinar inactivation by GABA receptor agonist injections lowered cortical firing rates in monkeys (Purushothaman et al., 2012; Zhou et al., 2016), but such injections cause changes to thalamic physiology, as well as potentially causing damage to cortex (Lomber, 1999; Majchrzak & Di Scala, 2000). Correlations between activity in the pulvinar with activity in the cortex also showed that pulvinar might drive synchronization between visual areas (Saalmann et al., 2012), but these results are inconsistent between studies (Zhou et al., 2016) due to a lack of causality. A better approach is to carefully review functional changes in visual cortex following finer scale manipulations of pulvinar.

In this dissertation we aim to directly measure the properties of cells in the pulvinar and the effects pulvinar has on visual cortex using a combination of electrophysiological and optogenetic techniques in rats. In rodents the pulvinar is called the lateral posterior nucleus (LP) and consists of three highly-conserved subregions, caudomedial (LPcm), rostromedial (LPrm), and lateral (LPl) portions (Takahashi, 1985; Nakamura et al., 2015; see Figure 1). These regions are homologous to the three pulvinar subdivisions in squirrel, caudal (Pc), rostromedial (Prm) and rostrolateral (Prl), a highly visual rodent, and tree shrew, dorsal (Pd), ventral (Pv), central (Pc), a close primate relative (Lyon et al., 2003; Baldwin et al., 2011); and share anatomical similarities to dorsomedial (PLdm), ventrolateral (PLvl), and inferior (PI) subdivisions of the primate pulvinar (Lyon et al., 2003; Kaas and Lyon, 2007), although the inferior pulvinar can be further subdivided into five more subdivisions (Lyon et al., 2010). These similarities, along with the benefits of using transgenic animals, make

rats a suitable model for studying pulvinar function. We aim to simultaneously improve the understanding of structure-function relationships in the pulvinar, while also showing that the rodent LP shares many physiological features with primate pulvinar.

1.3 Specific aims

In the first aim, we evaluated the responses of rat pulvinar neurons to drifting sine wave grating visual stimuli and characterized populations of cells within subdivisions of the nucleus. In both primates and rats, as well as a number of other species, one subdivision of pulvinar receives dense input from the superior colliculus (SC), one receives sparse SC input, and one receives input primarily from visual cortex. We hypothesized that the difference in collicular connectivity between the two rostral subdivisions may be reflected in different profiles of visual information processing. Aim 1 is addressed in chapter 2.

In the second aim, we sought to understand from where the functional properties of pulvinar neurons arise. We used modified rabies viruses to retrogradely trace connections between pulvinar and visual cortex to identify the areas with which pulvinar is best connected. We hypothesized that differences in subdivision physiology might arise from anatomical differences with the cortex. Aim 2 is addressed in chapter 3.

In the third aim, we developed a novel rabies virus for optical interrogation of thalamocortical circuits. Optogenetics have greatly contributed to the study of neural circuits over the past decade. In mice it is now possible to genetically introduce both excitatory and inhibitory light-driven proteins in order to manipulate circuit dynamics without altering mean firing rates, or to study the effects of both excitation and inhibition of a single population of cells (Han and Boyden, 2007; Zhang et al, 2007). However, this level of control is not currently available without the use of transgenic animal models, which take time to develop

and are not suitable for large animals. We developed a novel G-deleted rabies virus that expresses two independent channelrhodopsin proteins, providing the ability to introduce opsins *in vivo* where genetic manipulation is not practical. Neurons infected with this virus are susceptible to light-driven depolarization and hyperpolarization, providing full control over activity in areas with neurons projecting to injection sites. We utilized this technique to probe the inputs from the pulvinar to visual cortex to determine what downstream effect these spatiotemporally tuned neurons have, hypothesizing that the large receptive field sizes found in pulvinar might drive surround suppression in cortex. The third aim is addressed in chapter 4.

1.4 References

Ahmadlou, M., Zweifel, L. S., and Heimel, J. A. (2018). Functional modulation of primary visual cortex by the superior colliculus in the mouse. *Nature Communications*, 9(1):3895.

Baldwin, M. K. L., Wong, P., Reed, J. L., and Kaas, J. H. (2011). Superior colliculus connections with visual thalamus in gray squirrels (Sciurus carolinensis): Evidence for four subdivisions within the pulvinar complex. *Journal of Comparative Neurology*, 519(6):1071–1094.

Bender, D. B. (1982). Receptive-field properties of neurons in the macaque inferior pulvinar. *Journal of Neurophysiology*, 48(1):1–17.

Benevento, L. a. and Rezak, M. (1976). The cortical projections of the inferior pulvinar and adjacent lateral pulvinar in the rhesus monkey (Macaca mulatta): an autoradiographic study. *Brain Research*, 108(1):1–24.

Bennett, C., Gale, S. D., Garrett, M. E., Newton, M. L., Callaway, E. M., Murphy, G. J., and Olsen, S. R. (2019). Higher-Order Thalamic Circuits Channel Parallel Streams of Visual Information in Mice. *Neuron*, pages 1–16.

Bickford, M. E. (2015). Thalamic circuit diversity: Modulation of the driver/modulator framework. *Frontiers in Neural Circuits*, 9(JAN2016):1–8.

Bridge, H., Leopold, D. A., and Bourne, J. A. (2016). Adaptive Pulvinar Circuitry Supports Visual Cognition. *Trends in Cognitive Sciences*, 20(2):146–157.

Byne, W., Hazlett, E. a., Buchsbaum, M. S., and Kemether, E. (2009). The thalamus and schizophrenia: current status of research. *Acta neuropathologica*, 117(4):347–368.

Cortes, N. and van Vreeswijk, C. (2012). The Role of Pulvinar in the Transmission of Information in the Visual Hierarchy. *Frontiers in Computational Neuroscience*, 6(May):1–21.

Cowey, A., Smith, B., and Butter, C. (1984). Effects of damage to superior colliculi and pre-tectum on movement discrimination in rhesus monkeys. *Experimental Brain Research*, 56(1).

Fabre-Thorpe, M., Viévard, A., and Buser, P. (1986). Role of the extra-geniculate pathway in visual guidance - II. Effects of lesioning the pulvinar-lateral posterior thalamic complex in the cat. *Experimental Brain Research*.

Fredericks, C. A., Brown, J. A., Deng, J., Kramer, A., Ossenkoppele, R., Rankin, K., Kramer, J. H., Miller, B. L., Rabinovici, G. D., and Seeley, W. W. (2019). Intrinsic connectivity networks in posterior cortical atrophy: A role for the pulvinar? *NeuroImage: Clinical*, 21(August 2018):101628.

Gattass, R., Oswaldo-Cruz, E., and Sousa, A. P. (1979). Visual receptive fields of units in the pulvinar of cebus monkey. *Brain Research*, 160(3):413–429.

Han, X. and Boyden, E. S. (2007). Multiple-color optical activation, silencing, and desynchronization of neural activity, with single-spike temporal resolution. *PloS one*, 2(3):e299.

Ivanov, I., Bansal, R., Hao, X., Zhu, H., Kellendonk, C., Miller, L., Sanchez-Pena, J., Miller, A. M., Chakravarty, M. M., Klahr, K., Durkin, K., Greenhill, L. L., and Peterson, B. S. (2010). Morphological Abnormalities of the Thalamus in Youths With Attention Deficit Hyperactivity Disorder. *American Journal of Psychiatry*, 167(4):397–408.

Kaas, J. H. and Lyon, D. C. (2007). Pulvinar contributions to the dorsal and ventral streams of visual processing in primates. *Brain Research Reviews*, 55(2 SPEC. ISS.):285–296.

Kamishina, H., Conte, W. L., Patel, S. S., Tai, R. J., Corwin, J. V., and Reep, R. L. (2009). Cortical connections of the rat lateral posterior thalamic nucleus. *Brain Research*, 1264:39–56.

Lomber, S. G. (1999). The advantages and limitations of permanent or reversible deactivation techniques in the assessment of neural function. *Journal of Neuroscience Methods*, 86(2):109–117.

Lyon, D. C., Jain, N., and Kaas, J. H. (2003). The visual pulvinar in tree shrews II. Projections of four nuclei to areas of visual cortex. *The Journal of Comparative Neurology*, 467(4):607–627.

Lyon, D. C., Nassi, J. J., and Callaway, E. M. (2010). A Disynaptic Relay from Superior Colliculus to Dorsal Stream Visual Cortex in Macaque Monkey. *Neuron*.

Majchrzak, M. and Di Scala, G. (2000). GABA and muscimol as reversible inactivation tools in learning and memory. *Neural Plasticity*, 7(1-2):19–29.

Montero, V. M., Brugge, J. F., and Beitel, R. E. (1968). Relation of the visual field to the lateral geniculate body of the albino rat. *Journal of neurophysiology*, 31(2):221–36.

Nakamura, H., Hioki, H., Furuta, T., and Kaneko, T. (2015). Different cortical projections from three subdivisions of the rat lateral posterior thalamic nucleus: A single-neuron tracing study with viral vectors. *European Journal of Neuroscience*, 41(10):1294–1310.

Nishio, N., Tsukano, H., Hishida, R., Abe, M., Nakai, J., Kawamura, M., Aiba, A., Sakimura, K., and Shibuki, K. (2018). Higher visual responses in the temporal cortex of mice. *Scientific Reports*, 8(1):1–12.

Partlow, G. D., Colonnier, M., and Szabo, J. (1977). Thalamic projections of the superior colliculus in the rhesus monkey,Macaca mulatta. A light and electron microscopic study. *The Journal of Comparative Neurology*, 171(3):285–317.

Pasquier, D. A. and Villar, M. J. (1982). Subcortical projections to the lateral geniculate body in the rat. *Experimental Brain Research*, 48(3):409–419.

Petersen, S. E., Robinson, D. L., and Keys, W. (1985). Pulvinar nuclei of the behaving rhesus monkey: Visual responses and their modulation. *Journal of Neurophysiology*, 54(4):867–886.

Purushothaman, G., Marion, R., Li, K., and Casagrande, V. a. (2012). Gating and control of primary visual cortex by pulvinar. *Nature neuroscience*, 15(6):905–12.

Robson, J. A. and Hall, W. C. (1977). The organization of the pulvinar in the grey squirrel (Sciurus carolinensis). I. Cytoarchitecture and connections. *Journal of Comparative Neurology*, 173(2):355–388.

Roth, M. M., Dahmen, J. C., Muir, D. R., Imhof, F., Martini, F. J., and Hofer, S. B. (2015). Thalamic nuclei convey diverse contextual information to layer 1 of visual cortex. *Nature Neuroscience*, 19(2):299–307.

Saalmann, Y. B. and Kastner, S. (2011). Cognitive and Perceptual Functions of the Visual Thalamus. *Neuron*, 71(2):209–223.

Schuetze, M., Park, M. T. M., Cho, I. Y., Macmaster, F. P., Chakravarty, M. M., and Bray, S. L. (2016). Morphological alterations in the thalamus, striatum, and pallidum in autism spectrum disorder. *Neuropsychopharmacology*, 41(11):2627–2637.

Sherman, S. M. and Guillery, R. W. (1998). On the actions that one nerve cell can have on another: Distinguishing "drivers" from "modulators". *Proceedings of the National Academy of Sciences of the United States of America*, 95(12):7121–7126.

Shetht, B. R. and Young, R. (2016). Two visual pathways in primates based on sampling of space: Exploitation and exploration of visual information. *Frontiers in Integrative Neuroscience*, 10(NOV2016).

Snow, J. C., Allen, H. A., Rafal, R. D., and Humphreys, G. W. (2009). Impaired attentional selection following lesions to human pulvinar: Evidence for homology between human and monkey. *Proceedings of the National Academy of Sciences of the United States of America*, 106(10):4054–4059.

Sprague, J. M. and Meikle, T. H. (1965). The role of the superior colliculus in visually guided behavior. *Experimental Neurology*, 11(1):115–146.

Takahashi, T. (1985). The organization of the lateral thalamus of the hooded rat. *The Journal of comparative neurology*, 231(3):281–309.

Theyel, B. B., Llano, D. A., and Sherman, S. M. (2010). The corticothalamocortical circuit drives higher-order cortex in the mouse. *Nature Neuroscience*, 13(1):84–88.

Tohmi, M., Meguro, R., Tsukano, H., Hishida, R., and Shibuki, K. (2014). The extrageniculate visual pathway generates distinct response properties in the higher visual areas of mice. *Current biology : CB*, 24(6):587–97.

Trageser, J. C. and Keller, A. (2004). Reducing the uncertainty: gating of peripheral inputs by zona incerta. *The Journal of neuroscience : the official journal of the Society for Neuroscience*, 24(40):8911–5.

Vermaercke, B., Gerich, F. J., Ytebrouck, E., Arckens, L., Op de Beeck, H. P., and Van den Bergh, G. (2014). Functional specialization in rat occipital and temporal visual cortex. *Journal of Neurophysiology*, 112(8):1963–1983.

Zhou, H., Schafer, R. J., and Desimone, R. (2016). Pulvinar-Cortex Interactions in Vision and Attention. *Neuron*, 89(1):209–220.

Zhou, N., Masterson, S., Damron, J., Guido, W., and Bickford, M. (2017). The mouse pulvinar nucleus links the lateral extrastriate cortex, striatum, and amygdala. *The Journal of Neuroscience*, pages 1279–17.

2. Characterizing visual responses to grating stimuli in the rat pulvinar nucleus

2.1 Abstract

The extrageniculate visual pathway has a perplexing role in visual cognition as no clear link has been found between the functional properties of neurons in the pathway and behavioral deficits that arise when it is damaged. The pulvinar nucleus, called the lateral posterior nucleus (LP) in rats, is a higher order thalamic relay and a major component of the extrageniculate pathway, with input from the superior colliculus and visual cortex and output to all of visual cortex. To better understand what visual information is relayed and what kinds of computations the pulvinar might support, we characterized the response properties of populations of cells in two rostral LP subdivisions and in primary visual cortex by recording activity evoked by drifting sine wave gratings.

2.2 Introduction

In the mammalian visual system, there are two major pathways for visual information to reach visual cortex. The geniculostriate pathway carries signals from the retina through the lateral geniculate nucleus (LGN) to primary visual cortex (V1), and accounts for the majority of the visual information flow to the cortex (Jones, 1985). The extrageniculate

pathway starts in the retina and leads through the superior colliculus and pulvinar to primary and higher order visual cortex; its function is less well understood (Waleszczyk et al., 1999, 2004; Lyon et al., 2010). Whereas damage to the LGN or optic radiations from the LGN lead to profound loss of vision (Purves et al., 2001; Pula & Yuen, 2017), the secondary visual pathway has a more subtle role in guiding visual behavior, as injury to the superior colliculus and pulvinar leads to impairments of visually guided behavior and deficits in spatial attention, but not blindness (Sprague & Meikle, 1965; Cowey et al., 1984; Fabre-Thorpe et al., 1986). In stroke patients with damage to the thalamus encompassing the pulvinar but not the LGN, for example, visual discrimination was comprimised when salient distractors were present, but rescued when the stimulus contrast was increased (Snow et al., 2008), indicating that the extrageniculate pathway is involved in filtering irrelevant stimuli rather than driving conscious vision. Indeed, the pulvinar nucleus has been implicated in a wide range of visual attention tasks including directing attention to different spatial locations, filtering of unwanted information, and shifts of attention across the visual field (Saalmann & Kastner, 2011; Bridge et al., 2016). Thus, the extrageniculate visual pathway has an important, albeit perplexing role in visual cognition.

The pulvinar receives significant corticothalamic modulatory efferents (Benevento & Rezak, 1976), and sends many modulatory projections to all of visual cortex (Trageser & Keller, 1995), making it well suited to mediate information transfer between cortical areas. In monkeys, parts of the pulvinar are well connected with areas processing the guidance of action and object recognition (Kaas & Lyon, 2007), positioning the pulvinar as a likely player in the modulation of information flow from V1 to the so-called dorsal and ventral visual streams (Goodale, 2005; 2013). Recent behavioral studies have implicated the pulvinar in directing visually guided actions — inactivation of the pulvinar nucleus in primates caused hemispatial neglect during a visually guided reaching task (Wilke et al., 2010), and projections from pulvinar to V1 in mice have been shown to carry information about discrepancy between visual and motor inputs (Roth et al., 2016). Recent in vitro work has also demonstrated that

pulvino-recipient extrastriate neurons in mice typically respond strongly to pulvinar activity only if they in turn project to areas that are involved in guiding visual movement (Zhou et al., 2017). The pulvinar has also been implicated in object recognition, perhaps providing contextual information such as salience or foreground detection to ventral stream areas. As early as V1 there exists a discrepancy in firing rates related to the saliency of visual stimuli (Zhang et al, 2012). However, it is unclear where this map is generated; Chen et al. (2016) place it in V1, but others have argued that the extrageniculate pathway may play a large role in driving salience-based selection, in particular the pulvinar nucleus (Mizzi & Michael, 2014; Veale et al., 2016). Pulvinar neurons could also aide object recognition by encoding other forms of context; for instance Wilke et al. (2009) demonstrated that some primate pulvinar neurons encode illusory stimuli that match the animal's percept but not the visual stimulus.

Single unit recordings in the pulvinar nucleus of primates have identified basic receptive field properties and highlighted important differences between subregions of the nucleus. In monkeys, cells in the dorsomedial pulvinar (Pdm) have much larger receptive fields, longer response latencies, and are less retinotopically organized than cells in inferior (PI) and lateral (PL) pulvinar (Petersen et al., 1985), which have well-defined receptive fields selective to orientation or direction (Bender et al., 1982; Petersen et al., 1985; Gattass et al., 1979). These differences could contribute to the respective role of each subdivision in guiding visual behavior, since receptive fields with faster response latencies are more suited for motion processing and dorsal stream vision whereas cells with higher spatial acuity are more likely to process ventral stream object vision (Shetht & Young, 2016).

Given the limitations of primate research, including the small number of animals available for research and difficulty in developing genetically modified primates (Izpisua Belmonte et al., 2015), and the relative advantages of rodents, mice and rats are becoming a more popular animal model to study pulvinar anatomy and function (Carandini & Churchland,

2013; Schmitt & Halassa, 2017). In addition, anatomical similarities across species suggest that the pulvinar has remained largely unchanged over evolutionary time scales (Lyon et al., 2003; Zhou et al., 2017; see Figure 2.1). In rodents, the pulvinar is called the lateral posterior nucleus (LP) and consists of three highly-conserved subregions. In mice and rats, the LP is divided based on cytoarchitecture and connectivity into caudomedial (LPcm), rostromedial (LPrm), and lateral (LPl) portions (Takahashi, 1985; Nakamura et al., 2015; see Figure 2.1). These regions are homologous to the three pulvinar subdivisions in squirrel, caudal (Pc), rostromedial (Prm) and rostrolateral (Prl), a highly visual rodent (Robson & Hall, 1977; Baldwin et al., 2011), and in tree shrew, dorsal (Pd), ventral (Pv), central (Pc), a close primate relative (Lyon et al., 2003); and share anatomical similarities to dorsomedial (PLdm), ventrolateral (PLvl), and inferior (PI) subdivisions of the primate pulvinar (Lyon et al., 2003; Kaas & Lyon, 2007), although the inferior pulvinar can be further subdivided into five more subdivisions (Lyon et al., 2010). While in some species there may be additional specializations of subnuclei – for example in monkeys there are reports of snake-selective cells in the dorsomedial subdivision (Van Le et al., 2014) – these likely aren't the primary evolutionary purpose of the pulvinar. That the rodent LP conserves only the basic functional organization found in other mammals is possibly an advantage for understanding its fundamental role in the visual system.

However, little is known about receptive field properties of LPrm and LPl neurons in mice (Roth et al., 2015; Ahmadlou et al., 2018; Bennett et al., 2019) and even less so in rats (Montero et al., 1968), making it difficult to predict what role these regions have in modulating cortical activity. This lack of basic knowledge also makes it unclear whether or not rodent LP would be a useful model of human and non-human primate pulvinar. Thus, in order to address the lack of rodent pulvinar single unit data, we collected and compared spatiotemporal receptive fields of single units recorded in LPrm and LPl subdivisions to those in V1 of rats. We hypothesized that the difference in collicular connectivity between the two subdivisions may be reflected in different profiles of visual information processing.

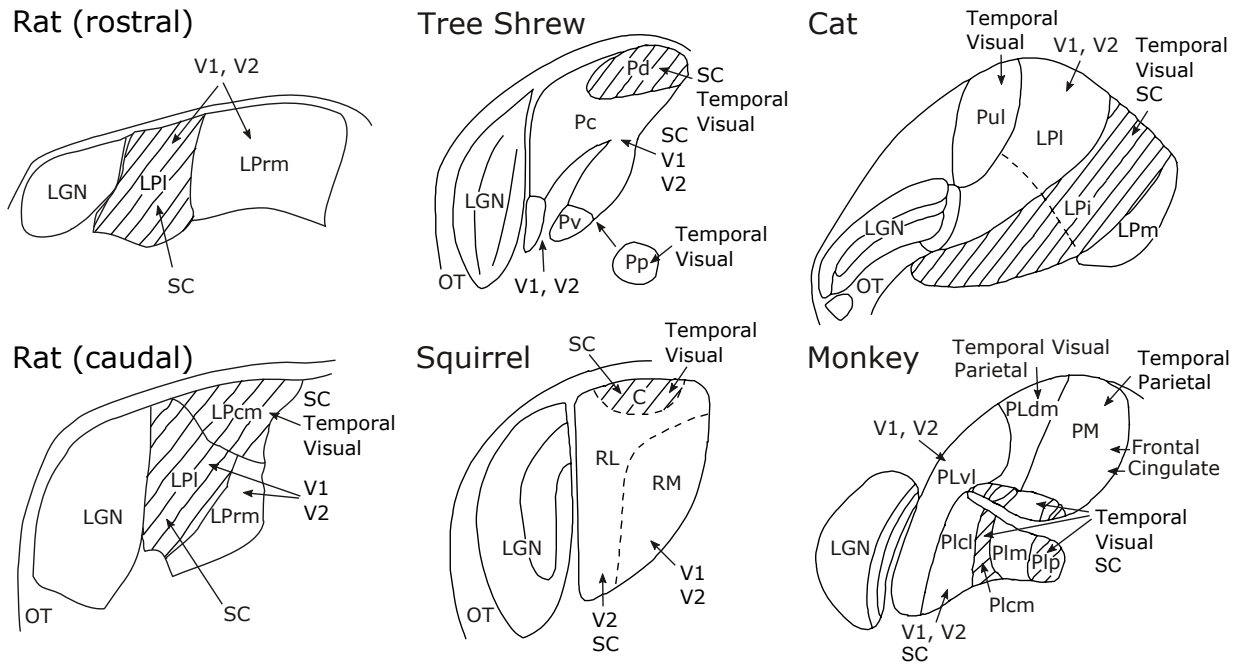

Figure 2.1: Schematic of pulvinar anatomy across five species. Regions receiving dense superior colliculus input and with connections to temporal visual cortex (shaded) include caudomedial pulvinar (LPcm) in rat, dorsal pulvinar (Pd) in tree shrew, caudal pulvinar (C) in squirrel, intermediate LP (LPi) in cat, and inferior pulvinar (PI) in monkey, although not all of PI receives input from the superior colliculus. Regions receiving sparse input from superior colliculus with connections to V1 and V2 include lateral pulvinar (LPl) in rat, caudal pulvinar in the tree shrew (Pc), rostrolateral pulvinar (RL) in squirrel, and caudolateral inferior pulvinar (PIcl) in monkey. Regions with visual cortex connections only include rostromedial pulvinar (LPrm) in rat, ventral pulvinar (Pv) in tree shrew, rostromedial pulvinar (RM) in squirrel, lateral LP (LPl) in cat, and ventrolateral lateral pulvinar (PLvl) in monkey. Additional subregions include posterior pulvinar (Pp) in tree shrew, the pulvinar (Pul) and medial LP (LPm) in cat, and the medial (PM) and dorsomedial lateral (PLdm) pulvinar in monkey. Optic tract (OT) and lateral geniculate nucleus (LGN) are shown for reference. Adapted from Lyon et al. (2003) and Nakamura et al., (2015). Not to scale.

2.3 Methods

Experiments were performed on 21 adult Long-Evans rats of either sex. All procedures were performed in accordance with the NIH guidelines for the care and use of laboratory animals, the ARVO Statement for the Use of Animals in Ophthalmic and Vision Research, and under a protocol approved by the Institutional Animal Care and Use Committee of UC Irvine.

Rats were initially anesthetized with 2% isoflurane in a mixture of N_2O/O_2 (70%/30%), then placed into a stereotaxic apparatus. Animals were given dexamethasone injections prior to surgery and flunixin meglumine injections after surgery. A small plastic chamber was glued to the exposed skull using dental cement. After one day of recovery, re-anesthetized animals were placed in a woven hammock, maintained under isoflurane anesthesia (1% in a mixture of N_2O/O_2), and one to four tungsten electrodes were inserted perpendicular to midline into a small craniotomy above neocortex using a stereotaxic micromanipulator and electronic microdrive. For V1 recordings, electrodes were targeted between -7 and -9 mm from bregma and 4 mm lateral from midline. For LP recordings, electrodes were targeted between -3.5 and -4.5 mm from bregma and 1 to 4 mm lateral from the midline. Electrodes were coated with 1,1'-dioctadecyl-3,3,3',3'-tetramethyl-indocarbocyanine perchlorate fluorescent dye (DiI, Sigma-Aldrich; Di Carlo, 1996) to facilitate later reconstruction of recording tracks. During recording sessions, animals were kept sedated under light isoflurane anesthesia (0.2 – 0.4%) in a mixture of N_2O/O_2. EEG and EKG were monitored throughout the experiments and body temperature was maintained with a heating pad (Harvard Apparatus, Holliston, MA). Following several recording sessions, rats were deeply anesthetized with isoflurane and sodium pentobarbital, then perfused transcardially first with saline, then 4% paraformaldehyde. Brains were removed and stored in 30% sucrose in phosphate buffer for histology.

Brains were sectioned coronally at 40 µm thickness on a freezing microtome and observed

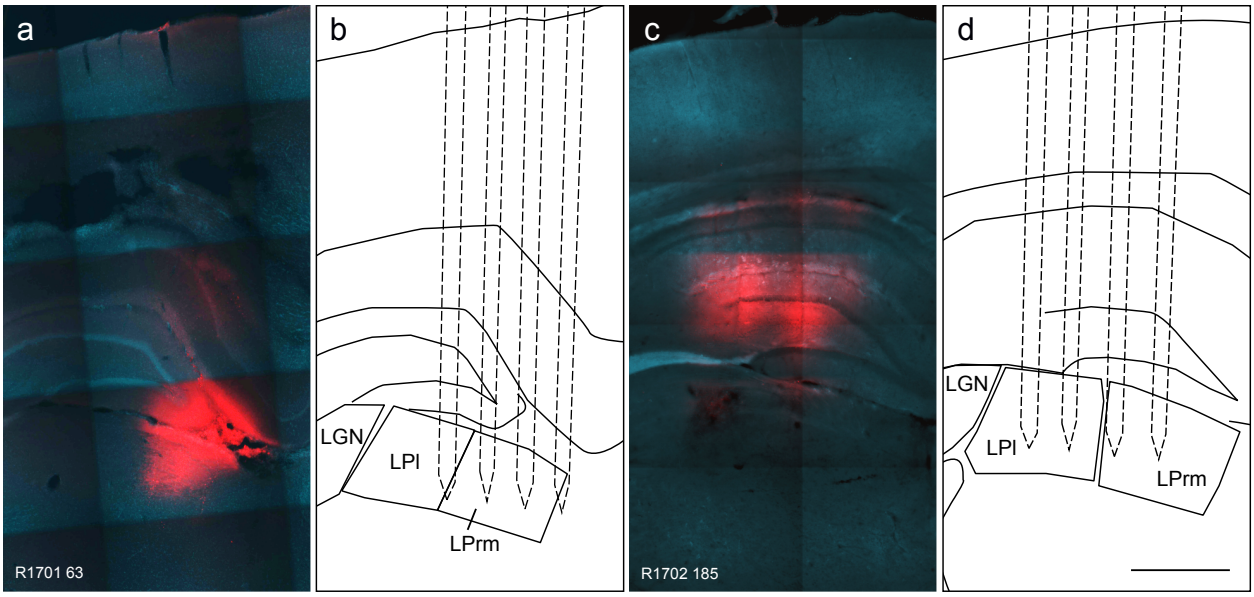

Figure 2.2: Electrode tracks in LPrm and LPl left by fluorescent dye. Case R1701 had six penetrations of four electrodes each, the most caudal set of penetrations is shown in (a) and reconstructed in (b). In case R1702 there were four penetrations of four electrodes each, the most caudal is shown in (c) and reconstructed in (d). Fluorescent DiI dye (a,c) helped to reconstruct electrode tracks, but in some cases the tracks were clearly visible even without dye (c). Scale bar equals 1 mm.

untreated under fluorescent and bright-field light using a fluorescent microscope (Axioplan 2; Zeiss, White Plains, NY). Digital images of electrodes tracks stained with DiI fluorescent dye were captured using a low-light-sensitive monochrome camera (Sensicam QE; PCO AG, Kelheim, Germany) and appropriate filters using Neurolucida software (MBF Bioscience, Williston, VT). Brain sections were visually inspected for the presence of DiI fluorescent electrode tracks (see Figure 2.2). Tracks were annotated with coordinates according to the rat brain atlas by Paxinos and Watson (2013) and assigned to a recording session according to their relative position to other tracks in the same case (see Figure 2.3). The maximum depth of each track was measured so that single units could be annotated along its length, then assigned to LP subdivisions based on stereotaxic coordinates (Figure 2.4).

Multichannel recordings were acquired using a 32-channel Scout recording system (Ripple Neuro, Salt Lake City, UT). Signals containing spikes were bandpass filtered from 500 Hz to 7 kHz and stored on a computer hard drive at 30 kHz sampling frequency. Spikes were

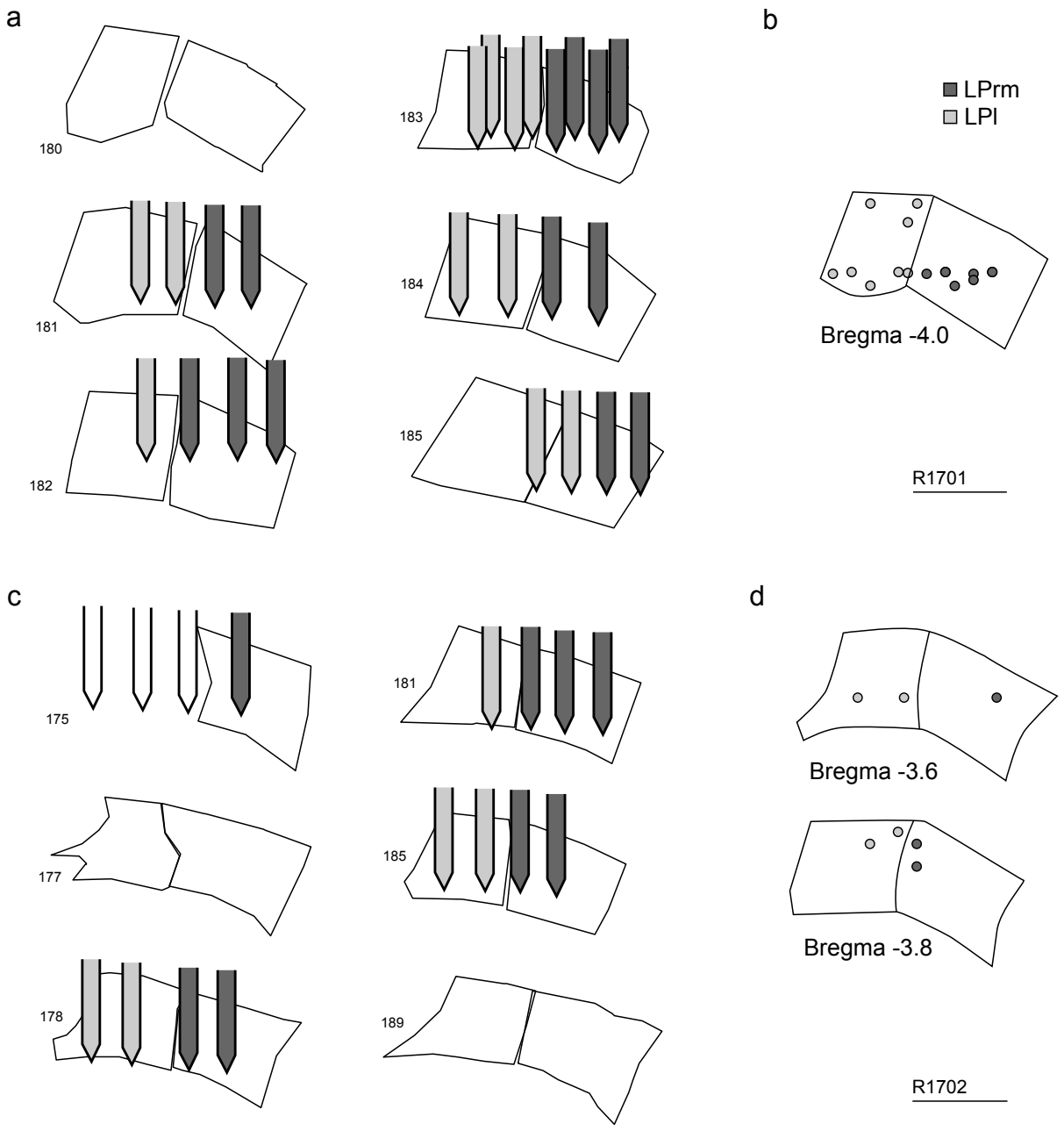

Figure 2.3: Reconstructions of electrode tracks and single unit locations for two cases. Electrode tracks (a, c) were reconstructed for each coronal brain slice where fluorescent dye was visible at the maximum depth from the corresponding recording session. Then each recording site (location and depth) was recorded and assigned to its anatomical region (b, d) according to the atlas by Paxinos and Watson (2013). Scale bars equal 1 mm.

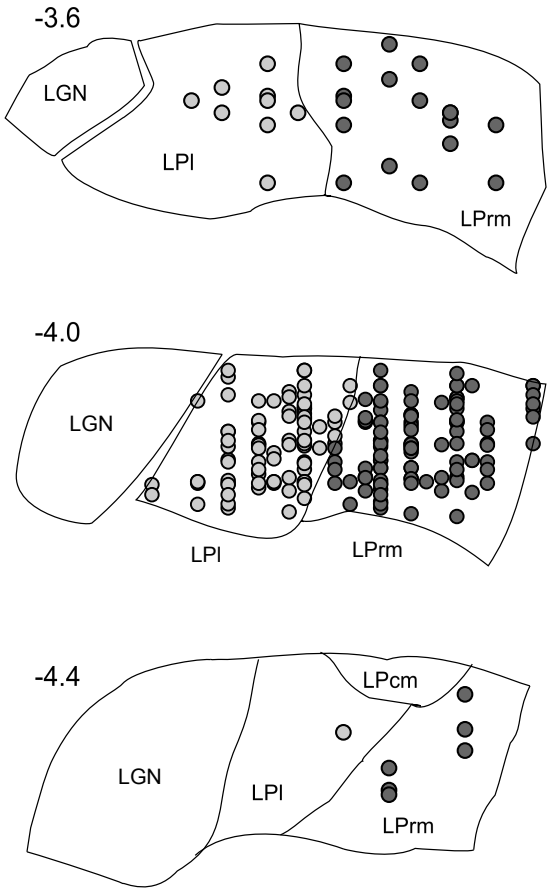

Figure 2.4: Reconstruction of all recorded cells in LP in three coronal planes. Dark circles are single units assigned to rostromedial pulvinar (LPrm), light circles are units assigned to lateral pulvinar (LPl). No units were assigned to caudomedial pulvinar (LPcm). Regions were anatomically conformed to the atlas by Paxinos and Watson (2013) using stereotaxic coordinates relative to Bregma.

sorted online in Trellis software (Ripple Neuro) while performing visual stimulation. Visual stimuli were generated in Matlab (Mathworks, Natick, MA) using Psychophysics Toolbox (Brainard, 1997; Pelli, 1997; Kleiner et al., 2007) and displayed on a gamma-corrected LCD monitor (55 inches, 60 Hz; RCA, NY, USA) at 1920x1080 pixels resolution and 52 $\mathrm{cd\,m^{-2}}$ mean luminance. Stimulus onset times were corrected for LCD monitor response time using a photodiode and microcontroller (in-house design based on an Arduino microcontroller board). Visually responsive cells were found using either 100% contrast isoluminant drifting grating stimuli or brief (500 ms) flashes of white on a black background. Cells with firing rates modulated by grating presentation were further tested with circular masked drifting sinusoidal gratings to determine their receptive field locations and optimal parameters for spatial frequency, temporal frequency, orientation, direction, size, and contrast. Not all tests were performed on every cell.

Peri-stimulus time histograms (PSTH) with 10 ms bin widths were constructed following flash stimulus onset and offset. Means and standard deviations of spontaneous background activity were calculated using the 100 ms before stimulus onset. Response latency was defined as the time at which instantaneous firing rate exceeded mean background activity plus two standard deviations.

Tuning curves were constructed using mean firing rates during stimulus presentation averaged over multiple repetitions (8 for grating stimuli, 100 to 300 for flash stimulus). Orientation selectivity index (OSI) and direction selectivity index (DI) were calculated as 1 - Var(r), where Var(r) is the circular variance of the responses at each orientation or direction.

To calculate orientation tuning bandwidth, size, contrast, and frequency preferences, cell responses were first fit to appropriate models using an unconstrained nonlinear optimization procedure (MATLAB function: FMINSEARCH; Mathworks, Natick, MA) to minimize the sum of squared residuals. Orientation responses were fit to double Gaussian distributions (Carandini & Ferster, 2000; Alitto & Usrey, 2004) without subtracting spontaneous activity.

Size tuning curves were fit using the difference of Gaussians (DoG), and spatial and temporal frequency responses were fit to Gaussian distributions (DeAngelis et al., 1993; Van der Bergh et al., 2010). The orientation tuning bandwidth of each tuning curve was measured in degrees as the half-width at half-height (HWHH). All other optimal parameters were chosen as the value with the maximum firing rate.

Cells were considered visually responsive if they had a response to any stimulus (flash or grating) above two standard deviations of mean pre-stimulus firing rate. Of these, some cells did not have strong responses to any of the grating stimuli we tested, and were not considered for further analysis of receptive field tuning preferences. Differences were considered significant at $p \leq 0.05$ for two-tailed Mann-Whitney U-tests and Pearson's χ^2 tests. Error bars indicate standard error of the mean (SEM). All offline data analysis and statistics were performed using Matlab (Mathworks, Natick, MA).

2.4 Results

Recordings in the lateral posterior nucleus (LP) in 18 rats and V1 in 9 rats revealed a total of 470 single units in LP and 101 units in V1. A summary of reconstructed recording sites is shown in Figure 2.4. Recordings in LPl were confirmed to be around -4 mm from Bregma (M = -3.9 mm, SD = 0.1 mm) and -2.5 mm from the midline (M = 2.6 mm, SD = 0.3 mm) and in LPrm around -4 mm from Bregma (M = -4.0 mm, SD = 0.2 mm) and 1.5 mm from the midline (M = 1.8 mm, SD = 0.3 mm). In V1, most cells were visually responsive and easy to find using high contrast grating stimuli (Table 1). In LP, cells had less robust responses to gratings but were easier to identify using flash stimuli. Significantly fewer cells were visually responsive in both LPrm ($\chi^2(1) = 4.08$, $p = 0.04$) and LPl ($\chi^2(1) = 8.43$, $p = 0.004$) compared to V1 (see Table 1). Visually evoked responses of neurons to brief (500 ms) flashes of light also revealed differences in latency between LP and V1 neurons. Both

Table 2.1: Percentage of visually responsive and grating selective neurons in each region.

	Number of cells	Visually responsive (%)	Drifting grating responsive (%)
LPrm	241	79	52
LPl	229	74	43
V1	101	88	79

LPrm ($p < 0.001$; U-test) and LPl ($p = 0.001$; U-test) had significantly longer latencies than V1 on average, although the shortest response latencies were observed in LP rather than V1 (Figure 2.5a, 2.5c). Mean spontaneous firing rate was also significantly higher in LPrm ($p = 0.018$; U-test) and LPl ($p = 0.009$; U-test) compared to V1.

Some cells in LP that were identified as visually responsive by flash stimuli did not have strong responses to drifting grating stimuli, even with low spatial frequencies (0.001 °/cycle). Of all visually responsive cells, a significantly lower percentage were responsive to drifting grating stimuli in both LPrm ($\chi^2(1) = 18.06$, $p < 0.001$) and LPl ($\chi^2(1) = 26.90$, $p < 0.001$) compared to V1. The remaining cells (125 in LPrm, 99 in LPl, and 80 in V1) were tested for preferences to spatial frequency, temporal frequency, orientation, direction, size, and contrast. Figure 2.6 shows typical experimental data recorded from cells in LPrm, LPl, and V1.

In the left column of Figure 2.6 are the responses to drifting sinusoidal gratings of an example cell in LPrm. This cell responded maximally to gratings oriented at 90°, with only a very small increase in firing rate to gratings in the opposite direction (270°). Likewise, in the middle column of Figure 2.6 is an example cell in LPl with direction selectivity, having had no response to the stimulus oriented 180° from the optimal direction. In comparison, the V1 cell shown in the right column of Figure 2.6 had nonzero responses to both the optimal stimulus and the one oriented 180° from the optimal direction. Figure 2.6b shows the responses of the same cells to different size grating stimuli, illustrating that LPrm and LPl cells can have receptive fields as large as 85°. Illustrations of spatial frequency (6c) and temporal frequency (6d) tuning are also shown for the same cells.

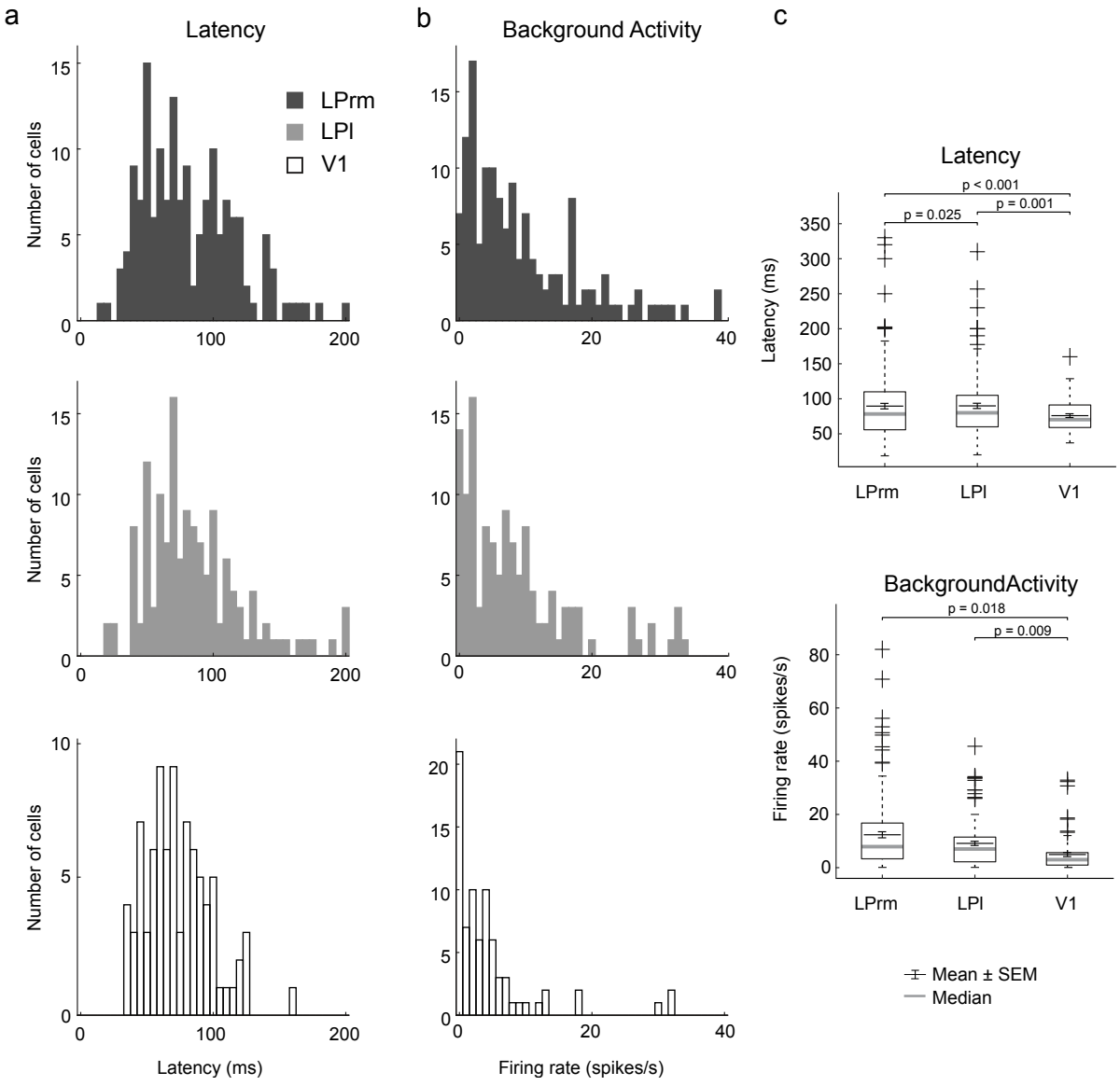

Figure 2.5: Response latency and spontaneous background activity of cells recorded from LPrm (top row, dark gray), LPl (middle row, gray), and V1 (bottom row, white). Response latencies (a) were sometimes very delayed in LP compared to V1. Spontaneous activity in LP cells was also higher on average compared to V1 cells. Mean and median responses are compared in (c).

Of the neurons in each region with responses to drifting sinusoidal gratings, average spatiotemporal receptive field properties were markedly different between LP and V1. Most noticeably, receptive field sizes in LP, at an average of 69° diameter, were significantly larger than in V1, where receptive fields averaged 22° diameter ($p < 0.001$; U-test; Figure 2.7c). Most receptive fields in LP were not suppressed by large stimuli and were facilitated by large stimuli up to the maximum diameter we tested (110°; see Figure 2.6b for example). The majority of cells we tested preferred spatial frequencies (SF) between 0.01 and 0.08 cycle/°, and there was no statistical difference in mean SF preference between LP and V1 ($p = 0.80$; U-test; Figure 2.6a), nor in preferred temporal frequencies (TF) between LP and V1 ($p = 0.13$; U-test).

Figure 2.6: Examples of spatiotemporal response properties of one cell each in LPrm (left column), LPl (middle column) and V1 (right column), before (dotted lines) and after (solid lines) curve fitting. In (a), direction tuning bandwidth was calculated based on the half width at half height (HWHH) of the preferred direction. Size (b), spatial frequency (c), and temporal frequency (d) were calculated based on the value realizing the highest firing rate.

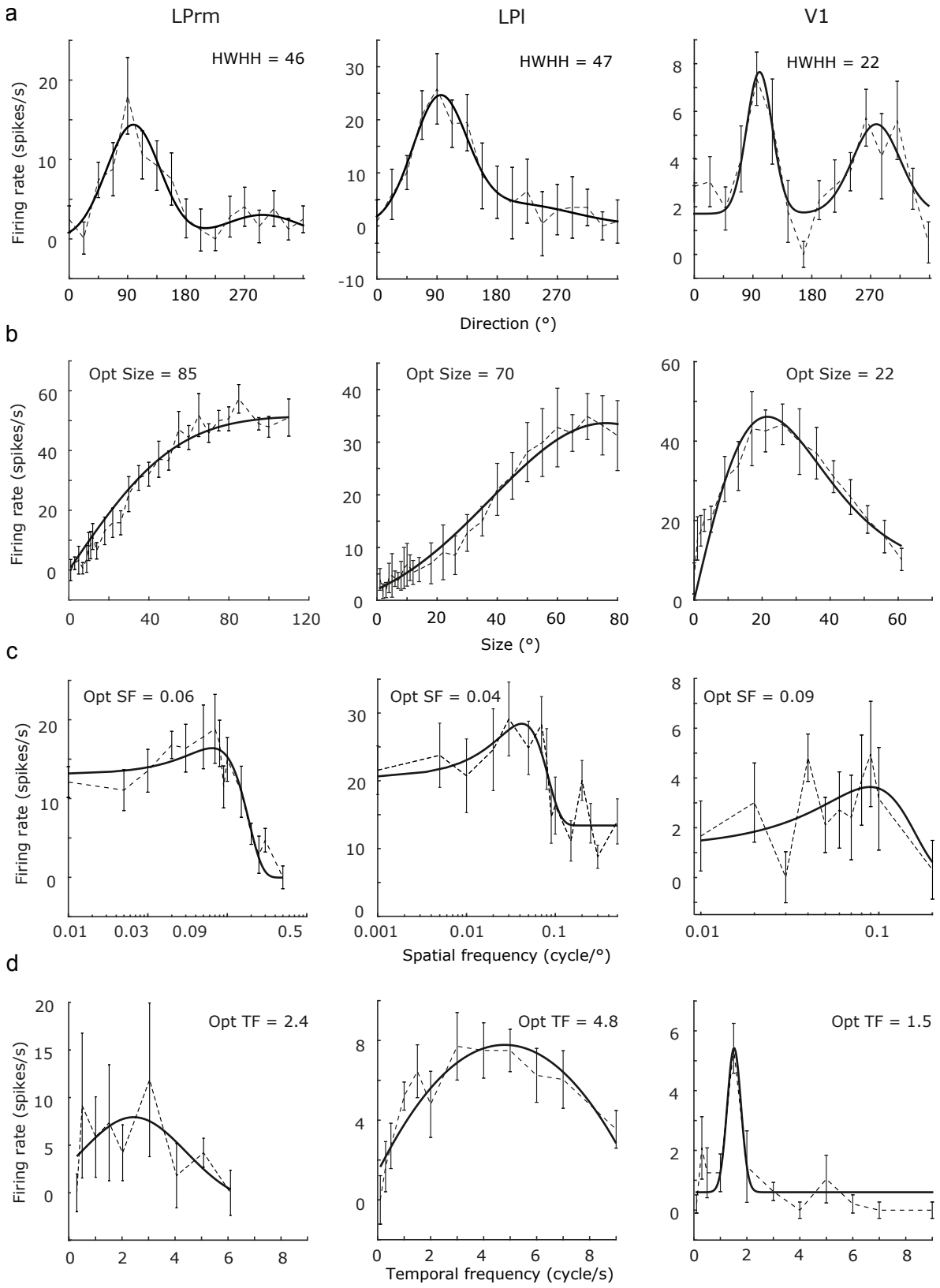
a
LPrm
LPl
V1
HWHH = 46
HWHH = 47
HWHH = 22
Firing rate (spikes/s)
Direction (°)
b
Opt Size = 85
Opt Size = 70
Opt Size = 22
Size (°)
c
Opt SF = 0.06
Opt SF = 0.04
Opt SF = 0.09
Spatial frequency (cycle/°)
d
Opt TF = 2.4
Opt TF = 4.8
Opt TF = 1.5
Temporal frequency (cycle/s)

Figure 2.7: Spatial frequency, temporal frequency, and size tuning. Spatial frequency preferences (a) were comparable between V1 and LP subdivisions. Optimal temporal frequency (b) was higher on average in LPl than in LPrm or V1. Receptive field size (c) was larger in both LP subdivisions compared to V1. Comparison of mean and median values for each parameter are shown in (d).

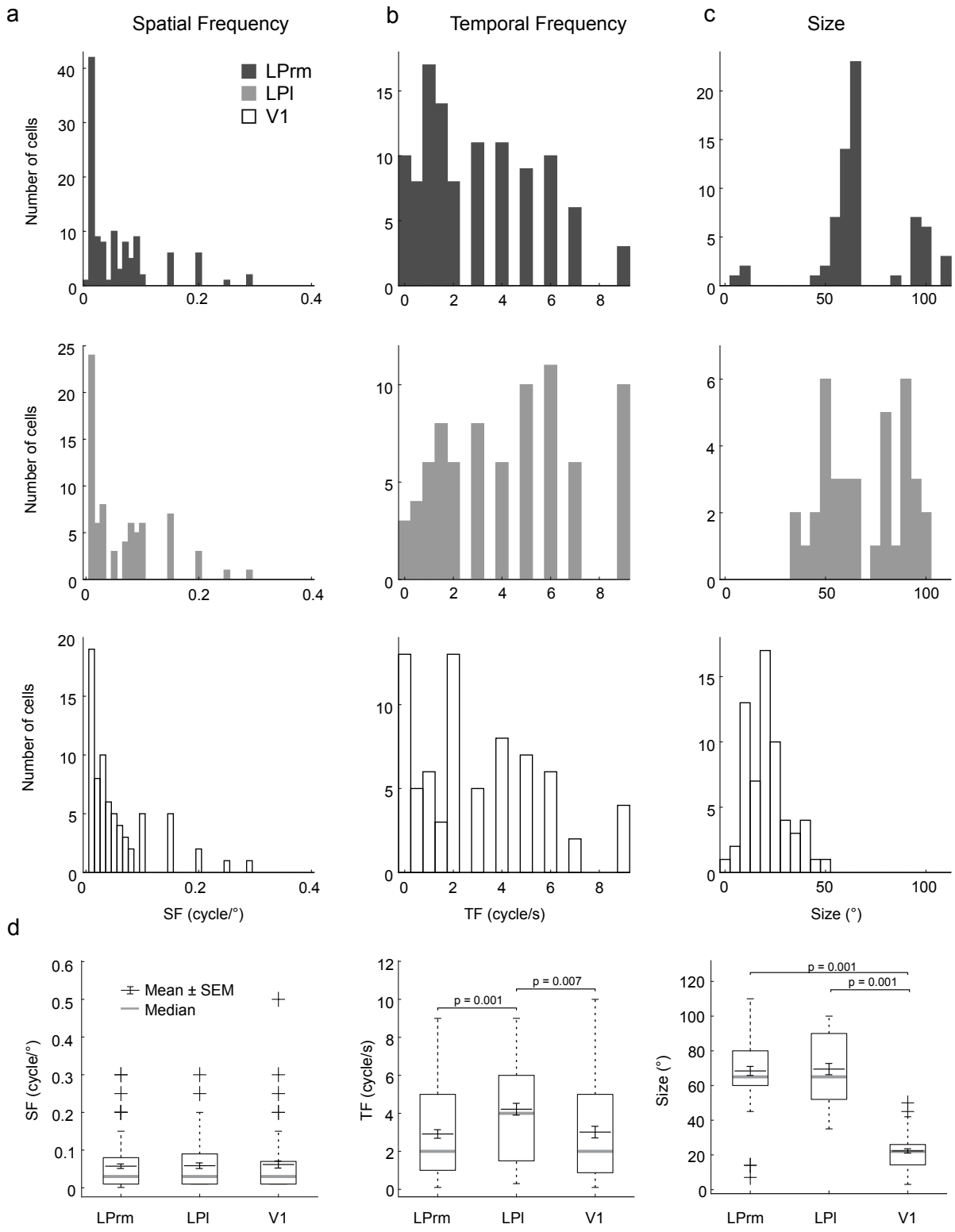
a
Spatial Frequency
b
Temporal Frequency
c
Size
LPrm
LPl
V1
Number of cells
SF (cycle/°)
TF (cycle/s)
Size (°)
d
Mean ± SEM
Median
SF (cycle/°)
TF (cycle/s)
Size (°)
p = 0.001
p = 0.007
p = 0.001
p = 0.001
LPrm
LPl
V1

We also compared preferences between the two rostral subdivisions to test whether collicular input had an impact on response properties in LPl. The mean temporal frequency preference was significantly higher in LPl than in LPrm ($p = 0.001$; U-test; see Figure 2.7). Out of 78 neurons tested for TF in LPl, ten responded optimally to 9 cycles/s, the highest frequency we tested. Average TF preference in LPl was also significantly higher than TF preference in V1 ($p = 0.007$; U-test). There was no significant difference in TF preference between LPrm and V1 ($p = 0.91$; U-test). There was also no significant difference in mean SF ($p = 0.27$; U-test) or size ($p = 0.59$; U-test) preference between the two pulvinar subdivisions.

Whereas all cells in LP and V1 with responses to grating stimuli displayed selective responses to certain spatial frequencies, temporal frequencies, and stimulus sizes, some cells were not selective to orientation or direction, and instead fired in response to all grating directions equally (Figure 2.8). To quantify the degree to which LP cells were direction or orientation selective, we compared orientation selectivity index (OSI) and direction selectivity index (DI) between the two rostral LP subdivisions and V1 (Figure 2.9). Mean OSI in V1 was 0.41 versus 0.36 in LP. On average, OSI was significantly lower in LPl than in V1 ($p = 0.012$; U-test).

Many cells in V1 and in both LP subdivisions were direction selective rather than orientation selective, having only a single preferred direction rather than a response at two orientations 180° apart (see Figure 2.6a). Direction tuning measured by DI was significantly higher on average in LPrm than in V1 ($p = 0.009$; U-test; Figure 2.9). Direction tuning bandwidth, measured for the preferred direction in cells with direction selectivity or for the direction with the highest firing rate for orientation tuned cells, was also compared between LP subdivisions and V1. Cells in V1 were more sharply tuned with significantly lower bandwidth measured by half width at half height (HWHH) than cells in LPrm ($p = 0.001$; U-test) and cells in LPl ($p = 0.002$; U-test; Figure 2.9). There was no significant difference between direction bandwidth between LPrm and LPl.

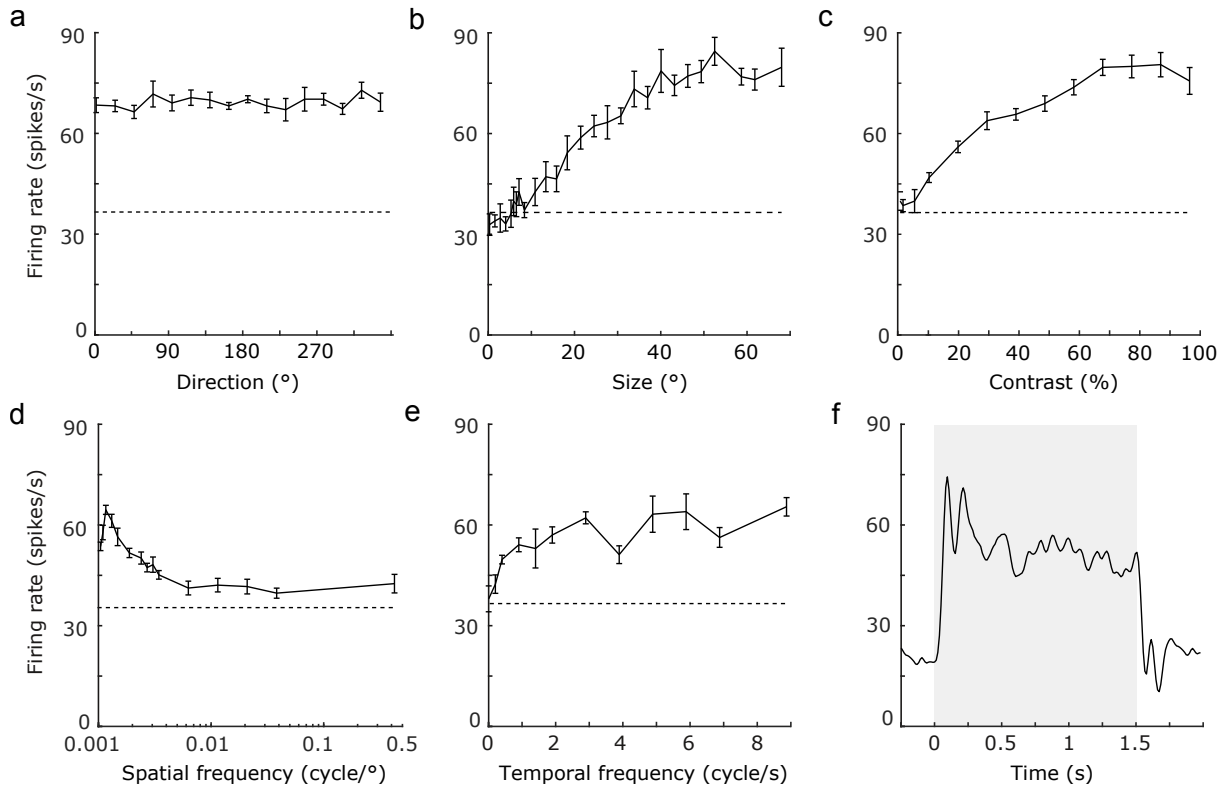

Figure 2.8: Example responses from an LPrm cell with no direction preference. This cell had strong responses to grating stimuli (a-e) and flash stimulus (f), but no preference for direction (a). Dotted lines indicate average spontaneous firing rate during each experiment. PSTH in (f) shows the cell's response to a black screen (shaded area) following brief (500 ms) periods of white, averaged across 100 trials and smoothed by a moving gaussian filter.

2.5 Discussion

The aim of this project was to test response selectivity in the rat lateral posterior thalamic nucleus (LP or pulvinar). To our knowledge such detailed studies in the rat LP have not been done in the past. Characteristics of single unit responses from rostro-medial (LPrm) and lateral (LPl) subdivisions of the LP revealed that only 40-50% of the population had robust responses to drifting gratings, whereas around 75% of the population was visually responsive. Close to 90% of V1 cells were responsive to both types of visual stimulus. Further analysis revealed that LPrm and LPl cells had significantly larger receptive field sizes, wider orientation tuning bandwidths, and higher spontaneous firing rates compared to cells in V1. We also examined differences between pulvinar subdivisions, finding that cells in the colliculo-recipient LPl had a higher mean temporal frequency preference than cells in LPrm. Compared to V1, LPl also had lower average orientation selectivity, whereas LPrm had higher average direction selectivity, indicating that LPl cells may inherit spatiotemporal properties primarily from superior colliculus, whereas in LPrm these properties are more likely derived from cortex.

The difference between LP and V1 receptive field sizes is indicative of the pulvinar's role as an integrating higher-order thalamic relay (Sherman & Guillery, 1998). The lateral geniculate nucleus (LGN), a first order relay, receives its driving input directly from the retina, giving its cells receptive fields that are smaller than those found in V1 (Rodieck, 1979; Gao et al., 2010). But in the LP, receptive fields were large compared to V1, meaning that LP cells

Figure 2.9: Orientation and direction selectivity compared between LPrm (dark gray bars), LPl (light gray bars), and V1 (white bars). (a) Orientation selectivity index (OSI) was higher in V1 compared to LPl, but similar between V1 and LPrm. (b) Direction selectivity index (DI) was higher on average in LPrm than in V1. (c) Direction tuning bandwidth was higher in both LP subdivisions compared to V1. (d) Comparisons of mean and median values for OSI, DI, and bandwidth.

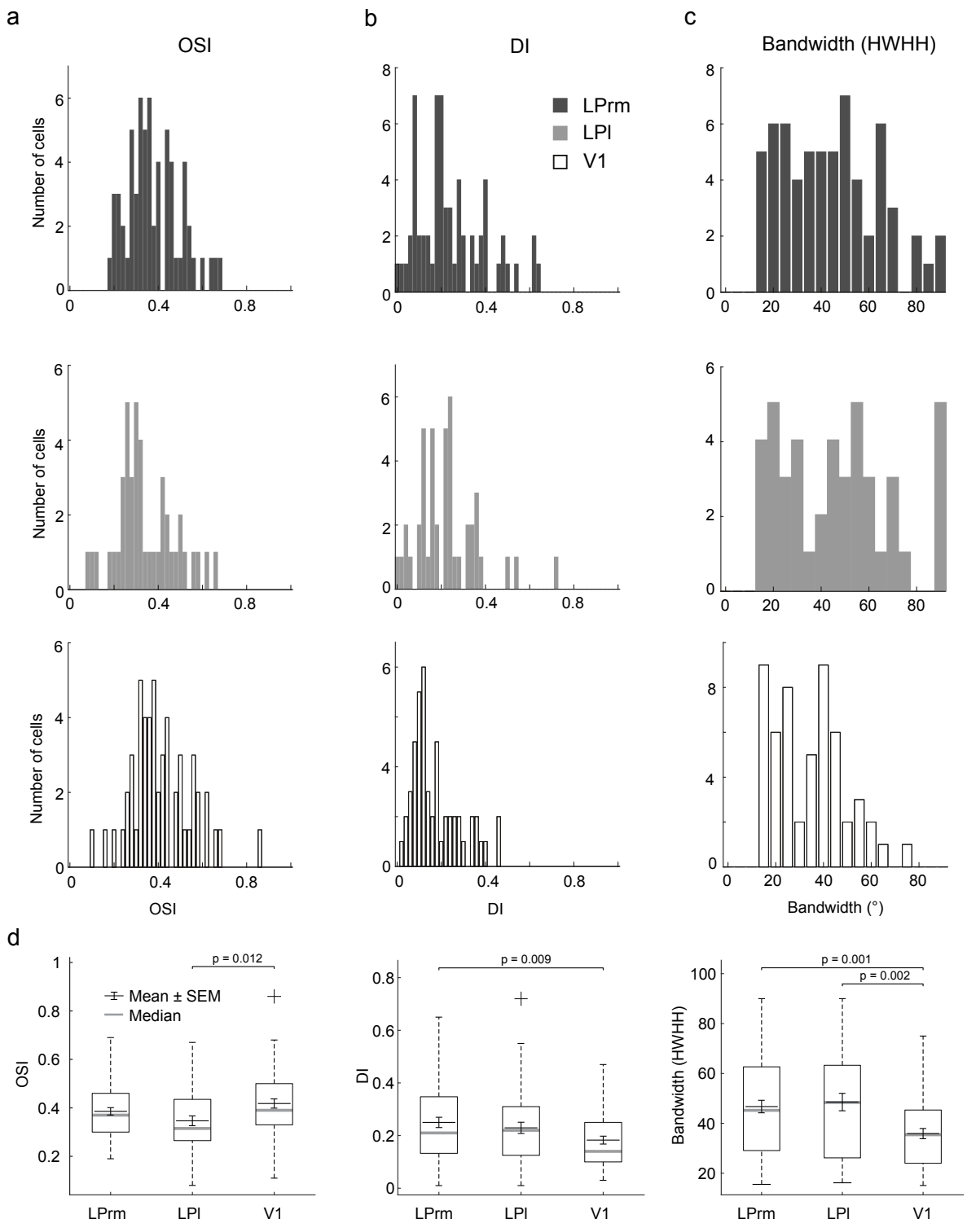
a
b
c
OSI
DI
Bandwidth (HWHH)
LPrm
LPl
V1
Number of cells
OSI
DI
Bandwidth (°)
d
p = 0.012
p = 0.009
p = 0.001
p = 0.002
Mean ± SEM
Median
OSI
DI
Bandwidth (HWHH)
LPrm
LPl
V1

may integrate input from many V1 cells, or inherit large receptive field sizes from higher visual cortex or, in the case of LPl, from the superior colliculus. Relatively large pulvinar receptive fields have also been found in the cat, where receptive fields in striate-recipient pulvinar average 8° diameter (Casanova et al., 1989), versus 2° in V1 (Albus, 1975), and in monkeys, where receptive fields average 5° diameter in the ventrolateral pulvinar (Gattass et al., 1979) and dorsomedial pulvinar (Petersen et al., 1985), versus diameters typically less than 1° in V1 (Hubel & Wiesel, 1968). We found V1 receptive field sizes of about 20° on average, similar to previously reported values in rat (Girman et al., 1999; Foik et al., 2018), and LP receptive field sizes of 70° on average. Superior colliculus receptive fields in rat have been reported with diameters ranging from 10° to 60° (Fukuda & Iwama, 1978).

The higher average temporal frequency preference in LPl compared to V1 (Figure 2.7) suggests that some pulvinar neurons might be involved in circuitry to filter visual input based on speed. This would be congruent with the results of Tohmi et al. (2014), who showed that velocity tuning differences between areas in higher visual cortex are lost when superior colliculus is ablated, presumably because pulvinar cells carry the information from temporal-frequency tuned superior colliculus cells which receive input mostly from Y-like and W-like channels (Waleszczyk et al., 2007; Prévost et al., 2007). The longer response latencies we observed in LP compared to V1 (Figure 2.5) suggest that feedback from spatially tuned visual cortex cells might combine with superior colliculus input in the pulvinar (Jarosiewicz et al, 2012).

Longer latencies might also be caused by cortical input alone. Cells in the higher visual cortex of macaque are known to have longer latencies than in V1 on average, although the distribution of latencies within any one particular visual area is large (Schmolesky et al., 1998). In LPrm in particular, which receives no collicular input but does receive cortical projections from V1 and V2 (Takahashi, 1985; Masterson et al., 2009), the additional delay versus V1 likely arises from the addition of synapses from cortex to LP. Similar latency to

what we found has been previously reported in V1 of rat (Wang et al., 2006; Foik et al., 2018) and mouse (Durand et al., 2016), but response latencies in some areas of higher visual cortex in mouse are much longer than in V1 on average (Polack & Contreras, 2012), which could account for longer response delays in LP cells.

Orientation selectivity and direction selectivity have both been demonstrated in rat V1 previously (Girman et al., 1999), and have also been reported in the pulvinar of cat (Casanova et al., 1989) and monkey (Gattass et al., 1979). Here we confirm that cells in rat LP also respond preferentially to specific orientations or directions of sinusoidal drifting gratings, with broader tuning bandwidth compared to V1 cells (Figure 2.9). This difference between LP and V1 in tuning broadness is consistent with studies performed in cats (Casanova et al., 1989; Chalupa & Abramson, 1989). We found subtle differences in responses between lateral and medial portions of the LP, as cells in the colliculo-recipient LPl had lower orientation selectivity compared to V1, whereas cells in LPrm had higher direction selectivity compared to V1. Again, this suggests that the superior colliculus, where direction selectivity is rare (Fukuda & Iwama, 1978), drives the difference between LPrm and LPl receptive field properties.

The inferior primate pulvinar has been subdivided into a medial portion involved in visually guided actions and a lateral portion involved in object vision (Kaas and Lyon, 2007). Given that both the inferior medial pulvinar and the LPl receive input from the superior colliculus as well as V1 and V2 (see Figure 2.1), in addition to the preference for higher temporal frequencies we observed in LPl, it is reasonable that LPl might be also involved in dorsal stream action-vision. Similarly, the lateral subdivision of the primate pulvinar and LPrm share anatomical input from V1 and V2 without any collicular input, and we observed the strongest direction tuning in LPrm, suggesting that LPrm may be involved in ventral stream object-vision. More conclusive evidence of specialization between these two rodent LP subdivisions requires further anatomical and functional confirmation of subdivisions within

rodent V2. In mouse, mounting evidence suggests areas in higher visual cortex can be grouped into dorsal and ventral stream classifications (Glickfeld et al., 2014), but no such map exists in rat. Bias in connectivity between LP subdivisions and different higher visual cortex areas would more clearly suggest a functional difference between LPrm and LPl in rodents. Future evaluation of rodent cortical responses will also be needed to more fully model the systems level functional properties of LPrm and LPl cells. For example, given that LPl encodes higher temporal frequencies than V1, and diversity in rodent V2 speed preferences are dependent on superior colliculus (Tohmi et al., 2014), it would be interesting to test whether the pulvinar has a direct influence on speed tuning in V2.

In summary, our findings suggest that the rat pulvinar is comparable to the pulvinar of other mammals in terms of visual stimuli processing. We verified the presence of orientation and direction tuned cells in LP, and identified receptive fields with large diameters compared to V1 cells. We also distinguished two distinct roles for the rostromedial and lateral portions of LP. The lateral part is more likely involved in temporal frequency and speed processing, whereas the rostromedial portion has stronger direction processing, perhaps due to differences in collicular input or connectivity with higher visual cortex. Further research aiming to identify differences in cortical connectivity with pulvinar subdivisions will help answer outstanding questions regarding the anatomical routes by which pulvinar might derive spatiotemporal receptive field properties.

2.6 References

Ahmadlou, M., Zweifel, L. S., and Heimel, J. A. (2018). Functional modulation of primary visual cortex by the superior colliculus in the mouse. *Nature Communications*, 9(1):3895.

Albus, K. (1975). A quantitative study of the projection area of the central and the paracentral visual field in area 17 of the cat. *Experimental Brain Research*, 24(2):159–179.

Alitto, H. J. and Usrey, W. M. (2004). Influence of contrast on orientation and temporal

frequency tuning in ferret primary visual cortex. *Journal of Neurophysiology*, 91(6):2797–2808.

Allen, A. E., Procyk, C. A., Howarth, M., Walmsley, L., and Brown, T. M. (2016). Visual input to the mouse lateral posterior and posterior thalamic nuclei: photoreceptive origins and retinotopic order. *The Journal of Physiology*, 594(7):1911–1929.

Baldwin, M. K. L., Balaram, P., and Kaas, J. H. (2013). Projections of the superior colliculus to the pulvinar in prosimian galagos (Otolemur garnettii) and VGLUT2 staining of the visual pulvinar. *Journal of Comparative Neurology*, 521(7):1664–1682.

Baldwin, M. K. L., Wong, P., Reed, J. L., and Kaas, J. H. (2011). Superior colliculus connections with visual thalamus in gray squirrels (Sciurus carolinensis): Evidence for four subdivisions within the pulvinar complex. *Journal of Comparative Neurology*, 519(6):1071–1094.

Bender, D. B. (1982). Receptive-field properties of neurons in the macaque inferior pulvinar. *Journal of Neurophysiology*, 48(1):1–17.

Benevento, L. a. and Rezak, M. (1976). The cortical projections of the inferior pulvinar and adjacent lateral pulvinar in the rhesus monkey (Macaca mulatta): an autoradiographic study. *Brain Research*, 108(1):1–24.

Bennett, C., Gale, S. D., Garrett, M. E., Newton, M. L., Callaway, E. M., Murphy, G. J., and Olsen, S. R. (2019). Higher-Order Thalamic Circuits Channel Parallel Streams of Visual Information in Mice. *Neuron*, pages 1–16.

Bridge, H., Leopold, D. A., and Bourne, J. A. (2016). Adaptive Pulvinar Circuitry Supports Visual Cognition. *Trends in Cognitive Sciences*, 20(2):146–157.

Carandini, M. and Churchland, A. K. (2013). Probing perceptual decisions in rodents. *Nature neuroscience*, 16(7):824–31.

Casanova, C., Freeman, R. D., and Nordmann, J. P. (1989). Monocular and binocular response properties of cells in the striate-recipient zone of the cat's lateral posterior-pulvinar complex. *J Neurophysiol*, 62(2):544–557.

Chalupa, L. M. and Abramsow, P. (1989). Visual Receptive Fields in the Striate-Recipient Complex Zone of the Lateral. *Physiology*, 9(January).

Chen, C., Zhang, X., Wang, Y., Zhou, T., and Fang, F. (2016). Neural activities in V1 create the bottom-up saliency map of natural scenes. *Experimental Brain Research*, 234(6):1769–1780.

Cowey, A., Smith, B., and Butter, C. (1984). Effects of damage to superior colliculi and pre-tectum on movement discrimination in rhesus monkeys. *Experimental Brain Research*, 56(1).

DeAngelis, G. C., Ohzawa, I., and Freeman, R. D. (1993). Spatiotemporal organization of simple-cell receptive fields in the cat's striate cortex. I. General characteristics and postnatal development. *Journal of Neurophysiology*, 69(4):1091–1117.

DiCarlo, J. J., Lane, J. W., Hsiao, S. S., and Johnson, K. O. (1996). Marking microelectrode penetrations with fluorescent dyes. *Journal of Neuroscience Methods*, 64(1):75–81.

Durand, S., Iyer, R., Mizuseki, K., De Vries, S., Mihalas, S., and Reid, R. C. (2016). A comparison of visual response properties in the lateral geniculate nucleus and primary visual cortex of awake and anesthetized mice. *Journal of Neuroscience*, 36(48):12144–12156.

Fabre-Thorpe, M., Viévard, A., and Buser, P. (1986). Role of the extra-geniculate pathway in visual guidance - II. Effects of lesioning the pulvinar-lateral posterior thalamic complex in the cat. *Experimental Brain Research*.

Foik, A. T., Scholl, L. R., Lean, G. A., Aramant, R. B., McLelland, B. T., Seiler, M. J., Mathur, A., and Lyon, D. C. (2018). Detailed Visual Cortical Responses Generated by Retinal Sheet Transplants in Rats with Severe Retinal Degeneration. *The Journal of Neuroscience*, 38(50):10709–10724.

Fukuda, Y. and Iwama, K. (1978). Visual Receptive-field Properties of Single Cells in the Rat Superior Colliculus. *The Japanese Journal of Physiology*, 28(3):385–400.

Gao, E., DeAngelis, G. C., and Burkhalter, A. (2010). Parallel Input Channels to Mouse Primary Visual Cortex. *Journal of Neuroscience*, 30(17):5912–5926.

Gattass, R., Oswaldo-Cruz, E., and Sousa, A. P. (1979). Visual receptive fields of units in the pulvinar of cebus monkey. *Brain Research*, 160(3):413–429.

Girman, S. V., Sauvé, Y., and Lund, R. D. (1999). Receptive field properties of single neurons in rat primary visual cortex. *Journal of Neurophysiology*, 82(1):301–311.

Glickfeld, L. L., Reid, R. C., and Andermann, M. L. (2014). A mouse model of higher visual cortical function. *Current Opinion in Neurobiology*, 24(1):28–33.

Goodale, M. A. (2005). Action insight: The role of the dorsal stream in the perception of grasping.

Goodale, M. A. (2013). Separate visual systems for perception and action: a framework for understanding cortical visual impairment. *Developmental Medicine & Child Neurology*.

Hubel, D. H. and Wiesel, T. N. (1968). Receptive fields and functional architecture of monkey striate cortex. *Journal of Physiology*, 195(1):215–243.

Izpisua Belmonte, J. C., Callaway, E. M., Churchland, P., Caddick, S. J., Feng, G., Homanics, G. E., Lee, K. F., Leopold, D. A., Miller, C. T., Mitchell, J. F., Mitalipov, S., Moutri, A. R., Movshon, J. A., Okano, H., Reynolds, J. H., Ringach, D., Sejnowski, T. J., Silva, A. C., Strick, P. L., Wu, J., and Zhang, F. (2015). Brains, Genes, and Primates. *Neuron*, 86(3):617–631.

Jarosiewicz, B., Schummers, J., Malik, W. Q., Brown, E. N., and Sur, M. (2012). Functional biases in visual cortex neurons with identified projections to higher cortical targets.

Jones, E. G. (1985). *The Thalamus*. Springer US, Boston, MA.

Kaas, J. H. and Lyon, D. C. (2007). Pulvinar contributions to the dorsal and ventral streams of visual processing in primates. *Brain Research Reviews*, 55(2 SPEC. ISS.):285–296.

Lyon, D. C., Jain, N., and Kaas, J. H. (2003). The visual pulvinar in tree shrews II. Projections of four nuclei to areas of visual cortex. *The Journal of Comparative Neurology*, 467(4):607–627.

Lyon, D. C., Nassi, J. J., and Callaway, E. M. (2010). A Disynaptic Relay from Superior Colliculus to Dorsal Stream Visual Cortex in Macaque Monkey. *Neuron*.

Masterson, S. P., Li, J., and Bickford, M. E. (2009). Synaptic organization of the tectorecipient zone of the rat lateral posterior nucleus. *Journal of Comparative Neurology*, 515(6):647–663.

Mizzi, R. and Michael, G. a. (2014). The role of the collicular pathway in the salience-based progression of visual attention. *Behavioural Brain Research*, 270:330–338.

Montero, V. M., Brugge, J. F., and Beitel, R. E. (1968). Relation of the visual field to the lateral geniculate body of the albino rat. *Journal of neurophysiology*, 31(2):221–36.

Nakamura, H., Hioki, H., Furuta, T., and Kaneko, T. (2015). Different cortical projections from three subdivisions of the rat lateral posterior thalamic nucleus: A single-neuron tracing study with viral vectors. *European Journal of Neuroscience*, 41(10):1294–1310.

Paxinos, G. and Watson, C. (2013). The rat brain in stereotaxic coordinates. *London: Academic press*.

Petersen, S. E., Robinson, D. L., and Keys, W. (1985). Pulvinar nuclei of the behaving rhesus monkey: Visual responses and their modulation. *Journal of Neurophysiology*, 54(4):867–886.

Polack, P. O. and Contreras, D. (2012). Long-range parallel processing and local recurrent activity in the visual cortex of the mouse. *Journal of Neuroscience*, 32(32):11120–11131.

Pula, J. H. and Yuen, C. A. (2017). Eyes and stroke: The visual aspects of cerebrovascular disease.

Purves, D., Augustine, G., Fitzpatrick, D., Katz, L., LaMantia, A.-S., McNamara, J., and Williams, M. (2001). Visual Field Deficits. In *Neuroscience (2nd ed.). Sunderland (MA): Sinauer Associates*.

Robson, J. A. and Hall, W. C. (1977). The organization of the pulvinar in the grey squirrel (Sciurus carolinensis). I. Cytoarchitecture and connections. *Journal of Comparative Neurology*, 173(2):355–388.

Rodieck, R. (1979). Visual pathways. *Annual review of neuroscience*, pages 193–225.

Roth, M. M., Dahmen, J. C., Muir, D. R., Imhof, F., Martini, F. J., and Hofer, S. B. (2015). Thalamic nuclei convey diverse contextual information to layer 1 of visual cortex. *Nature Neuroscience*, 19(2):299–307.

Saalmann, Y. B. and Kastner, S. (2011). Cognitive and Perceptual Functions of the Visual Thalamus. *Neuron*, 71(2):209–223.

Schmitt, L. I. and Halassa, M. M. (2017). Interrogating the mouse thalamus to correct human neurodevelopmental disorders. *Molecular Psychiatry*, 22(2):183–191.

Schmolesky, M. T., Wang, Y., Hanes, D. P., Thompson, K. G., Leutgeb, S., Schall, J. D., and Leventhal, A. G. (1998). Signal timing access the macaque visual system. *Journal of Neurophysiology*, 79(6):3272–3278.

Shetht, B. R. and Young, R. (2016). Two visual pathways in primates based on sampling of space: Exploitation and exploration of visual information. *Frontiers in Integrative Neuroscience*, 10(NOV2016).

Snow, J. C., Allen, H. A., Rafal, R. D., and Humphreys, G. W. (2009). Impaired attentional selection following lesions to human pulvinar: Evidence for homology between human and monkey. *Proceedings of the National Academy of Sciences of the United States of America*, 106(10):4054–4059.

Sprague, J. M. and Meikle, T. H. (1965). The role of the superior colliculus in visually guided behavior. *Experimental Neurology*, 11(1):115–146.

Takahashi, T. (1985). The organization of the lateral thalamus of the hooded rat. *The Journal of comparative neurology*, 231(3):281–309.

Tohmi, M., Meguro, R., Tsukano, H., Hishida, R., and Shibuki, K. (2014). The extrageniculate visual pathway generates distinct response properties in the higher visual areas of mice. *Current biology : CB*, 24(6):587–97.

Trageser, J. C. and Keller, A. (2004). Reducing the uncertainty: gating of peripheral inputs by zona incerta. *The Journal of neuroscience : the official journal of the Society for Neuroscience*, 24(40):8911–5.

Van Den Bergh, G., Zhang, B., Arckens, L., and Chino, Y. M. (2010). Receptive-field properties of V1 and V2 neurons in mice and macaque monkeys. *Journal of Comparative Neurology*, 518(11):2051–2070.

Van Le, Q., Isbell, L. A., Matsumoto, J., Le, V. Q., Hori, E., Tran, A. H., Maior, R. S., Tomaz, C., Ono, T., and Nishijo, H. (2014). Monkey pulvinar neurons fire differentially to snake postures. *PLoS ONE*, 9(12):e114258.

Veale, R., Hafed, Z. M., and Yoshida, M. (2017). How is visual salience computed in the brain? Insights from behaviour, neurobiology and modeling. *Philosophical Transactions of the Royal Society B: Biological Sciences*, 372(1714).

Waleszczyk, W. J., Nagy, A., Wypych, M., Berényi, A., Paróczy, Z., Eördegh, G., Ghazaryan, A., and Benedek, G. (2007). Spectral receptive field properties of neurons in the feline superior colliculus. *Experimental Brain Research*, 181(1):87–98.

Waleszczyk, W. J., Wang, C., Benedek, G., Burke, W., and Dreher, B. (2004). Motion sensitivity in cat's superior colliculus: Contribution of different visual processing channels to response properties of collicular neurons. *Acta Neurobiologiae Experimentalis*, 64(2):209–228.

Waleszczyk, W. J., Wang, C., Burke, W., and Dreher, B. (1999). Velocity response profiles of collicular neurons: Parallel and convergent visual information channels. *Neuroscience*, 93(3):1063–1076.

Wang, H., Xie, X., Li, X., Chen, B., and Zhou, Y. (2006). Functional degradation of visual cortical cells in aged rats. *Brain Research*, 1122(1):93–98.

Wilke, M., Mueller, K.-M., and Leopold, D. A. (2009). Neural activity in the visual thalamus reflects perceptual suppression. *Proceedings of the National Academy of Sciences*, 106(23):9465–9470.

Wilke, M., Turchi, J., Smith, K., Mishkin, M., and Leopold, D. A. (2010). Pulvinar Inactivation Disrupts Selection of Movement Plans. *Journal of Neuroscience*, 30(25):8650–8659.

Zhang, X., Zhaoping, L., Zhou, T., and Fang, F. (2012). Neural Activities in V1 Create a Bottom-Up Saliency Map. *Neuron*, 73(1):183–192.

Zhou, N., Masterson, S., Damron, J., Guido, W., and Bickford, M. (2017). The mouse pulvinar nucleus links the lateral extrastriate cortex, striatum, and amygdala. *The Journal of Neuroscience*, pages 1279–17.

3. Projections between visual cortex and pulvinar nucleus in the rat

3.1 Abstract

The extrageniculate visual pathway, which carries visual information from the retina through the superficial layers of the superior colliculus and the pulvinar nucleus, is poorly understood. The pulvinar is thought to modulate information flow between cortical areas, and has been implicated in cognitive tasks like directing visually guided actions. In order to better understand the underlying circuitry, we performed retrograde injections of modified rabies virus in the visual cortex and pulvinar of the Long-Evans rat. We found a relatively small population of cells projecting to primary visual cortex (V1), compared to a much larger population projecting to higher visual cortex. Reciprocal corticothalamic projections showed a similar result, implying that pulvinar does not play as big a role in directly modulating V1 activity as previously thought.

3.2 Introduction

Most visual information in primary visual cortex (V1) is delivered from the retina via the lateral geniculate nucleus (LGN; Jones, 1985). However, the extrageniculate visual pathway, which carries information from the retina through the superficial layers of the superior colliculus (SC) and the pulvinar nucleus (Kaas and Huerta, 1988; Stepniewska, 2003; Lyon et al., 2010), also makes major contributions to visual processing, having been implicated

in gating visual cortex activity both in primates (Purushothaman et al., 2012; Zhou et al., 2016) and in rodents (Tohmi et al., 2014; Roth et al., 2015). In comparison to the LGN, less is known about the structure and function of the extrageniculate thalamic nuclei, yet these structures have a big impact on cognition and behavior. Early behavioral studies in primates identified cells in the pulvinar that are enhanced by shifts in gaze (Petersen et al., 1985; Robinson et al., 1986; Bender, 1982), leading many to think the pulvinar is involved in directing spatial attention. Modern theories of pulvinar's role in attention include its driving of salience-based selection (Mizzi & Michael, 2014; Veale et al., 2016), guiding visual actions (Wilke et al., 2010; Zhou et al., 2017), and providing contextual information to visual cortex (Wilke et al., 2009; Roth et al., 2015; Jaramillo et al., 2019). Because of its reciprocal connections with so many visual areas and its behavioral role in both action and object vision, the pulvinar is a likely player in the modulation of information flow to the so-called dorsal and ventral visual streams (Kaas and Lyon, 2007), processing the guidance of action and object recognition, respectively (Goodale, 2005; 2013).

The rat pulvinar, also called the lateral posterior nucleus (LP), consists of three highly-conserved subregions based on cytoarchitecture and connectivity: caudomedial (LPcm), lateral (LPl), and rostromedial (LPrm) pulvinar (Takahashi, 1985; Nakamura et al., 2015; see Figure 3.1). Caudal LP receives input primarily from SC and pretectum (Takahashi, 1985; Mason & Groos, 1981; Shi & Davis, 2001) and sends projections mostly to temporal association cortex and postrhinal cortex (Nakamura et al., 2015; Shi & Davis, 2001), whereas rostral LP receives and sends most of its projections to visual cortex (Takahashi, 1985; Nakamura, 2015; Masterson, 2009; Bourassa & Deschenes, 1995). However, while some projections, such as retrosplenial cortex and amygdala projections from rostral LP have been studied in detail (Kamishina, et al., 2009), a quantitative analysis of rat pulvinar connectivity with visual cortex has not yet been made. The pulvinar nucleus is known to send projections broadly to visual cortex in several other species (Zhou et al., 2017), including mice (Tohmi et al., 2014; Bennett et al., 2019), gray squirrels (Robson and Hall, 1977), carnivores (Hutchins

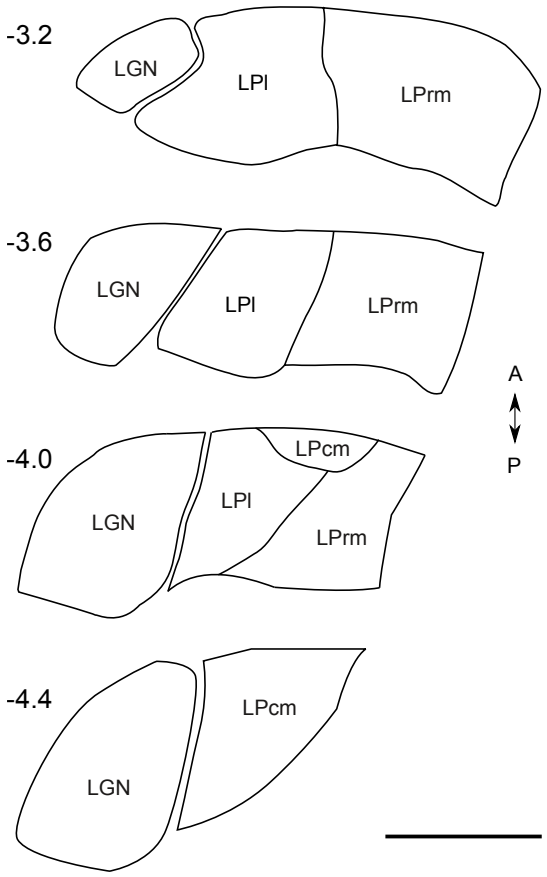

Figure 3.1: Schematic of rat lateral (LPl), rostromedial (LPrm) and caudomedial (LPcm) pulvinar subdivisions and the lateral geniculate nucleus (LGN) between -3.2 and -4.4 mm from bregma. Based on the cytoarchitectonic divisions by Nakamura (2015), conformed to the atlas by Paxinos and Watson (2013).

& Updyke, 1989; Mason, 1978) and primates (Benevento & Rezak, 1976; Asanuma et al., 1985; Adams et al., 2000). Nevertheless, it is difficult to interpret the role of the pulvinar on cortical activity without a more precise understanding of the relative weights of these connections, as well as the details of where in the pulvinar these projections originate.

Of particular interest to us was whether pulvinar in rats projects more to V1 or V2. In rodents, V1 is homologous to primate V1, whereas higher visual cortex is called V2 and is subdivided into areas receiving retinotopically organized input from V1, including medial areas anteromedial (AM) and posteromedial (PM), as well as lateral areas anterolateral (AL) and lateromedial (LM) (Olavarria and Montero, 1984; Glickfeld, et al., 2014). Each of

these areas likely receives some LP input, as has been demonstrated in mouse (Tohmi et al., 2014; Juavinett et al., 2019), but it remains unclear how contributions from pulvinar differ between higher visual cortex and V1. After lesions in mouse SC, higher visual cortex activity becomes more similar to activity in V1, suggesting that only higher visual cortex is affected by pulvinar (Tohmi et al., 2014). Yet mouse LP axon terminals do confer information to V1, as demonstrated by Roth et al. (2015), although it is unclear from how many LP cells these axons originate. To better understand the contributions of the pulvinar to visual cortical cells, a more complete map of its connectivity is needed.

To address these issues, we made injections of glycoprotein-deleted rabies virus in V1 and higher visual cortex, as well as in lateral and rostromedial subdivisions of LP, to retrogradely label projection neurons. In this way, we are able to determine whether or not there are quantitative differences in the thalamocortical and corticothalamic projections between V1 and higher visual cortex with the rat pulvinar.

3.3 Methods

Injections of modified rabies virus were carried out in nine adult female Long-Evans rats in order to retrogradely label connected cells (Foik et al., 2018). All procedures were approved by the University of California, Irvine Institutional Animal Care and Use Committee and the Institutional Biosafety Committee, and followed the guidelines of the National Institutes of Health.

G-deleted rabies viruses (RV; Wickersham et al., 2007) modified with either green fluorescent protein (GFP) or mCherry transgenes (provided by the Callaway laboratory) were amplified and purified as described by Osakada & Callaway (2013). For each virus, BHK cells expressing rabies glycoprotein SADB19G (B7GG, provided by the Callaway laboratory) were

infected with 1 µl of stock virus and maintained at 3% CO_2 and 35°C for 5-6 d in order to produce viral supernatant (Figure 3.2a and 3.2b). The supernatants for each virus were subsequently used to infect five 150 mm dishes of the same cell line in order to amplify the viruses. Supernatants were collected twice during incubation at 3% CO_2 and 35 °C after 6 and 10 days, then passed through a 0.45 µm polyethersulfone filter, and transferred to an ultracentrifuge (rotor SW28, Beckman Coulter) for 2 h at 19,400 g and 4°C. Purified virus was resuspended in phosphate buffered saline (PBS) for 1 h at 4°C before 2% fetal bovine serum was added. Aliquots for injection were stored at -80°C. Titer was assessed by infecting HEK 293T cells (Sigma-Aldrich) with serial dilutions of modified virus, to ensure at least 1×10^9 infectious units ml^{-1} was achieved. Figure 3.2 shows infected B7GG cells prior to amplification and infected 293T cells during titration.

Prior to surgery, rats were initially anesthetized with 2% isoflurane in a mixture of 30% oxygen and 70% nitrous oxide, and maintained with 1 to 1.5% isoflurane in the same mixture. Using a stereotaxic apparatus, a craniotomy was performed to expose the caudal neocortex of one hemisphere. A glass micropipette was cut to approximately 20 µm in diameter, filled with rabies virus suspension, and lowered into the brain using a motorized microdrive to a depth of roughly 800 µm for cortical injections or 4,250 µm for LP injections. Stereotaxic coordinates were used to target each structure: for V1 injections, between -6 and -8 mm from bregma and between 3.75 and 4.25 mm from the midline; for medial V2 injections, -5.5 to -6.5 mm from bregma, 2.25 mm lateral; for lateral V2 injections, -6 to -7 mm from bregma, 5.5 mm lateral; for LPrm injections, -3.75 to -4 from bregma, 1.75 mm lateral; for LPl injections, -3.75 to -4 from bregma, 2.75 mm lateral. Viral suspensions were injected at a rate of approximately 1 µl/ min using an adjustable regulator and pressures below 35 kPa, to a volume of no more than 1.2 µl per injection, as larger injection volumes can cause damage to surrounding tissue. To increase total injection volume, multiple injections were made at nearby depths or nearby sites within the target area in most cases. Total injection volumes, summed across all depths and all sites for each case, are listed in Table 3.1 (M = 3.1µl,

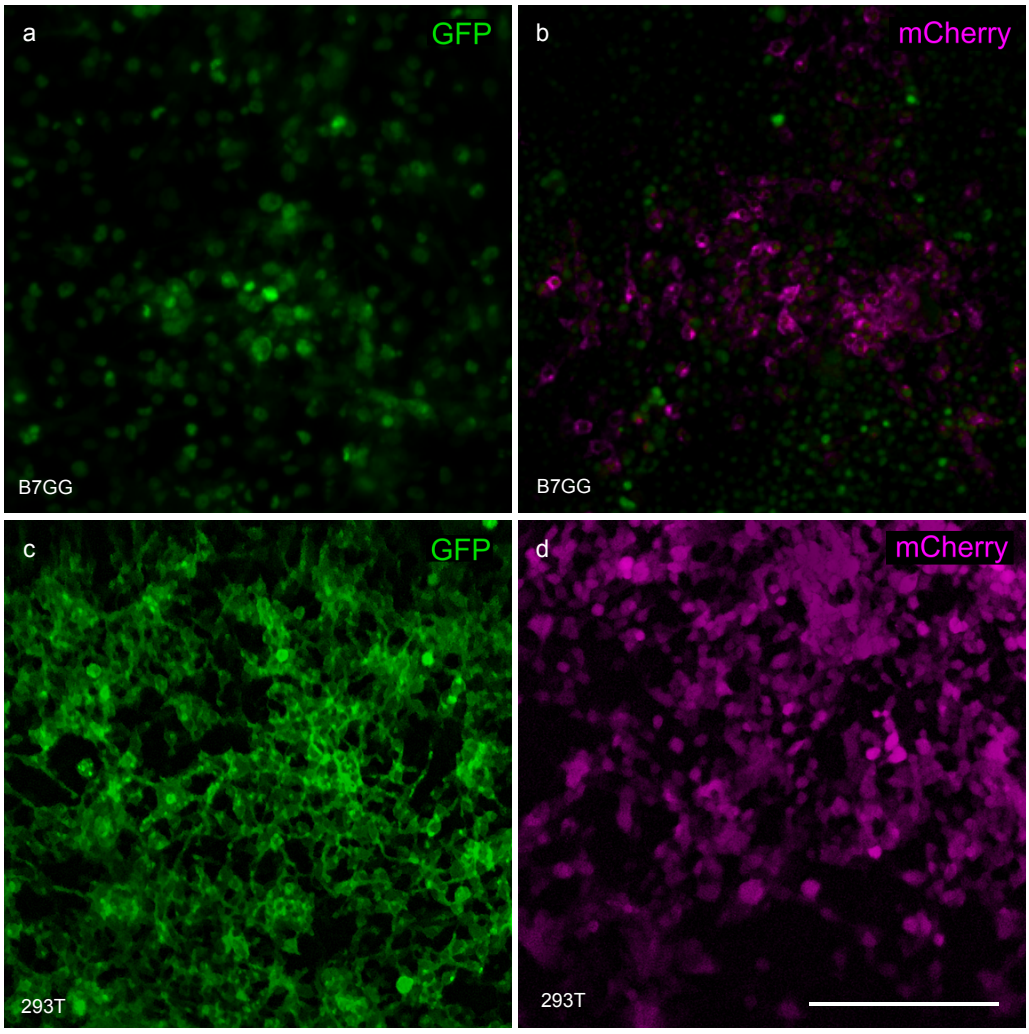

Figure 3.2: Amplification and titration of GFP and mCherry modified rabies viruses. B7GG cells in (a) and (b) express nuclear GFP in addition to the rabies viruses being amplified. 293T cells shown in (c) and (d) were used to verify expression of the viruses without the presence of cellular rabies glycoprotein and to quantify the virus titers. Scale bar equals 250 µm.

Table 3.1: Injection sites and total injection volumes for each case. mCherry and GFP refer to mCherry and GFP modified rabies viruses.

Rat	Virus	Inj site	Injection volume (uL)
R1630	mCherry	AL	1.2
R1703	mCherry	V1	3.6
	GFP	V1	3.6
R1802	mCherry	V1	2.4
	GFP	V1	2.4
R1803	GFP	LM	1.2
R1902	mCherry	AM	4.8
	GFP	PM	4.8
R1903	mCherry	LPrm	3.6
	GFP	LPl	3.6
R1905	mCherry	LPl	1.8
	GFP	LPrm	1.8
R1908	mCherry	LPrm	3.6
	GFP	LPl	3.6
R1909	mCherry	LPl	3.6
	GFP	LPrm	3.6

$SD = 1.1$µl, $n = 16$). Following injections, the skull was sealed with dental cement before closing the scalp with surgical staples and reviving the rat.

Following a 7-14 day survival period, rats were deeply anesthetized with Euthasol and transcardially perfused first with saline, then with 4% paraformaldehyde in PBS. Brains were removed and cryoprotected in 30% sucrose for at least 24 hours, then sectioned coronally on a freezing microtome to 40 µm thickness, mounted on glass microscope slides, and coverslipped using polyvinyl alcohol mounting medium with 1,4-diazabicyclo-octane (PVA-DABCO, prepared in-house).

To assess corticothalamic connectivity, every fourth section was scanned using a fluorescent microscope (Axioplan 2, Zeiss, White Plains, NY) equipped with a 10x objective and motorized stage. Images were captured with a monochromatic low-noise CCD camera (Sensicam qe, PCO AG, Kelheim, Germany) and corrected for lamp misalignment by dividing each pixel by corresponding pixels in a flat field image acquired for each color channel. Corrected

images were stitched using stage coordinates with regions of 10 overlapping pixels between images in which average pixel values were used. False colors were applied to each image before each brain section was counted manually for labeled cells. Neurons were identified based on the presence of the cell soma and dendrites. Fluorescently labeled neurons were then annotated by anatomical brain region based on the rat brain atlas by Paxinos and Watson (2013). Injection sites were identified in histology by tracks left by the glass micropipette (see Figure 3.3b). Image correction and stitching were performed in MATLAB (Mathworks, Natick, MA) using the multisection-imager toolbox (http://github.com/leoscholl/multisection-imager).

Statistical significance was determined based on uncorrected cell counts. P values lower than 0.05 were considered significant for Student's t-tests and two-way ANOVAs. All statistical analyses were carried out in MATLAB.

3.4 Results

To assess the strength and size of input from LP to V1, we made four injections of the retrograde fluorescent-protein-expressing g-deleted rabies virus into V1 of two rats. In each case, substantial thalamic labeling was observed when calculated as a percentage of the total number of labeled neurons in each case ($M = 11\%$, $SD = 6\%$, $n = 4$).

In rat R1703, one large injection was made in anterior V1 (GFP; Figure 3.4a), and a second in posterior V1 (mCherry; Figure 3.4a). The resulting fluorescent labeling included a large number of cortical cells in and around the injection sites. In the thalamus, 30 labeled cells were found in LGN and only seven in LP across the two injections (see Table 3.2). Topographic organization of LGN labeling was observed between the two injection sites, with the posterior V1 injection labeling anterior LGN and vice versa, consistent with previous findings in the rat (Sauve & Gaillard, 2007). No such topography was seen for LP cells in

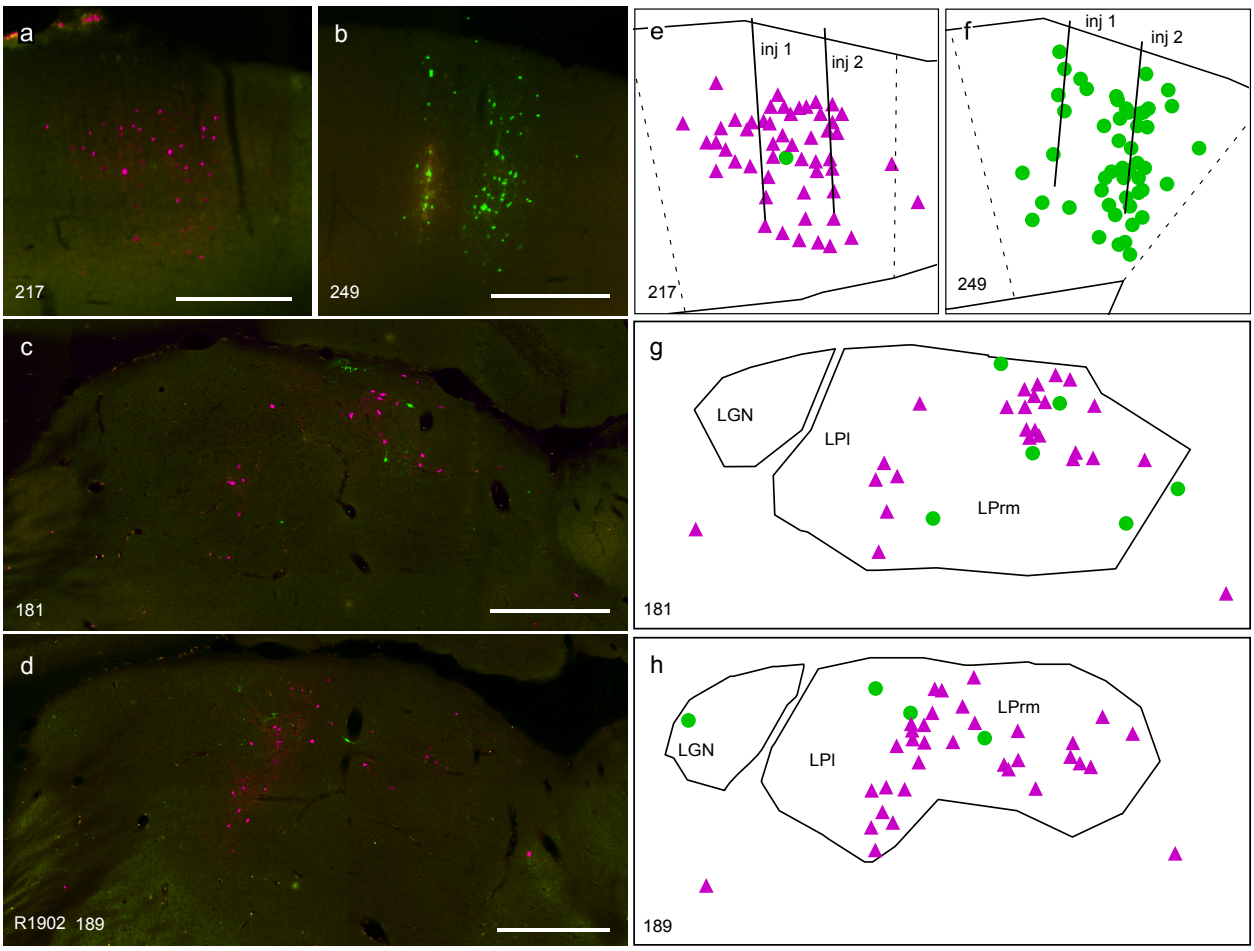

Figure 3.3: Example reconstruction of fluorescent labeling. Representative example showing fluorescently labeled thalamic inputs to anterior and posterior medial V2 areas AM and PM after injections of mCherry (a and e; magenta) and GFP (b and f; green) modified rabies viruses in rat R1902. Thalamic labeling (c-h) reveals a large population of LPl and LPrm projections to V2. False-color stitched fluorescent images are shown in a-d. Reconstructions of the same sections are shown in e-h. Scale bars equal 500 µm.

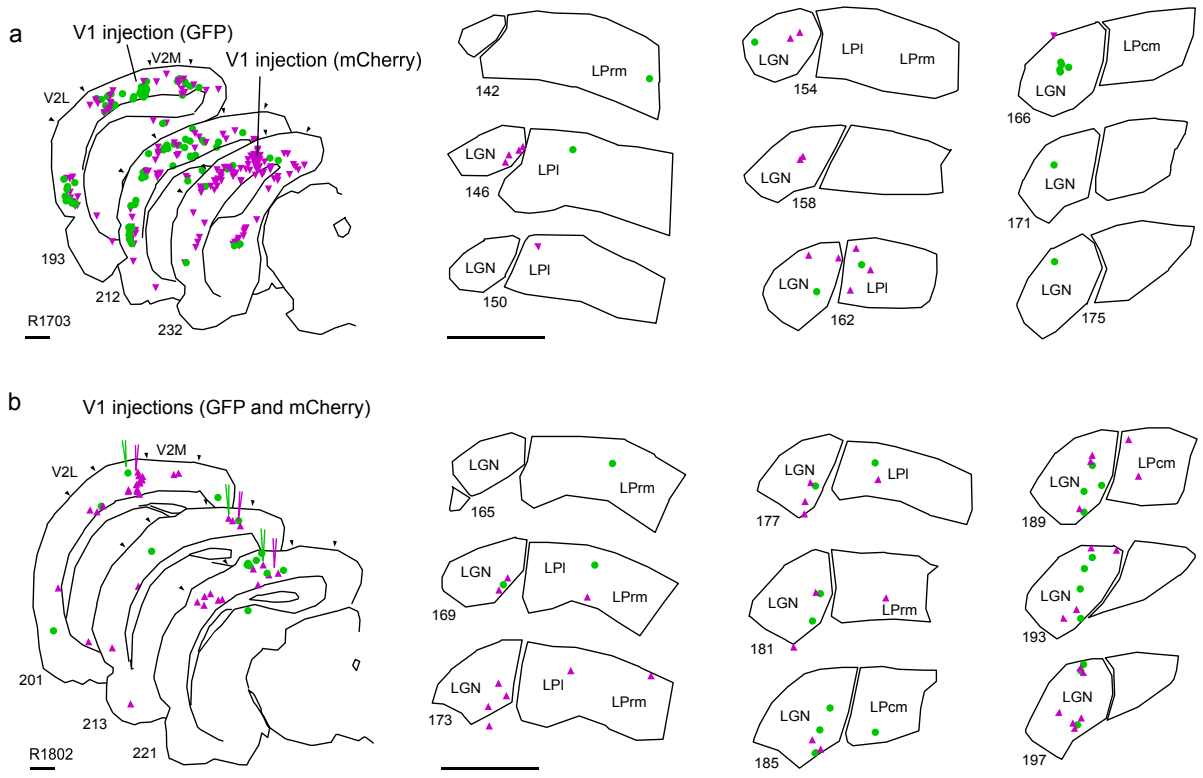

Figure 3.4: Reconstructions of fluorescently labeled neurons identified after retrograde RV injections in V1. In rat R1703 (a), the GFP virus was injected into the anterior portion of V1 and the mCherry virus was injected into posterior V1. In rat R1802 (b), three smaller injections were made along the anterior-posterior axis of V1 for each virus, covering a large portion of V1. In all cases, more labeled neurons were present in LGN than in pulvinar. Magenta triangles indicate mCherry fluorescence, green circles indicate GFP. Scale bars equal 1 mm.

this case, although it has been reported in mice (Roth et al., 2015; Juavinett et al., 2019).

Across the four cases with V1 injections (see Table 3.2), there were significantly fewer inputs from LP to V1 compared to the number of inputs from LGN to V1 ($p = 0.01$, paired samples t-test). Infecting a large area of V1 on the possibility that LP input to V1 is sparse made no difference; there was one fifth as many cells in LP as in LGN in both R1703 and R1802.

In contrast to V1, injections in V2 labeled proportionately fewer neurons in LGN and many more neurons in LP. In rat R1902, the anterior and posterior medial V2 areas, AM and PM, were each injected with rabies virus (Figure 3.5a). The resulting fluorescence in the

Table 3.2: Percent of retrogradely labeled thalamic cells following cortical rabies virus injections.

Rat	Virus	Target	No of cells	LPrm	LPl	LPcm	LGN
R1703	GFP	V1 anterior	16	6	13	0	81
	mCherry	V1 posterior	21	0	19	0	81
R1802	mCherry	V1	34	6	9	6	79
	GFP	V1	26	4	8	4	85
			Mean	**4**	**12**	**2**	**82**
R1630	mCherry	V2L (AL)	19	11	63	11	16
R1803	GFP	V2L (LM)	15	7	53	13	27
R1902	mCherry	V2M (AM)	124	44	54	2	0
	GFP	V2M (PM)	61	41	46	3	10
			Mean	**26**	**54**	**7**	**13**
			Total Mean	**15**	**33**	**5**	**47**

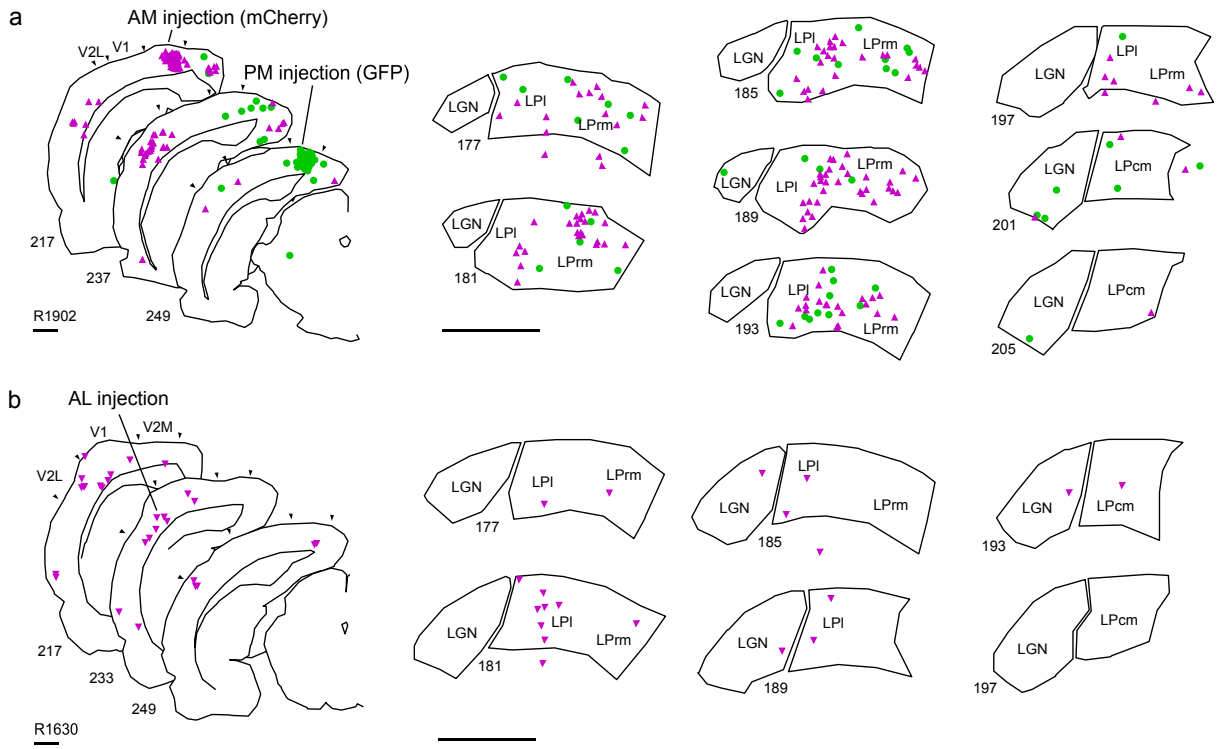

Figure 3.5: Reconstructed fluorescent labeling for rats with injections in V2 areas. Rat R1902 (a) was injected with mCherry virus targeting anteromedial V2 area (AM), and GFP virus targeting the posteromedial V2 area (PM). Labeling in the thalamus was strong in both LPrm and LPl, with only a few labeled cells in the lateral geniculate nucleus (LGN). Rat R1630 (b) was injected with mCherry virus targeting anterolateral V2 (AL), resulting in thalamic labeling mostly in LPl. Magenta triangles indicate mCherry fluorescence, green circles indicate GFP. Scale bars equal 1 mm.

thalamus was primarily located within LP, 179 cells, compared to the LGN, 6 cells, indicating the injections were well contained outside V1. Between LP subdivisions, only four cells were labeled in LPcm, while 95 were labeled in LPl and 80 in LPrm (see Table 3.2 for summary). The cells in LPl and LPrm were not distributed throughout each subdivision, rather they were clustered along the medial margin of LPl and central LPrm (see Figure 3.5a).

Lateral V2 areas AL and LM were targeted with single injections into rats R1630 and R1803, respectively. These injections were three times smaller than the injections in R1902, yet thalamic labeling was also limited primarily to the LP in these cases, as 26 neurons were located in LP and 7 in the LGN. Between LP subdivisions, LPl had the majority of fluorescent

cells in both cases, with 73% of LP cells being found within LPl in R1630 and 80% in R1803 (see Table 3.2).

Across all four cases with V2 injections, there was a significantly higher percentage of cells labeled in LP than in LGN ($p < 0.01$, paired samples t-test; see Table 3.2). Moreover, compared with V1 injections, V2 injections revealed that LP sends significantly more projections to V2 than it does to V1. The number of labeled cells in LP following V2 virus injections was significantly larger than the number following V1 injections ($F(1, 12) = 6.1$, $p = 0.03$, ANOVA). Additionally, medial V2 areas AM and PM were both observed to receive more LP input than lateral V2 areas AL and LM, especially from LPrm. There was also some indication that lateral V2 areas receive less input from medial LP (*n.s.*), however there was no difference between overall input to V2 between the two rostral subdivisions of LP ($F(1, 12) = 0.28$, $p = 0.6$, ANOVA).

Injections of modified rabies virus were also made into LPrm and LPl to retrogradely determine the strength of corticothalamic inputs from V1 and V2 to each pulvinar subdivision. Figure 3.6 illustrates three cases with injections targeting similar stereotaxic coordinates for LPrm and LPl. Rats R1903 (Figure 3.6a) and R1909 (Figure 3.6c) had large injections targeting central LPl and LPrm; rat R1909 (Figure 3.6b) had large injections targeting central LPl but more posterior LPrm; and rat R1905 (Figure 3.7) had small injections into anterior LPl and LPrm (see Table 3.1). Cortical labeling was assessed in each case to determine the relative strength of inputs from V1 and V2 to each rostral LP subdivision. In all cases, V2 labeling accounted for most of the cortical fluorescence. Rat R1903 additionally had significant reticular thalamic nucleus labeling following injection into LPl (Figure 3.6a), which is known to project to the pulvinar and many other neighboring thalamic nuclei (Lyon et al., 2010; Bourassa & Deschenes, 1995; Zikopoulos & Barbas, 2007; Hirsch et al., 2015). Also of note, rat R1909 had significant amygdala labeling following injection into LPrm, but this is perhaps due to leakage of virus into the hippocampus directly dorsal to LP.

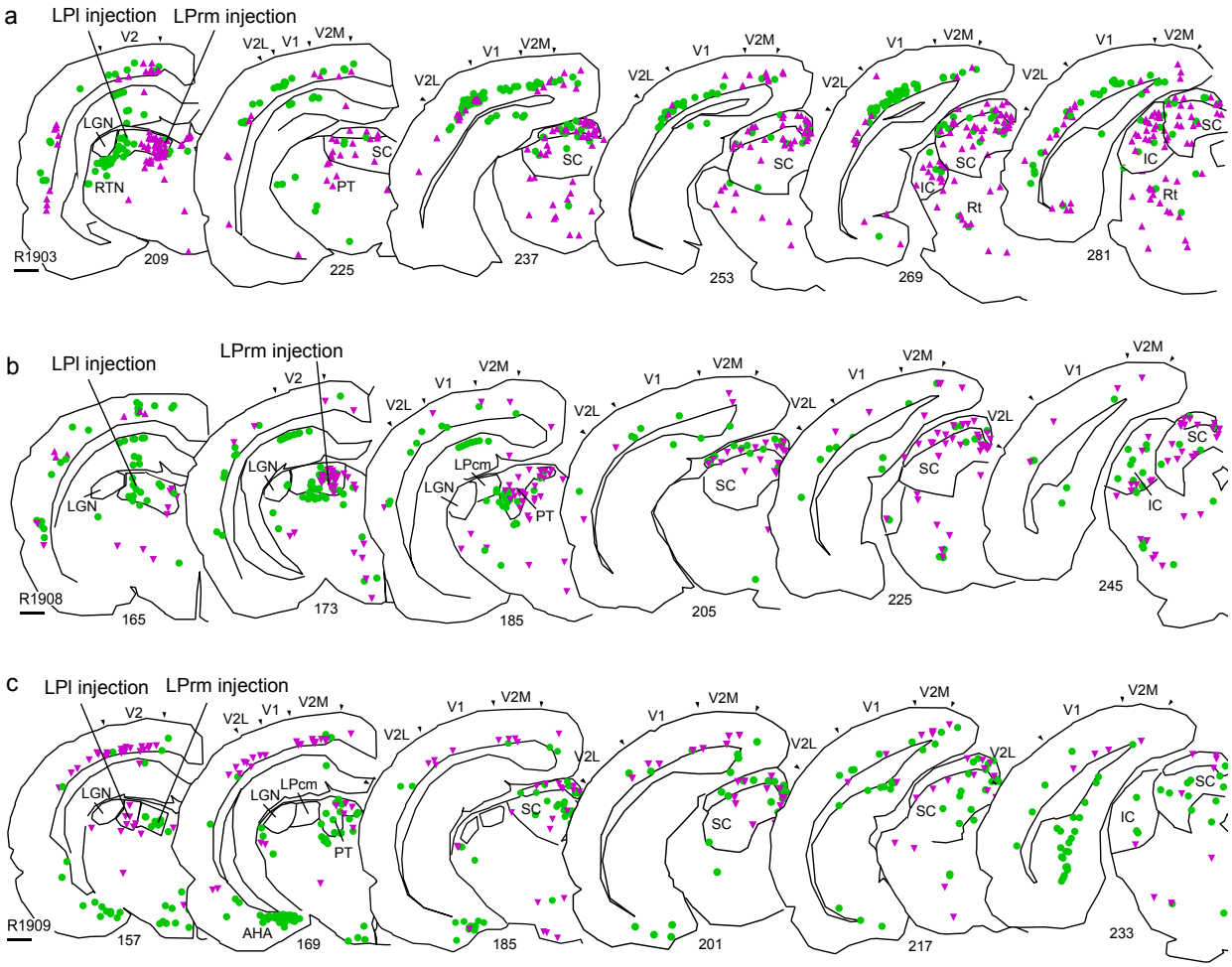

Figure 3.6: Reconstructions of fluorescently labeled neurons identified following rabies injections in LPrm and LPl in three rats. Each LPl injection and each LPrm injection was targeted to the same stereotaxic coordinates and used the same volume, with the exception of rat R1908 (b), where more posterior LPrm was targeted to avoid a blood vessel. The superficial layers of the superior colliculus are demarcated. Magenta triangles indicate mCherry fluorescence, green circles indicate GFP. IC inferior colliculus, RTN reticular thalamic nucleus, PT pretectal nucleus, Rt reticular formation. AHA amygdalohippocampal area. Scale bars equal 1 mm.

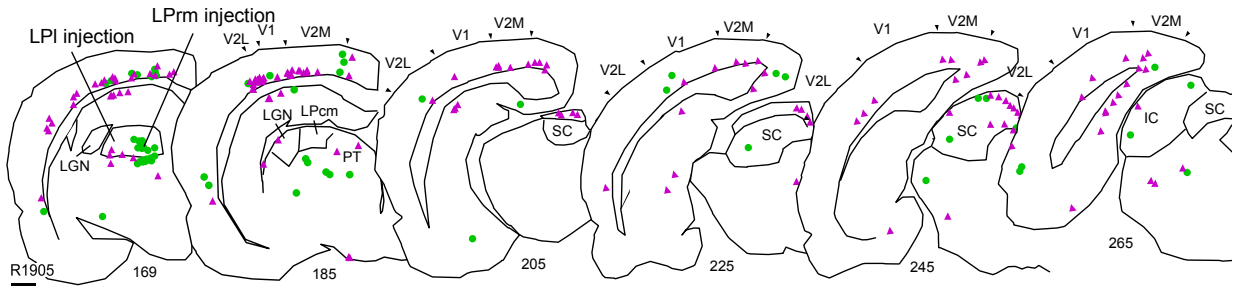

Figure 3.7: Reconstruction of rat R1905, in which retrograde injections were made in the rostral portions of LPl and LPrm. Very little labeling is apparent in pretectum (PT) and superior colliculus (SC) following GFP virus injection into LPrm in this case (green circles). Injection of mCherry virus (magenta triangles) yielded similar results to previous injections. Scale bar equals 1 mm.

Across all eight LP injections, there were a similar number of neurons labeled in SC as in visual cortex ($p = 0.3$, paired samples t-test). Since rostral LP receives most of its input from cortex, and caudal LP receives most of its input from SC (in rats: Mason and Groos, 1980, Takahashi, 1985, Masterson, 2009; in mice: Bennett, et al., 2019, Juavinett et al., 2019), this is a good indication that caudal and rostral LP in this study were infected at similar rates.

A significantly higher number of cells were labeled in V2 areas than in V1 ($F(1, 12) = 5.39$, $p = 0.04$, ANOVA; see Table 3.3). Furthermore, injections in lateral LP led to significantly more labeling in visual cortex than injections in medial LP ($F(1, 12) = 5.35$, $p = 0.04$, ANOVA), implying that rat pulvinar receives differential visual cortical inputs along its medial-lateral axis.

3.5 Discussion

The purpose of this study was to compare the connections of V1 and higher visual cortex with the pulvinar as well as to determine any anatomical differences between lateral and medial pulvinar subdivisions in the rat. We demonstrated that the projections between

Table 3.3: Percent of retrogradely labeled cortical cells following LP injections

Rat	Virus	Target	No of cells	V1	V2	medial V2	lateral V2
R1903	mCherry	LPrm	159	14	86	34	52
R1905	GFP	LPrm anterior	35	17	83	77	6
R1908	mCherry	LPrm	76	30	70	30	39
R1909	GFP	LPrm	74	31	69	30	39
			Mean	**23**	**77**	**43**	**34**
R1903	GFP	LPl	425	32	68	21	47
R1905	mCherry	LPl anterior	231	25	75	46	29
R1908	GFP	LPl	109	28	72	18	54
R1909	mCherry	LPl	131	35	65	37	28
			Mean	**30**	**70**	**31**	**40**
			Total Mean	**26**	**74**	**37**	**37**

pulvinar and V2 in rats are more frequent than those between pulvinar and V1, suggesting that the pulvinar has a greater influence on activity in higher visual cortex than in V1. We also observed differences in the number of inputs and outputs of LP subdivisions, with the lateral portion of the pulvinar having a stronger connection to visual cortex, for both V2 and V1. Together, these results provide a basis for understanding to which visual networks the rat pulvinar contributes.

In previous studies of the pulvinar, projections have been identified to both V1 and higher visual cortices, but no attempt to quantify these cells has been made. However, evidence consistent with our findings does exist. In rats, anterograde injections in LP labeled both V1 and V2, but V1 labeling was much more sparse, with many more fibers being labeled in both medial and lateral V2 (Nakamura et al., 2015, see their Figure 7). In mouse, retrograde injections in V1 produced fluorescent labeling that was confined to small regions within LP, whereas injections in other visual cortical areas led to larger and brighter patches of fluorescent labeling (Juavinett et al., 2019, see their Figure 4). Although qualitative, these previous findings are consistent with the difference in projection strength we observed in the present study.

In other species, there is also a trend in the existing literature of denser and more numerous projections from pulvinar to higher visual cortex compared to projections from pulvinar to V1. In squirrels, a highly visual rodent, dense pulvinar labeling was observed following retrograde tracer injections into the temporal posterior area and visual area 19, but very few cells were labeled following V1 (area 17) injection (Robson & Hall, 1977, see their Figures 15-17). Tree shrew, a close primate relative, exhibits a similar pattern of connectivity following retrograde tracer injections in V1 and V2; only sparse, topographic labeling was observed in caudal pulvinar following V1 injection, whereas V2 injection was followed by denser labeling spread across large regions of caudal and ventral pulvinar (Lyon et al., 2003, see their Figure 2). Similarly, in monkeys, retrograde injections in V1 of macaque labeled very few cells in

pulvinar compared to injections in V2 in marmoset (Kaas & Lyon, 2007, see their Figures 6-7). Although this pattern seems to have gone largely unnoticed, it is present in all of the anatomical literature we have come across.

Given that several high profile studies have found significant functional effects of pulvinar on V1 in other species (Purushothaman, et al., 2012, Roth et al., 2015, Sun et al., 2016), it is tempting to assume that there must be a significant population of pulvinar neurons projecting directly to V1 in these animal models. However, our results indicate that higher visual cortex receives significantly more input from the pulvinar than does V1, thus pulvinar would likely have a bigger impact on visual responses there, and the gating of V1 responses by pulvinar could be explained by indirect modulation via higher visual cortex. This view is consistent with the results of Tohmi et al. (2014), who showed higher visual areas in mice behave more like V1 when the extrageniculate pathway is damaged by superior colliculus lesions. In addition, Zhou et al. (2016) found that deactivation of the ventrolateral pulvinar in monkeys led to inactivity in V4, without evidence for change in V1 activity, implying a direct influence of pulvinar on V4. Nevertheless, as we and others do observe some pulvinar projections to V1, direct effects on V1 are not out of the question.

In primates, the pulvinar is divided by its connectivity with cortical areas into a dorsal-ventral stream classification for visually guided actions and object vision, respectively. The posterior and caudomedial inferior pulvinar (PIp and PIcm) as well as the medial inferior pulvinar (PIm) are associated with the dorsal stream because they project to dorsal stream areas such as the middle temporal visual area (MT), whereas the caudolateral inferior (PIcl) portion and lateral (PL) portions of the pulvinar are associated with the ventral stream because of their projections to early visual areas and inferior temporal cortex (Kaas and Lyon, 2007). As illustrated in Figure 3.8, SC and visual cortex input to pulvinar is highly conserved across species, with regions of dense bilateral input from SC, ipsilateral input from SC, and cortical input only. These include rat (Takahashi, 1985; Mason & Groos, 1980),

mouse (Zhou et al., 2017), gray squirrel (Baldwin et al., 2011), tree shrew (Lyon et al., 2003), and primate (Baldwin et al., 2013). Given that they share anatomical features with primates, rodents might be a suitable model animal for studying pulvinar contributions to the two visual streams, as there is growing evidence for such a classification in rodents (see Figure 3.9; Wang et al., 2011; Glickfeld, 2014; Nishio et al., 2018). However, previous studies have shown that tectorecipient LPcm in rats sends most of its projections to ventral stream areas such as postrhinal cortex (POR) and temporal association cortex (Nakamura et al., 2015), and our results show that LPrm and LPl are well connected with dorsal stream areas AM and PM, opposite to the pattern of tecto- and striate-recipient zones of the pulvinar in monkeys. In mice, however, LPrm was observed to receive significant input from POR, and LPl significant input from LM (Juavinett et al., 2019), so the distinctions may not be so clear cut.

In monkeys, disruption of the dorsolateral pulvinar has been shown to cause deficits to spatial attention (Wilke et al., 2010). It is unclear which pathways the pulvinar influences, and whether it generates salience-based signals or receives top-down influence from other cortical areas. If pulvinar is responsible for modulating cortex based on salience cues, it seems unlikely that these salience maps would follow the hierarchy of visual areas as suggested by Zhang et al. (2012), since pulvinar is only weakly connected to V1. Instead, V1 salience maps might derive from LGN, while pulvinar modulates higher-level features such as motion or texture in other cortical areas (Schiller, 1993; Saalmann et al., 2012; Perry & Fallah, 2014). If, on the other hand, pulvinar receives attention signals from higher visual cortex, such as by V4 as demonstrated by Zhou et al. (2016), then reciprocal connections with these areas, but not V1, would be sufficient. Further research will be needed to evaluate pulvinar's functional role in attention.

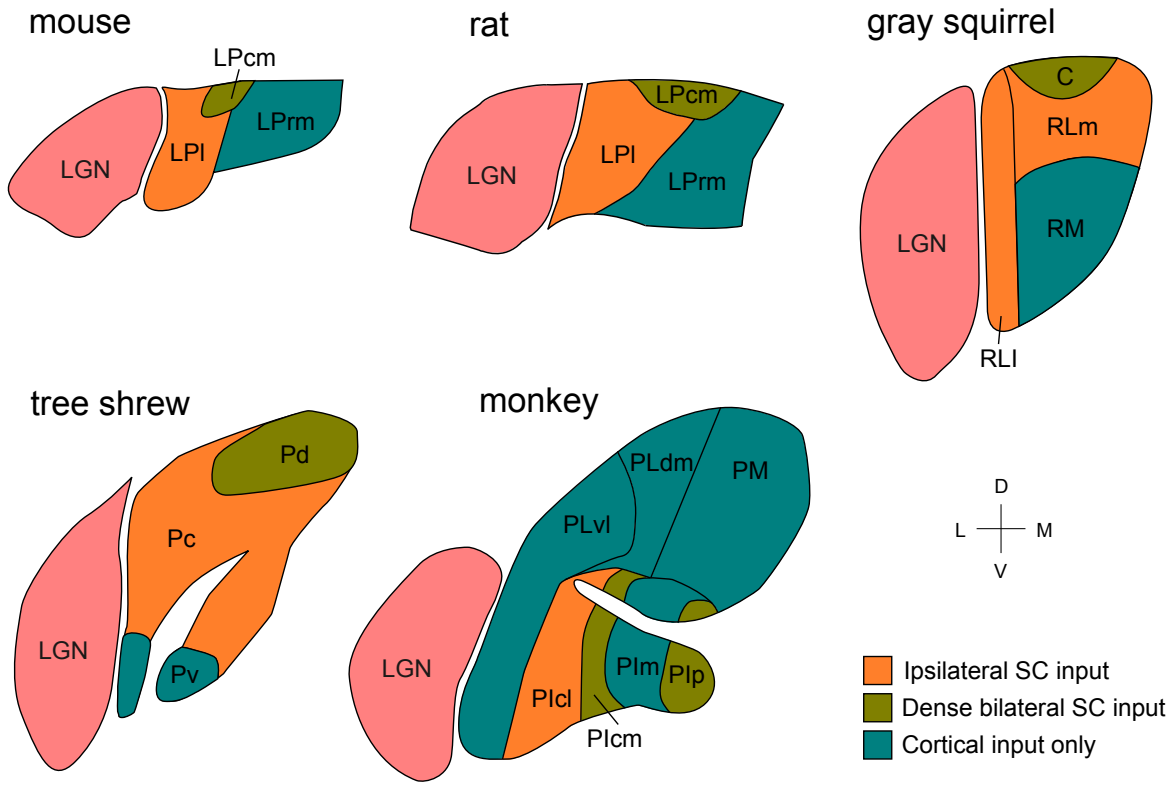

Figure 3.8: Conserved pulvinar input scheme from SC and visual cortex across species. Schematic diagrams of the pulvinar in mouse, rat, gray squirrel, tree shrew, and monkey are shown. Areas with dense bilateral input from SC are shown in green, areas with ipsilateral SC input are shown in orange, and cortical recipient areas are shown in blue. Adapted from Lyon et al. (2003) and Zhou et al. (2017).

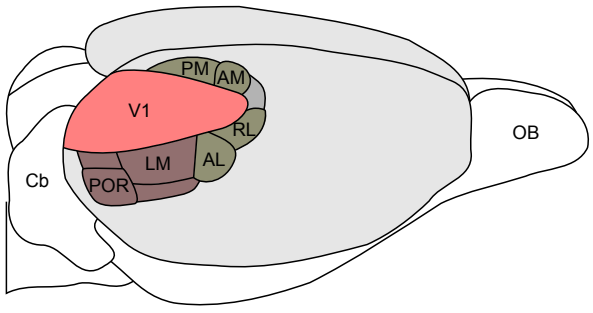

Figure 3.9: Summary of dorsal and ventral stream areas in the visual cortex of the rat. Modified from Sereno et al. (1991) based on Espinoza et al (1983), Glickfeld et al. (2014), and Wang et al. (2007). Cb cerebellum, OB olfactory bulb.

3.6 References

Adams, M. M., Hof, P. R., Gattass, R., Webster, M. J., and Ungerleider, L. G. (2000). Visual cortical projections and chemoarchitecture of macaque monkey pulvinar. *The Journal of Comparative Neurology*, 419(3):377–393.

Asanuma, C., Andersen, R. A., and Cowan, W. M. (1985). The thalamic relations of the caudal inferior parietal lobule and the lateral prefrontal cortex in monkeys: Divergent cortical projections from cell clusters in the medial pulvinar nucleus. *Journal of Comparative Neurology*, 241(3):357–381.

Baldwin, M. K. L., Balaram, P., and Kaas, J. H. (2013). Projections of the superior colliculus to the pulvinar in prosimian galagos (Otolemur garnettii) and VGLUT2 staining of the visual pulvinar. *Journal of Comparative Neurology*, 521(7):1664–1682.

Baldwin, M. K. L., Wong, P., Reed, J. L., and Kaas, J. H. (2011). Superior colliculus connections with visual thalamus in gray squirrels (Sciurus carolinensis): Evidence for four subdivisions within the pulvinar complex. *Journal of Comparative Neurology*, 519(6):1071–1094.

Bender, D. B. (1982). Receptive-field properties of neurons in the macaque inferior pulvinar. *Journal of Neurophysiology*, 48(1):1–17.

Benevento, L. a. and Rezak, M. (1976). The cortical projections of the inferior pulvinar and adjacent lateral pulvinar in the rhesus monkey (Macaca mulatta): an autoradiographic study. *Brain Research*, 108(1):1–24.

Bennett, C., Gale, S. D., Garrett, M. E., Newton, M. L., Callaway, E. M., Murphy, G. J., and Olsen, S. R. (2019). Higher-Order Thalamic Circuits Channel Parallel Streams of Visual Information in Mice. *Neuron*, pages 1–16.

Bourassa, J. and Deschenes, M. (1995). Corticothalamic projections from the primary visual cortex in rats: a single fiber study using biocytin as an anterograde tracer. *Neuroscience*, 66(2):253–263.

Brainard, D. H. (1997). The Psychophysics Toolbox. *Spatial Vision*.

Espinoza, S. G. and Thomas, H. C. (1983). Retinotopic organization of striate and extrastriate visual cortex in the hooded rat. *Brain Research*, 272(1):137–144.

Glickfeld, L. L., Reid, R. C., and Andermann, M. L. (2014). A mouse model of higher visual cortical function. *Current Opinion in Neurobiology*, 24(1):28–33.

Goodale, M. A. (2005). Action insight: The role of the dorsal stream in the perception of grasping.

Goodale, M. A. (2013). Separate visual systems for perception and action: a framework for understanding cortical visual impairment. *Developmental Medicine & Child Neurology*.

Hirsch, J. A., Wang, X., Sommer, F. T., and Martinez, L. M. (2015). How Inhibitory Circuits in the Thalamus Serve Vision. *Annual Review of Neuroscience*, 38(1):309–329.

Hutchins, B. and Updyke, B. V. (1989). Retinotopic organization within the lateral posterior complex of the cat. *Journal of Comparative Neurology*, 285(3):350–398.

Jaramillo, J., Mejias, J. F., and Wang, X. J. (2019). Engagement of Pulvino-cortical Feedforward and Feedback Pathways in Cognitive Computations. *Neuron*, 101(2):321–336.e9.

Juavinett, A. L., Kim, E. J., Collins, H. C., and Callaway, E. M. (2019). A systematic topographical relationship between mouse lateral posterior thalamic neurons and their visual cortical projection targets. *Journal of Comparative Neurology*, (July):cne.24737.

Kaas, J. H. and Lyon, D. C. (2007). Pulvinar contributions to the dorsal and ventral streams of visual processing in primates. *Brain Research Reviews*, 55(2 SPEC. ISS.):285–296.

Kamishina, H., Conte, W. L., Patel, S. S., Tai, R. J., Corwin, J. V., and Reep, R. L. (2009). Cortical connections of the rat lateral posterior thalamic nucleus. *Brain Research*, 1264:39–56.

Kleiner, M., Brainard, D. H., Pelli, D. G., Broussard, C., Wolf, T., and Niehorster, D. (2007). What's new in Psychtoolbox-3? *Perception*.

Lean, G. A., Liu, Y.-J., and Lyon, D. C. (2019). Cell type specific tracing of the subcortical input to primary visual cortex from the basal forebrain. *Journal of Comparative Neurology*, 527(3):589–599.

Lyon, D. C., Jain, N., and Kaas, J. H. (2003). The visual pulvinar in tree shrews II. Projections of four nuclei to areas of visual cortex. *The Journal of Comparative Neurology*, 467(4):607–627.

Lyon, D. C., Nassi, J. J., and Callaway, E. M. (2010). A Disynaptic Relay from Superior Colliculus to Dorsal Stream Visual Cortex in Macaque Monkey. *Neuron*.

Mason, R. (1978). Functional organization in the cat's pulvinar complex. *Experimental Brain Research*, 31(1):51–66.

Mason, R. and Groos, G. A. (1981). Cortico-recipient and tecto-recipient visual zones in the rat's lateral posterior (pulvinar) nucleus: An anatomical study. *Neuroscience Letters*, 25(2):107–112.

Masterson, S. P., Li, J., and Bickford, M. E. (2009). Synaptic organization of the tectorecipient zone of the rat lateral posterior nucleus. *Journal of Comparative Neurology*, 515(6):647–663.

Mizzi, R. and Michael, G. a. (2014). The role of the collicular pathway in the salience-based progression of visual attention. *Behavioural Brain Research*, 270:330–338.

Nakamura, H., Hioki, H., Furuta, T., and Kaneko, T. (2015). Different cortical projections from three subdivisions of the rat lateral posterior thalamic nucleus: A single-neuron tracing study with viral vectors. *European Journal of Neuroscience*, 41(10):1294–1310.

Nishio, N., Tsukano, H., Hishida, R., Abe, M., Nakai, J., Kawamura, M., Aiba, A., Sakimura, K., and Shibuki, K. (2018). Higher visual responses in the temporal cortex of mice. *Scientific Reports*, 8(1):1–12.

Olavarria, J. and Montero, V. M. (1984). Relation of callosal and striate-extrastriate cortical connections in the rat: Morphological definition of extrastriate visual areas. *Experimental Brain Research*, 54(2):240–252.

Osakada, F. and Callaway, E. E. M. (2013). Design and generation of recombinant rabies virus vectors. *Nature protocols*, 8(8):1583–1601.

Paxinos, G. and Watson, C. (2013). The rat brain in stereotaxic coordinates. *London: Academic press*.

Pelli, D. G. (1997). The VideoToolbox software for visual psychophysics: Transforming numbers into movies. *Spatial Vision*.

Perry, C. J. and Fallah, M. (2014). Feature integration and object representations along the dorsal stream visual hierarchy. *Frontiers in Computational Neuroscience*, 8(August):1–17.

Petersen, S. E., Robinson, D. L., and Keys, W. (1985). Pulvinar nuclei of the behaving rhesus monkey: Visual responses and their modulation. *Journal of Neurophysiology*, 54(4):867–886.

Purushothaman, G., Marion, R., Li, K., and Casagrande, V. a. (2012). Gating and control of primary visual cortex by pulvinar. *Nature neuroscience*, 15(6):905–12.

Robinson, D. L., Petersen, S. E., and Keys, W. (1986). Saccade-related and visual activities in the pulvinar nuclei of the behaving rhesus monkey. *Experimental brain research. Experimentelle Hirnforschung. Experimentation cerebrale*, 62(3):625–634.

Robson, J. A. and Hall, W. C. (1977). The organization of the pulvinar in the grey squirrel (Sciurus carolinensis). I. Cytoarchitecture and connections. *Journal of Comparative Neurology*, 173(2):355–388.

Roth, M. M., Dahmen, J. C., Muir, D. R., Imhof, F., Martini, F. J., and Hofer, S. B. (2015). Thalamic nuclei convey diverse contextual information to layer 1 of visual cortex. *Nature Neuroscience*, 19(2):299–307.

Saalmann, Y. B., Pinsk, M. a., Wang, L., Li, X., and Kastner, S. (2012). The Pulvinar Regulates Information Transmission Between Cortical Areas Based on Attention Demands. *Science*, 337(6095):753–756.

Schiller, P. H. (1993). The effects of V4 and middle temporal (MT) area lesions on visual performance in the rhesus monkey. *Visual Neuroscience*.

Sereno, M. I. and Allman, J. M. (1991). Cortical visual areas in mammals.

Shi, C. and Davis, M. (2001). Visual Pathways Involved in Fear Conditioning Measured with Fear-Potentiated Startle: Behavioral and Anatomic Studies. *The Journal of Neuroscience*, 21(24):9844–9855.

Sun, W., Tan, Z., Mensh, B. D., and Ji, N. (2016). Thalamus provides layer 4 of primary visual cortex with orientation- and direction-tuned inputs. *Nature Neuroscience*, 19(2):308–315.

Takahashi, T. (1985). The organization of the lateral thalamus of the hooded rat. *The Journal of comparative neurology*, 231(3):281–309.

Tohmi, M., Meguro, R., Tsukano, H., Hishida, R., and Shibuki, K. (2014). The extrageniculate visual pathway generates distinct response properties in the higher visual areas of mice. *Current biology : CB*, 24(6):587–97.

Veale, R., Hafed, Z. M., and Yoshida, M. (2017). How is visual salience computed in the brain? Insights from behaviour, neurobiology and modeling. *Philosophical Transactions of the Royal Society B: Biological Sciences*, 372(1714).

Wang, Q. and Burkhalter, A. (2007). Area map of mouse visual cortex. *The Journal of Comparative Neurology*, 502(3):339–357.

Wang, Q., Gao, E., and Burkhalter, A. (2011). Gateways of ventral and dorsal streams in mouse visual cortex. *Journal of Neuroscience*, 31(5):1905–1918.

Wickersham, I. R. I., Lyon, D. C. D., Barnard, R. J. R., Mori, T., Finke, S., Conzelmann, K. K., Young, J. A., and Callaway, E. M. (2007). Monosynaptic restriction of transsynaptic tracing from single, genetically targeted neurons. *Neuron*, 53(5):639–647.

Wilke, M., Mueller, K.-M., and Leopold, D. A. (2009). Neural activity in the visual thalamus reflects perceptual suppression. *Proceedings of the National Academy of Sciences*, 106(23):9465–9470.

Wilke, M., Turchi, J., Smith, K., Mishkin, M., and Leopold, D. A. (2010). Pulvinar Inactivation Disrupts Selection of Movement Plans. *Journal of Neuroscience*, 30(25):8650–8659.

Zhang, X., Zhaoping, L., Zhou, T., and Fang, F. (2012). Neural Activities in V1 Create a Bottom-Up Saliency Map. *Neuron*, 73(1):183–192.

Zhou, H., Schafer, R. J., and Desimone, R. (2016). Pulvinar-Cortex Interactions in Vision and Attention. *Neuron*, 89(1):209–220.

Zhou, N., Masterson, S., Damron, J., Guido, W., and Bickford, M. (2017a). The mouse pulvinar nucleus links the lateral extrastriate cortex, striatum, and amygdala. *The Journal of Neuroscience*, pages 1279–17.

Zhou, N. A., Maire, P. S., Masterson, S. P., and Bickford, M. E. (2017b). The mouse pulvinar nucleus: Organization of the tectorecipient zones.

Zikopoulos, B. and Barbas, H. (2007). Circuits for multisensory integration and attentional modulation through the prefrontal cortex and the thalamic reticular nucleus in primates. *Reviews in the neurosciences*, 18(6):417–38.

4. Thalamocortical modulation identified *in vivo* using new rabies virus variant for bi-directional optical control

4.1 Abstract

Optogenetic tools have become of great utility in the causal analysis of systems in the brain. However, current optogenetic techniques do not reliably support both excitation and suppression of the same cells *in vivo*, limiting analysis and slowing research. Here we developed a novel glycoprotein-deleted rabies virus expressing two channelrhodopsin proteins in order to independently manipulate excitatory and inhibitory transmembrane potentials. Using this approach, we demonstrated that rodent pulvinar neurons modulate cortical size tuning and suppress flash responses, but don't drive activity in visual cortex. While our goal was primarily to develop this novel method to study the structure-function organization of thalamocortical circuits, this technique is readily applicable to study any brain region.

4.2 Introduction

Manipulating neural activity is a highly effective way to deduce the role of complex cortical networks on sensory perception and behavior. More crude methods of ablation and lesion

have given way to small molecule receptor agonists and electrical microstimulation, and, more recently, to optogenetic proteins that are reversible, do not interfere with the normal physiology of cells, and can quickly and efficiently raise or lower membrane potentials (Deisseroth, 2011; Yizhar et al. 2011; Bernstein et al. 2012; Prigge et al. 2012). These recent optogenetic methods can reach high spatial and temporal resolutions making it possible to dissect cortical network connections and related functions on a fine scale (e.g., Adesnik et al. 2012; Lee et al. 2012; Olsen et al. 2012; Wilson et al. 2012; Xue et al. 2014). Even so, light-sensitive proteins only allow either anions or cations to flow across the neuronal membrane, inducing either depolarization or hyperpolarization, but not both. Introducing a single activating or inhibiting opsin does not provide absolute control over cell activity, making it impossible to drive or suppress downstream activity in all situations due to complex excitatory and inhibitory network structures. In addition, continuous excitation or inhibition can lead to adaptation and reduced efficacy (Lignani et al., 2013), and is impractical over the long-term because the balance between excitation and inhibition that is important for network dynamics (van Vreeswijk & Sompolinsky, 1996) is altered.

One system where these issues are apparent are the projections between the thalamus, in particular the pulvinar, and visual cortex. The pulvinar nucleus, called the lateral posterior nucleus (LP) in rodents, is known to have influence over activity in visual cortex (Saalmann et al., 2012; Tohmi et al., 2014; Zhou et al., 2016), but not much is known about what information is being transmitted (Roth et al., 2015; Zhou et al., 2017). The pulvinar receives diverse input (see Figure 4.1), ranging from attention signals from frontal cortex (Romanski et al., 1997; Wilke et al., 2009) to input from multiple sensory cortical areas (Kaas & Lyon, 2007; Kamishina et al., 2009; Juavinett et al., 2019) and superior colliculus (Benevento & Standage, 1983; Takahashi, 1985; Nakamura et al., 2015), to projections from melanopsin-containing retinal ganglion cells (Allen et al., 2016). It is unlikely that a nucleus with such diverse inputs has only one function, or that neurons in the pulvinar all have similar responses to the same stimulus. This makes it difficult to know in advance whether

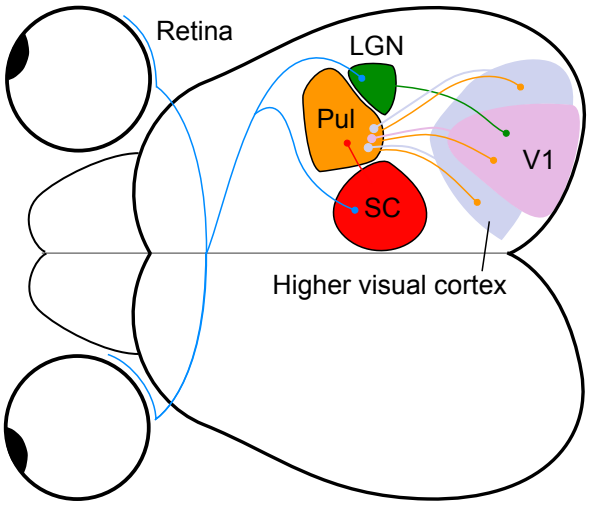

Figure 4.1: Rodent visual system overview. Retinal ganglion cells project to the lateral geniculate nucleus (LGN) and the superior colliculus (SC). Most of the pulvinar (Pul) receives driving input from cortex, including primary (V1) and higher visual cortex, but the caudal part also receives input from SC. Projections from the pulvinar mainly target higher visual cortex, with more sparse connections to V1. Not to scale.

activation or inactivation (or both) of pulvinar neurons will have an effect on cortical systems. Furthermore, projections from the thalamus can target both excitatory and inhibitory subnetworks (Bruno & Sakmann, 2006; Cruikshank et al., 2007), so although thalamocortical projections are typically excitatory in nature (Reid & Alonso, 1995; Gil et al., 1999), the same population of pulvinar cells might have a facilitating drive over one cortical system but an inhibitory drive over another.

Here we introduce a method to retrogradely deliver a pair of independently activated light-gated ion channels with selectivity for positively and negatively charged ions. With this new tool, we probe the inputs to visual cortex from the pulvinar to ask what modulatory effect pulvinar has on visually evoked responses in cortex. Since we can perform both activation and inactivation of projection neurons, we effectively cut experiment times in half, and increase statistical power by studying a single population. We also demonstrate the effectiveness of the virus by recording local cortical activity in response to multi wavelength laser activation.

4.3 Virus design

In order to independently excite and inhibit neurons, we selected two channelrhodopsin proteins with compatible spectral and electrochemical characteristics. These are Chrimson, a fast red-shifted channelrhodopsin variant (Klapoetke et al., 2014; Oda et al., 2018) and GtACR2, a blue-shifted mutant from a class of anion-channelrhodopsins (Govorunova et al., 2015). It has been demonstrated previously that Chrimson effectively induces cation flow and elicits neural spiking activity, while GtACR2 selectively passes anions and suppresses neural spiking. The combined absorption spectra allows a yellow colored laser around 630 nm to exclusively activate Chrimson but not GtACR2, and a blue colored laser around 450 nm to activate GtACR2, with only residual activation of Chrimson (Figure 4.2). Critically, this residual activation is overcome by the higher sensitivity of GtACR2 compared to Chrimson, such that with suitable laser power, GtACR2-driven anion flow should dominate. This design is superior to any utilizing light-driven anion pumps, such as halorhodopsin (Halo), due to the millisecond timescale of both channelrhodopsins, and offers greater spectral separation than other approaches, such as between ChR2 and Halo (see Figure 4.2; Han & Boyden, 2007; Zhang et al., 2007).

In order to visualize traced neurons *in vivo* or in histological slides, a fluorescent protein compatible with the two channelrhodopsins' absorption spectrums is needed. We employed the fluorescent protein mScarlet (Bindels et al. 2016); this reporter is suitable not only because of its near-infrared emission spectrum, giving the added benefit of having deep tissue penetration for *in vivo* imaging, but also because it is by far the brightest red fluorescent protein reported (Bindels et al., 2016). Moreover, the excitation spectrum of mScarlet avoids both laser wavelengths selected to activate Chimson and GtACR2, preventing any unwanted fluorescence during optogenetic manipulation (Figure 4.2).

To package the effector genes we used glycoprotein-deleted rabies virus (RVdG), which offers

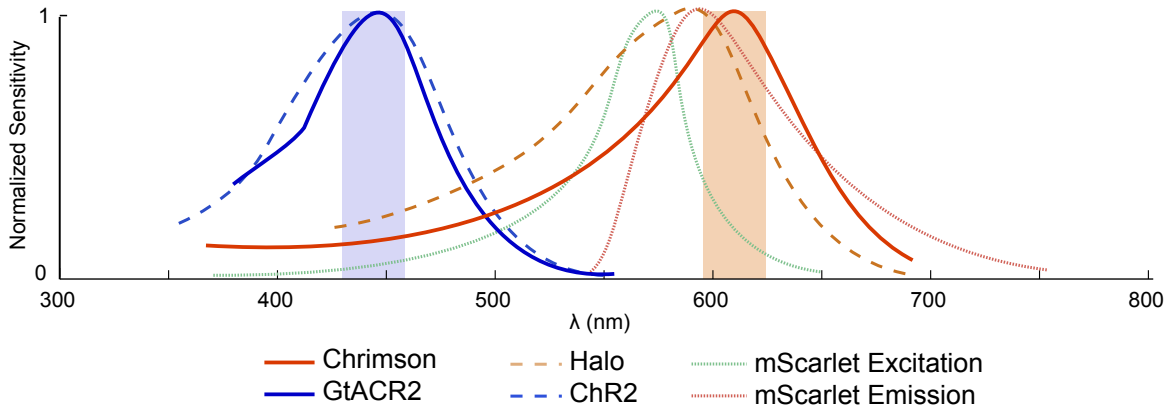

Figure 4.2: Combined spectra. Excitation spectra for Chrimson (solid orange; adapted from Klapoetke et al., 2014) and GtACR2 (solid blue; adapted from Govorunova et al., 2015). Halorhodopsin (Halo; dotted orange) and Channelrhodopsin-2 (ChR2; dotted blue) are included for reference (Adapted from Han & Boyden, 2007), as are the excitation and emission spectra for the fluorescent protein mScarlet (dotted green and red lines; adapted from Bindels et al., 2016). The overlap between GtACR2 and Chrimson excitation spectra is similar to the Halo-ChR2 overlap, which Han & Boyden (2007) have shown to work independently in the same cell.

several advantages over other methods of gene delivery (Figure 4.3; Wickersham et al. 2007a; Osakada et al. 2011). When enveloped with rabies glycoprotein or optimized glycoprotein (oG; Kim et al. 2016), RVdG is able to retrogradely trace and deliver genes to the cell body of all pre-synaptically connected neurons, revealing the projections of one brain area to another (e.g., Connolly et al. 2012; Negwer et al. 2017; Foik et al. 2018). In addition, a major benefit of using rabies virus to package channelrhodopsin genes is the ability to pseudotype the virus (Wickersham et al. 2007b) to target specific protein receptors delivered transgenically, via helper viruses, and through single cell electroporation (Marshel et al. 2010; Wall et al. 2010; Miyamichi et al. 2011; Rancz et al. 2011; Kim et al. 2015; Callaway and Luo, 2015; Wertz et al. 2015; Wall et al., 2016). For example, recently we developed a suite of helper viruses designed to transduce avian tumor virus receptor A (TVA) and oG to excitatory (LV-αCamKII) or inhibitory (AAV-GAD1) subpopulations (Liu et al., 2013; Lean et al., 2018). As such, RVdG pseudotyped with the ASLV-A envelope glycoprotein (EnvA) will selectively infect neurons expressing the TVA receptor, and the oG delivered in trans will enable monosynaptic infection of retrogradely connected neurons.

Several more considerations were made in designing the viral genome. Two measures were taken to reduce the likelihood of interactions between the opins. First, a faster variant of the Chrimson protein, ChrimsonSA (Oda et al., 2018), was chosen due to its reduced sensitivity to light, thus increasing the relative sensitivity of the anion-channelrhodopsin. To further increase this short-wavelength sensitivity, the transgenes were arranged in the genome such that GtACR2 was located near the beginning of the genome, leading to increased transcription efficiency (see Figure 4.3; Finke et al., 2000; Schnell et al., 2010). Finally, in order to restrict the channelrhodopsins to the cell soma, preventing unwanted axonal activation, both channelrhodopsins were fused with the soma-targeting signal (ST) from the voltage-gated potassium channel Kv2.1 (Lim et al., 2000; Mahn et al., 2018).

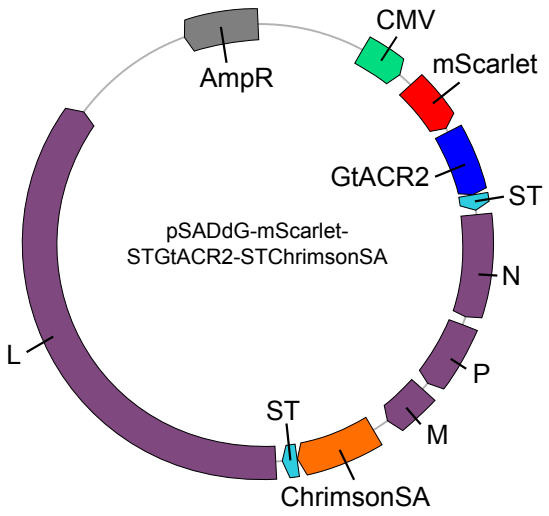

Figure 4.3: Plasmid encoding the modified rabies virus genome. mScarlet and GtACR2 transgenes were cloned immediately following the transcription start sequence with additional M/G intergenic region sequences between each coding region. ChrimsonSA was cloned in place of G. Soma-targeting sequences (ST) were fused to GtACR2 and ChrimsonSA to prevent axonal activation.

4.4 Methods

4.4.1 Virus production

Virus was prepared following the protocol by Osakada and Callaway (2013) and pseudotyped with oG following Ciabatti et al. (2017). Plasmid synthesis, sequence verification, and maxiprep were performed by Gene Universal Inc (Newark, DE). BHK cells expressing rabies glycoprotein SADB19G (B7GG, provided by the Callaway laboratory) were transfected with the genomic plasmid pSADdG-mScarlet-STGtACR2-STChrimsonSA in addition to plasmids encoding rabies viral proteins N, L, P, and G using Lipofectamine 2000 (Invitrogen, Waltham, MA) transfection reagent. Following transfection, the 100 mm dish was incubated for 6 d at 3% CO_2 and 35 °C, then transferred to a 150 mm dish and incubated for a further 6 d before the supernatant was removed and passed through a 0.45 µm polyethersulfone filter.

BHK cells expressing optimized rabies glycoprotein (TGoG, provided by the Tripodi laboratory) were infected with 5 ml of viral supernatant and maintained at 3% CO_2 and 35 °C for 1 d, then washed thoroughly and transferred to a clean dish for another 5-6 d to produce viral supernatant with only oG coated virus. This supernatant was subsequently used to infect five 150 mm dishes of the same cell line in order to amplify the virus. Supernatant was collected twice during incubation at 3% CO_2 and 35 °C after 6 and 10 days, then filtered and transferred to an ultracentrifuge (rotor SW28, Beckman Coulter) for 2 h at 19,400 g and 4 °C. Purified virus was resuspended in phosphate buffered saline for 1 h at 4 °C before 2% fetal bovine serum was added. Aliquots for injection were stored at -80 °C. Titer was assessed by infecting HEK 293T cells (Sigma-Aldrich) with serial dilutions of modified virus, to ensure at least 1×10^9 infectious units ml^{-1} was achieved. Figure 4.4 shows infected 293T cells during titration.

4.4.2 Electrophysiology

Injections of modified rabies virus were carried out in four adult female Long-Evans rats. All procedures were approved by the University of California, Irvine Institutional Animal Care and Use Committee and the Institutional Biosafety Committee, and followed the guidelines of the National Institutes of Health. Prior to surgery, rats were initially anesthetized with 2% isoflurane in a mixture of 30% oxygen and 70% nitrous oxide, and maintained with 1 to 1.5% isoflurane in the same mixture. Using a stereotaxic apparatus, a craniotomy was performed to expose the caudal neocortex of one hemisphere. A glass micropipette was cut to approximately 20 µm diameter, filled with rabies virus suspension, and lowered into the brain using a motorized microdrive. Multiple injections (spaced 1 mm) of rabies virus were made at several depths ranging from 200 to 1600 µm. Following a 6-7 d survival period to allow for infection and expression of transgenes, an eight-channel linear probe (U-probe; Plexon, Dallas, TX) was lowered into the injected site guided by *in vivo* fluorescent imaging, and a 100 µm diameter optic fiber was positioned at the surface of the injection site for cortical activation or at the apex of lateral posterior nucleus for thalamic activation (stereotaxic coordinates -4 mm from bregma, 1.75 to 2.75 mm lateral). Extracellular recordings were made with and without laser stimulation, with power ranging from 5 to 15 mW at the fiber tip. Light was delivered via the optic fiber to the brain using two diode lasers housed in a beam combiner (Omicron, Dudenhofen, Germany) coupled to the optic fiber. One 594 nm yellow laser (Mambo; Cobolt, Stockholm, Sweden) and one 473 nm blue laser (LuxX 473; Omicron) were triggered using the parallel port and synchronized within 10 ms of visual stimuli onset.

Multichannel recordings were acquired using a 32-channel Scout recording system (Ripple, UT, USA). Local field potentials (LFP) were captured at 1 kHz sampling frequency from signals filtered between 0.3 to 250 Hz and with 60 Hz noise removed. Signals containing spikes

were bandpass filtered from 500 Hz to 7 kHz and stored at 30 kHz sampling frequency. Spikes were sorted online in Trellis software (Ripple, UT, USA) while performing visual stimulation. For LFP recordings, only electrodes more than 250 um apart were considered for analysis (Katzner et al., 2009). Visual stimuli were generated in Experica (http://experica.github.io) and displayed on a gamma-corrected LCD monitor (55 inches, 60 Hz; RCA, New York, NY) at 1920x1080 pixels resolution and 52 $\mathrm{cd\,m^{-2}}$ mean luminance. Stimulus onset times were corrected for LCD monitor response time using a photodiode and microcontroller. Visually responsive cells were found using either 100% contrast drifting grating stimuli or brief (500 ms) flashes of white on a black background.

4.4.3 Histology

Following several recording sessions, but no more than 12 d post injection, rats were deeply anesthetized with Euthasol and transcardially perfused first with saline, then with 4% paraformaldehyde in phosphate buffered saline. Brains were removed and cryoprotected in 30% sucrose for at least 24 hours, then sectioned coronally on a freezing microtome to 40 µm thickness and mounted on glass microscope slides in polyvinyl alcohol mounting medium with 1,4-diazabicyclo-octane (PVA-DABCO, prepared in-house).

Sections were scanned using a fluorescent microscope (Axioplan 2; Zeiss, White Plains, NY) equipped with a 10x objective and motorized stage. Images were captured with a monochromatic low-noise CCD camera (Sensicam qe, PCO AG, Kelheim, Germany) and corrected for lamp misalignment by dividing each pixel by corresponding pixels in a flat field image acquired for each color channel. Corrected images were stitched using stage coordinates with regions of 10 overlapping pixels between images in which average pixel values were used. Neurons were identified based on the presence of the cell soma and dendrites. Fluorescently labeled neurons were then annotated by anatomical brain region based on the rat brain atlas

by Paxinos and Watson (2013). Image correction and stitching were performed in MATLAB using the multisection-imager toolbox (http://github.com/leoscholl/multisection-imager).

4.4.4 Data analysis and statistics

Visually evoked potentials (VEP) were averaged across 50 trials for laser and flash stimuli. Peri-stimulus time histograms (PSTH) were constructed using 20 ms bin widths and averaged across 50 trials for laser and flash stimuli. Mean firing rate (MFR) was calculated for spikes in the first 200 ms following stimulus presentation. Average data are presented as mean ± standard error of the mean (SEM) unless otherwise noted. Values of $p \leq 0.05$ were considered significant for Wilcoxon signed rank tests.

4.5 Results

The genomic plasmid encoding mScarlet-STGtACR2-STChrimsonSA rabies virus was successfully synthesized and its sequence verified before virus production. Following transfection, the virus was pseudotyped with optimized glycoprotein (oG) in order to increase infection efficiency (Kim et al. 2016). Rabies virus titer was verified in the 293T cell line (Figure 4.4a). The virus was injected into V2 in one adult rat (case LSR1906), revealing bright *in vivo* (Figure 4.4b) and *ex vivo* (Figure 4.4c) mScarlet fluorescence. Retrogradely labeled cells were visible not only locally near the injection site (Figure 4.4c) but also in the thalamus (Figure 4.4d), in particular the lateral posterior nucleus (LP). Subsequent injections of the same virus were made in medial V2 (V2M) of cases LSR1910 (reconstructed in Figure 4.5) and LSR1911 (reconstructed in Figure 4.8), and lateral V2 (V2L) of case LSR1912 (reconstructed in Figure 4.9).

Extracellular cortical recordings were made *in vivo* in case LSR1910 during simultaneous

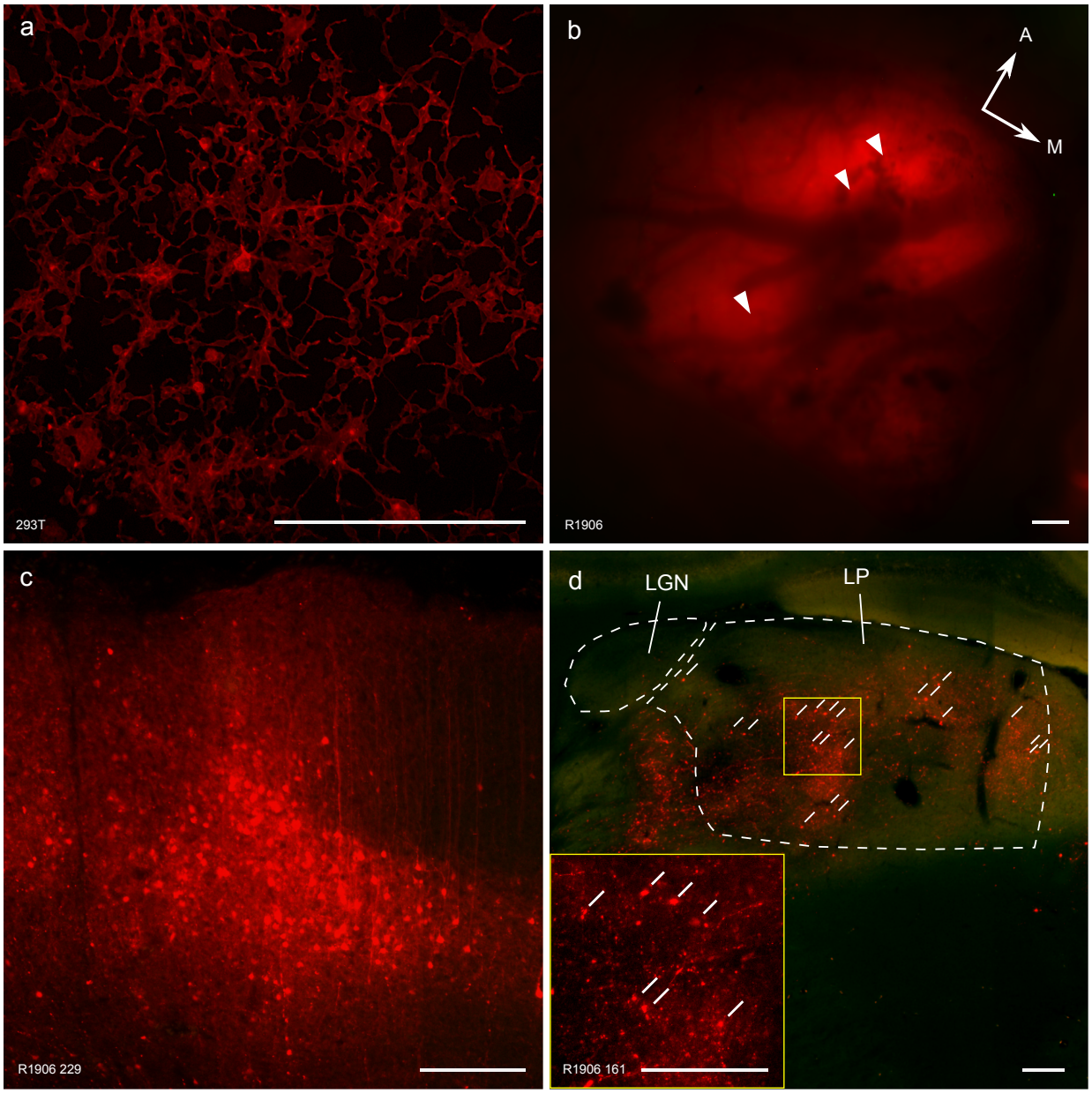

Figure 4.4: mScarlet fluorescence in cultured cells and rat neurons. (a) Infected 293T cells, (b) *in vivo* fluorescence one week after cortical injections (arrowheads), and the same case *ex vivo* with labeled neurons in cortex (c) and in LP (d). Scale bars equal 250 µm

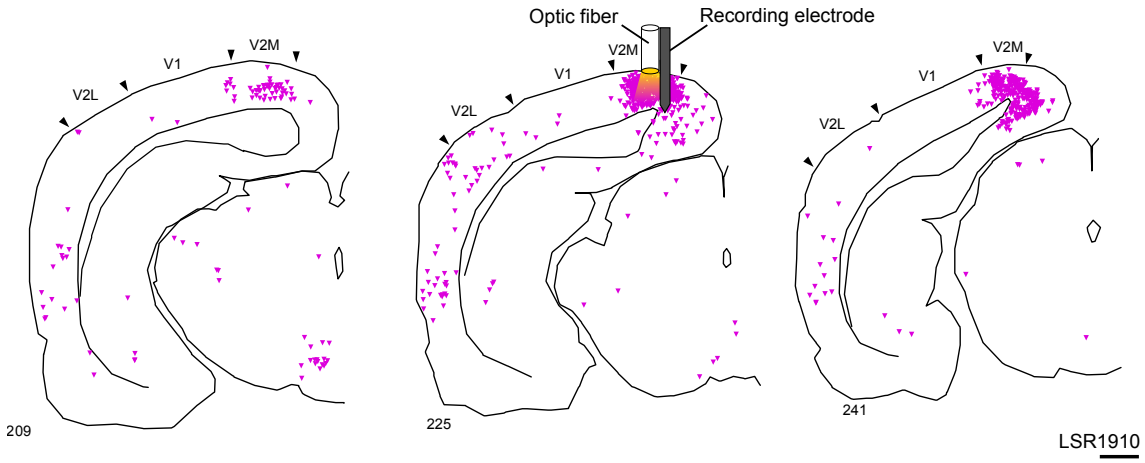

Figure 4.5: Reconstruction of case LSR1910 in which mScarlet-STGtACR2-STChrimsonSA rabies virus was injected into medial visual cortex where subsequent recordings and laser activation were performed. Scale bar equals 1 mm.

laser manipulation of local cortical neurons. Single units recorded near the injection site were excited by 5 Hz yellow laser stimulation at the brain surface and suppressed by 5 Hz blue laser stimulation (Figure 4.6), and were reliably excitable at and above 10 Hz laser stimulation (square wave, 50% duty cycle; see Figure 4.7).

To test the effectiveness of our virus in manipulating long-range connections, and to explore the causal effects of pulvinar activation and inhibition on cortical activity, we tested cortical responses to visual stimuli during laser manipulation of LP (Figure 4.8 and 4.9). Local field potential (LFP) and spiking activity were recorded during presentation of flash stimuli over six cortical penetrations and LP optic fiber sites. Visually evoked potentials (VEP) and mean firing rates (MFR) were measured in response to the onset of a white screen following periods of black. Offset responses were also recorded but not considered for analysis since typical VEPs and MFR were much larger at the stimulus onset (data not shown).

At several V2 recording sites, changes in VEP amplitude were immediately noticeable following both activation (594 nm laser) and inactivation (473 nm laser) of pulvinar neurons (Figure 4.10a, 4.10c). In these channels, activation of pulvinar lowered evoked amplitude,

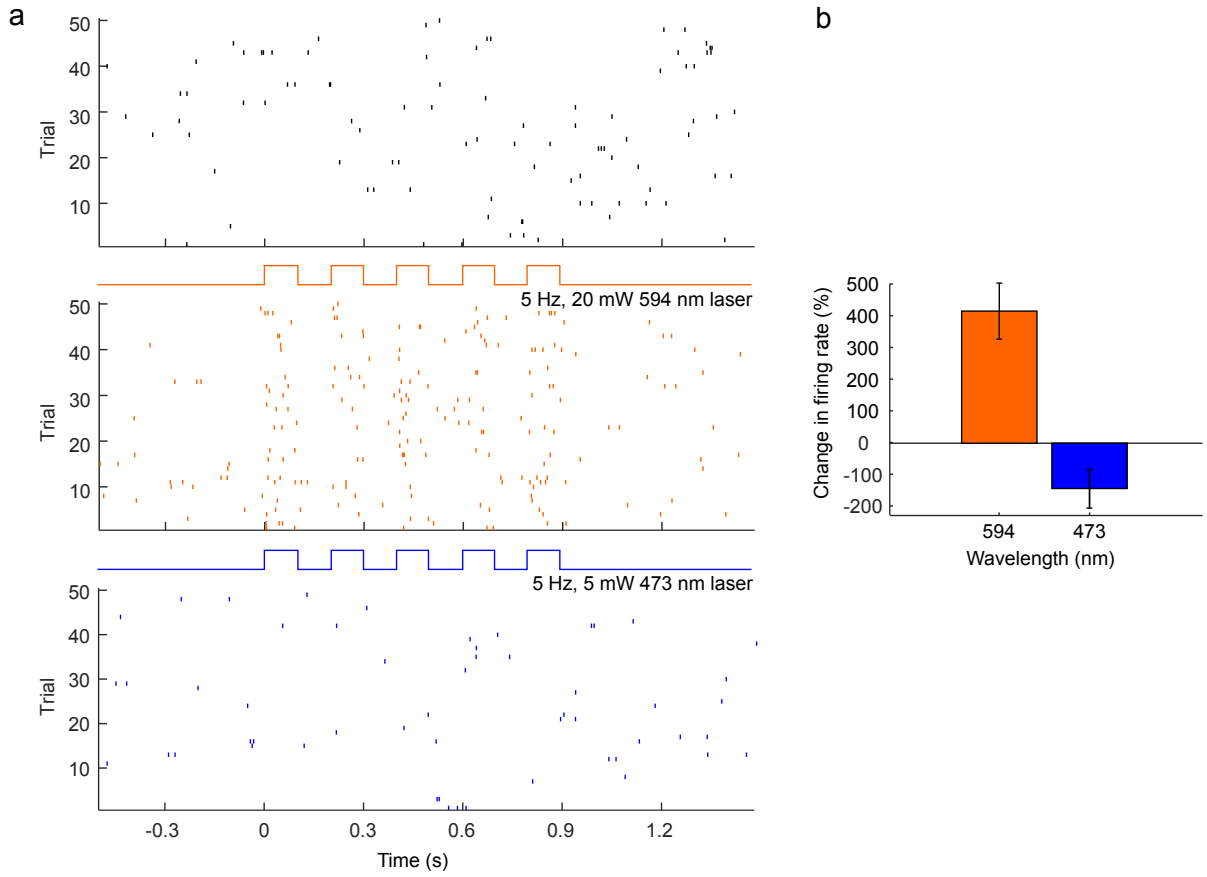

Figure 4.6: Cortical excitation with 594 nm and inhibition with 473 nm wavelength lasers with no visual stimulus. The firing rate of this cell is elevated by 400% under yellow laser light, and decreased by 140% under blue laser light. (a) Raster plots of each laser condition. Black marks indicate spikes during trials with no laser stimulation, yellow marks indicate spikes during yellow laser stimulation at 5 Hz, and blue marks indicate spikes during blue laser stimulation at 5 Hz. (b) Summary of the percent change in firing rate from baseline (no laser) to yellow (594 nm) or blue (473 nm) laser excitation.

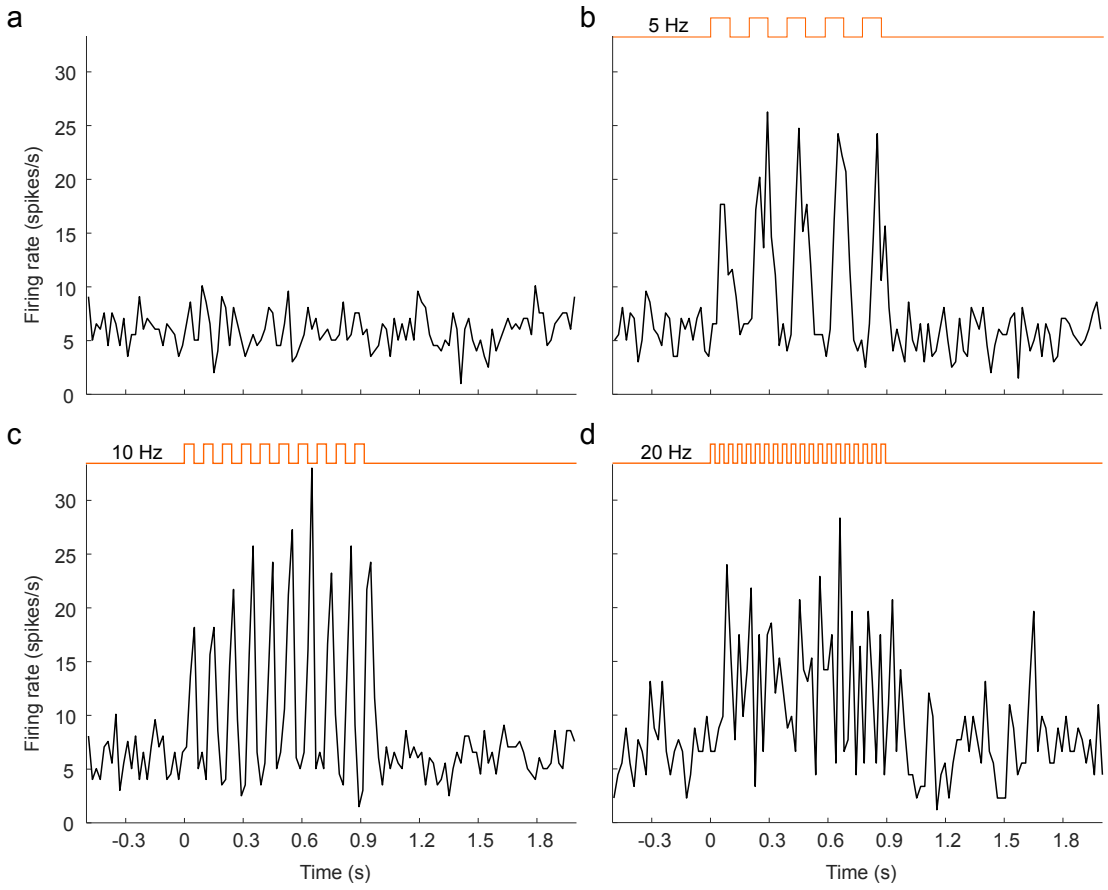

Figure 4.7: Excitation at multiple frequencies caused by 594 nm wavelength laser in cortical cells. Peri-stimulus time histogram with no laser activation (a), 5 Hz (b), 10 Hz (c), and 20 Hz (d) square wave laser stimulation. The cell response follows the laser pulses at 5 and 10 Hz, but breaks down at 20 Hz although the firing rate is still elevated above baseline.

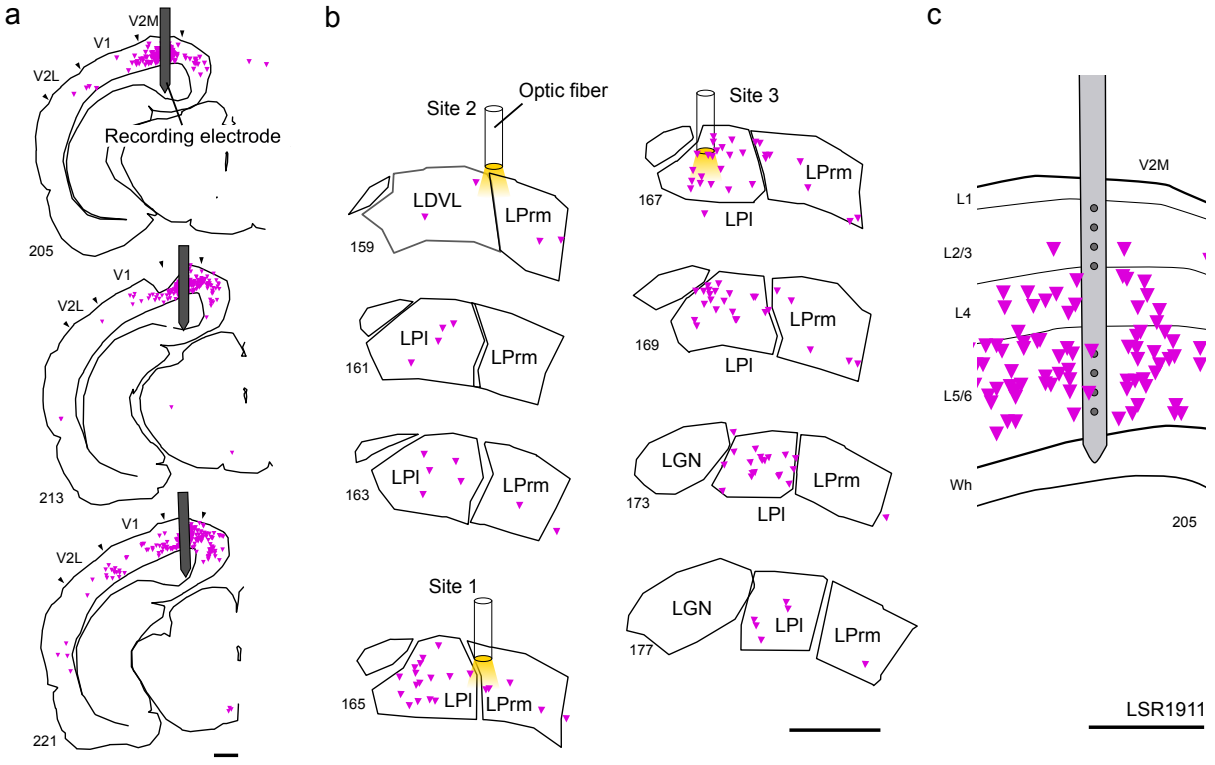

Figure 4.8: Reconstruction of case LSR1911. mScarlet-STGtACR2-STChrimsonSA rabies virus was injected into medial V2 (V2M; panel a) and retrogradely infected cells in LPl and LPrm (b). Recordings were made across several cortical layers at the injection site (c) while simultaneously activating or inhibiting cells in LP with 594 nm and 473 nm wavelength laser light in order to uncover thalamocortical modulation of activity in V2M. Three sites were targeted sequentially in LP. Site 1 targeted central LP, Site 2 targeted anterior LP, and Site 3 targeted LPl only. Scale bars in (a) and (b) equal 1 mm; scale bar in (c) equals 0.5 mm.

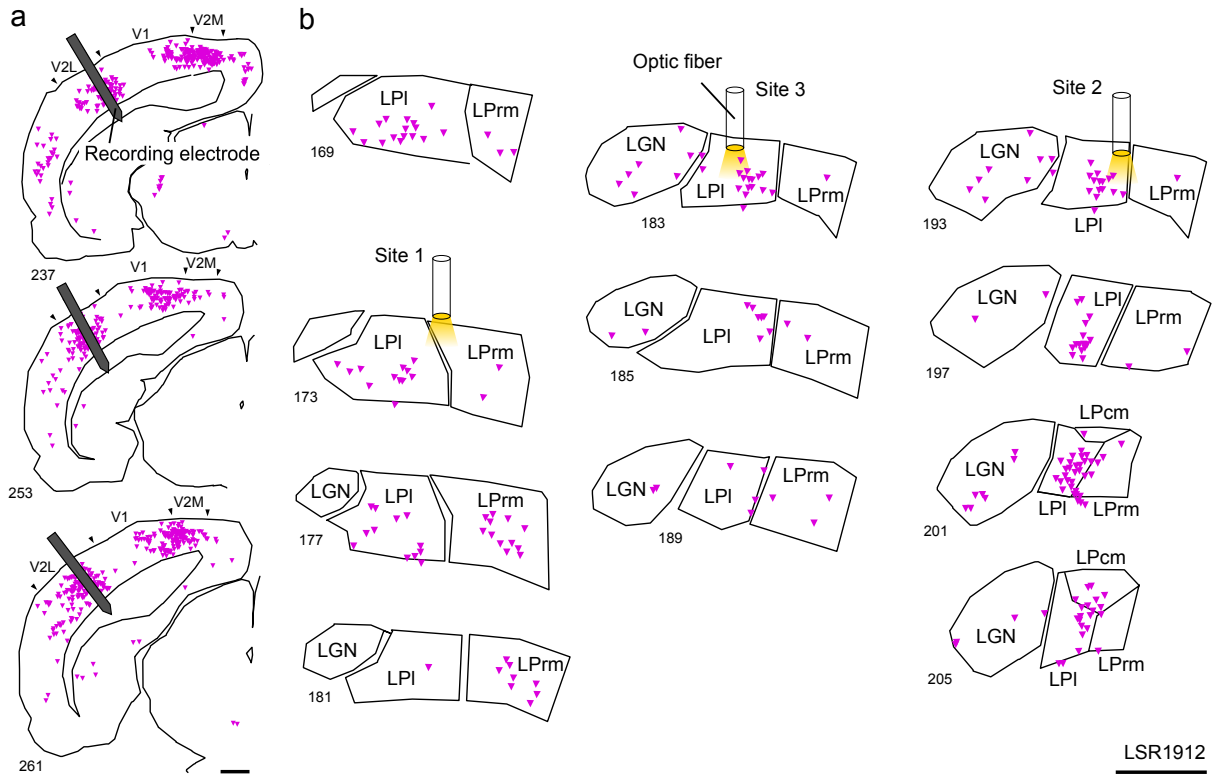

Figure 4.9: Reconstruction of case LSR1912. Virus was injected into lateral V2 (V2L, panel a), retrogradely infecting neurons in LPl, LPrm, and LPcm (b). An optic fiber was lowered sequentially into three sites targeting LPl during extracellular recordings of cells in V2L. Scale bars equal 1 mm.

whereas inactivation raised amplitude. This seemed to be consistent, with no channels having noticeable amplitude increase following pulvinar activation or amplitude decrease following pulvinar inactivation. Other recording sites showed signs of amplitude change in one direction but not the other as shown in Figure 4.10b, in which inactivation (blue laser) caused increased amplitude whereas activation caused no change.

On average, amplitude in response to stimulus onset was significantly lower during periods of LP activation (594 nm laser) compared to baseline ($n = 20$, $p = 0.025$, Wilcoxon sign test), and significantly higher for periods of LP inactivation (473 nm wavelength laser) compared to baseline ($p = 0.0008$, Wilcoxon sign test). Comparing the two laser wavelengths directly, there was a significantly higher amplitude for 473 nm wavelength light than for 594 nm wavelength light ($p = 0.0002$, Wilcoxon sign test). Without any visual stimulus, neither laser wavelength caused significant changes to amplitude.

The difference in amplitude between the two laser wavelengths essentially measured the strength LP manipulation had on a particular cortical recording site. We compared this manipulation strength against electrode depth to identify which cortical layers were most affected by pulvinar. Recording sites in superficial cortical layers were the most strongly manipulated. Across the whole population, electrode depth was negatively correlated with change in amplitude between the two laser wavelengths (Pearson's $r = -0.57$, $p = 0.009$; see

Figure 4.10: Visually evoked potentials (VEP) in V2 during pulvinar manipulation of mScarlet-STGtACR2-STChrimsonSA rabies virus infected cells. (a-d) Examples of VEP during no laser (dotted lines), yellow laser (orange lines) or blue laser (blue lines) stimulation of LP. (e) Population amplitude of VEPs in V2 when LP neurons were activated by yellow (594 nm) laser, when no laser was used, and when LP neurons were suppressed by blue (473 nm) laser. Evoked responses in V2 are strongest when LP neurons are inactivated and weakest when LP neurons are activated. (f) Percent change between activation, suppression, and no laser conditions. (g) Comparison of electrode depth and percent change between suppression and activation of LP neurons. Sites recorded in V2L are shaded; sites recorded in V2M are open circles. Solid line indicates a significant linear correlation between electrode depth and strength LP manipulation had on cells in V2 at that depth.

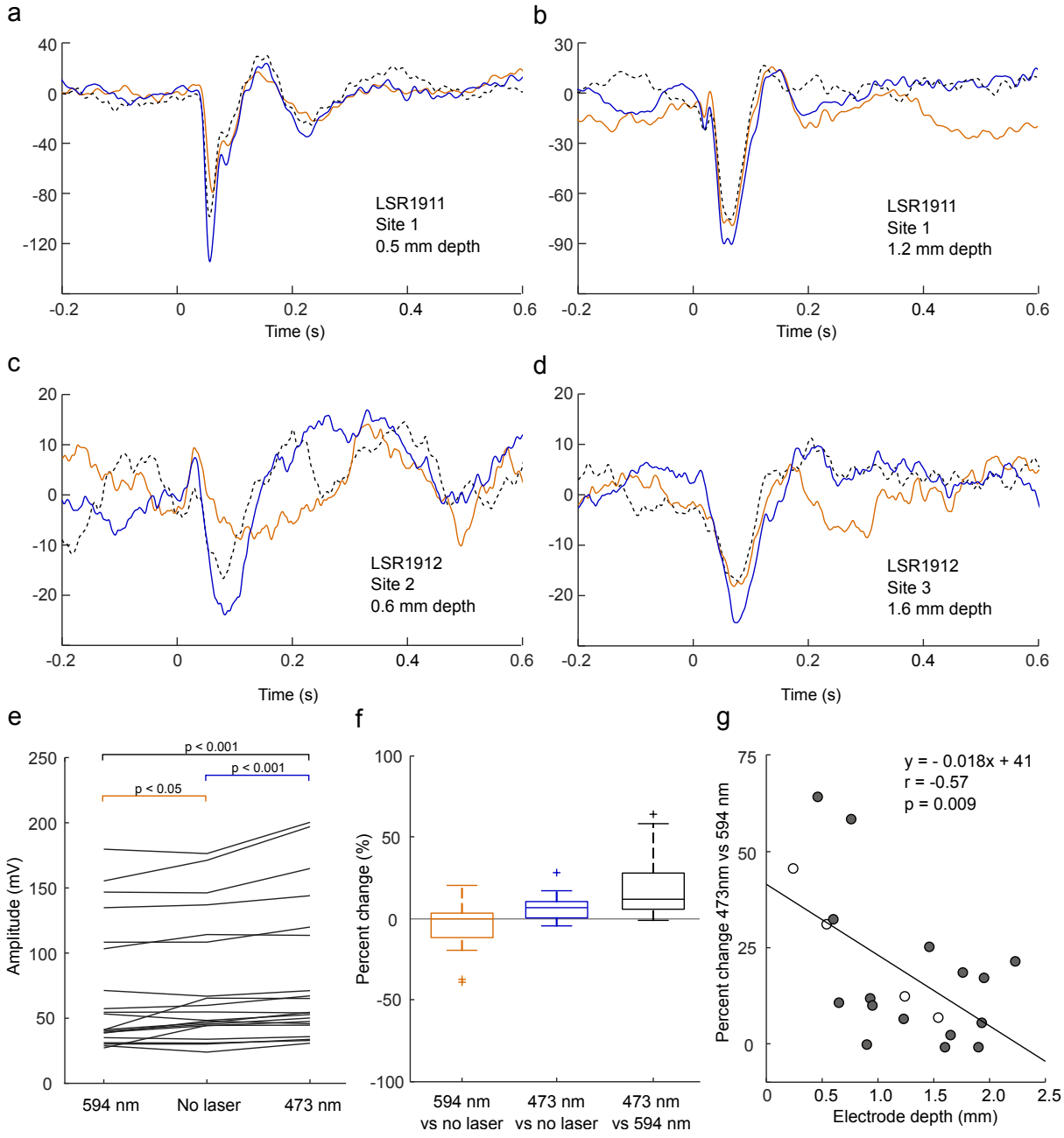
a
b
c
d
e
f
g
LSR1911
Site 1
0.5 mm depth
LSR1911
Site 1
1.2 mm depth
LSR1912
Site 2
0.6 mm depth
LSR1912
Site 3
1.6 mm depth
Time (s)
p < 0.001
p < 0.001
p < 0.05
Amplitude (mV)
594 nm
No laser
473 nm
Percent change (%)
594 nm
vs no laser
473 nm
vs no laser
473 nm
vs 594 nm
y = - 0.018x + 41
r = -0.57
p = 0.009
Percent change 473nm vs 594 nm
Electrode depth (mm)

Figure 4.10g).

Cortical single unit responses to the same stimuli were also affected by pulvinar manipulation. Three V2 neuron examples are shown in Figure 4.11. Firing rates were significantly lower on average during pulvinar activation compared to without modulation ($n = 28$, $p = 0.013$; Wilcoxon sign test), and significantly higher during pulvinar inactivation (473 nm laser) versus pulvinar activation (594 nm; $n = 28$, $p = 0.030$; Wilcoxon sign test). Cortical electrode depth was also significantly correlated with firing rate change (Pearson's $r = -0.35$, $p = 0.05$).

Cells in V2 were also tested for responses to sinusoidal drifting grating stimuli at different spatial frequencies, temporal frequencies, orientations, and sizes. A subset of these cells (n = 8) were tested for size preference during laser stimulation of pulvinar. These cells were highly selective to the diameter of the stimulus, with optimal responses at sizes ranging from 18° to 40° ($M = 26°$, $SD = 7°$, n = 8) and maximally suppressed at a size ranging from 50° to 80° ($M = 63°$, $SD = 12°$, n = 7). One cell was excluded from analysis of suppression because it was only tested at small diameters.

Mean firing rates at the optimal diameter were significantly lower when pulvinar was inactivated (473 nm laser) than without pulvinar modulation ($n = 8$; $p = 0.016$; Wilcoxon sign test; Figure 4.12a and 4.12b). No significant change in firing rate at the optimal size was observed during pulvinar activation (594 nm laser). In contrast, at the maximally suppressed size, cells in V2 were more clearly affected by pulvinar activation than inactivation (see Figure 4.12a). On average, firing rates at the suppressed size increased significantly during pulvinar activation (594 nm laser; $n = 7$; $p = 0.016$; Wilcoxon sign test). No significant change in firing rate at the suppressed size occurred during pulvinar inactivation (473 nm laser).

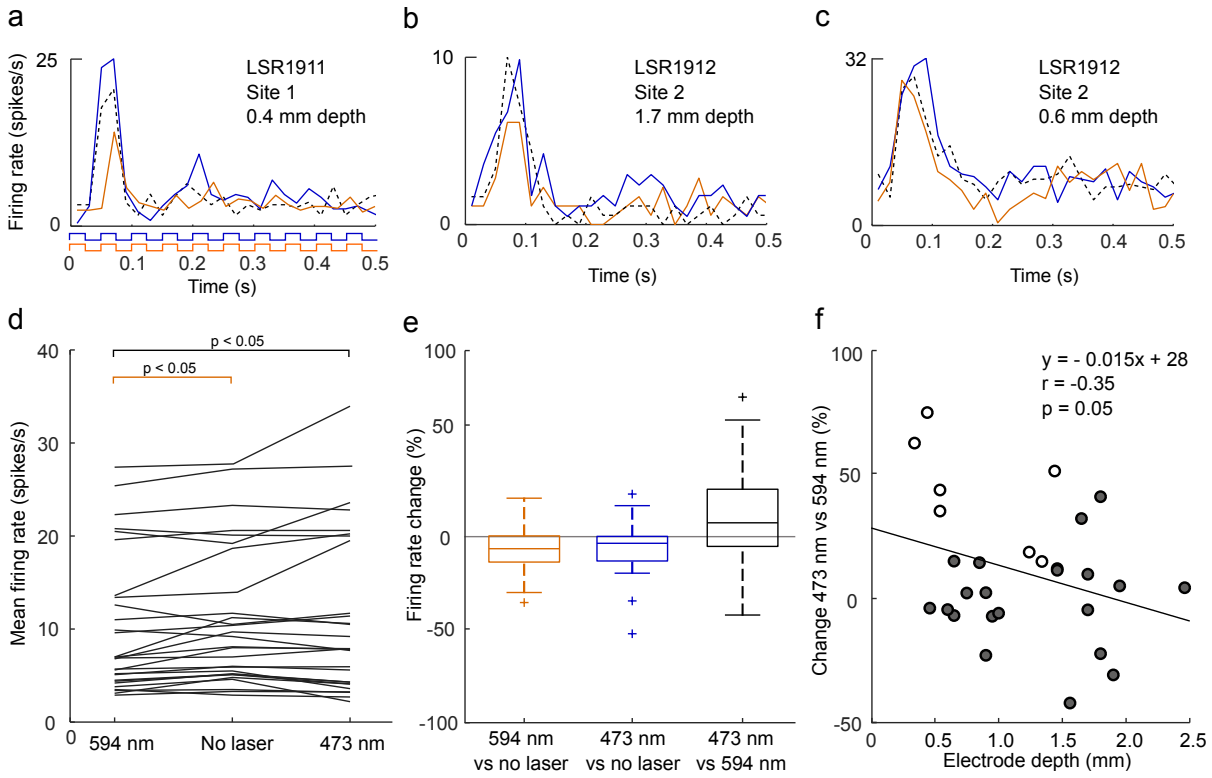

Figure 4.11: Single unit responses to flash stimulus with and without laser manipulation of pulvinar. (a-c) Three example cells with varying degrees of modulation from pulvinar. Colors indicate which laser manipulation was used, while dotted lines indicate no manipulation was used. (d) Population response during pulvinar stimulation with yellow laser (594 nm), no laser, or blue laser (473 nm) light. (e) Percent change over no laser condition for yellow and blue lasers, and percent change from yellow laser to blue laser conditions. (f) Comparison of electrode depth to percent change in firing rate between blue laser and yellow laser. Open circles indicate units were recorded from V2M while shaded circles indicate units were recorded from V2L.

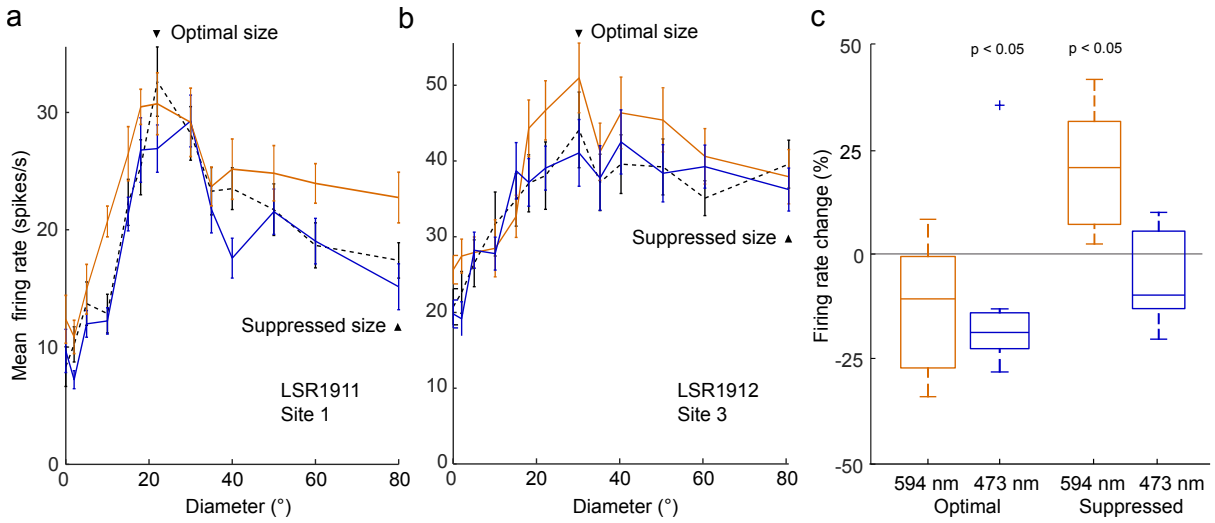

Figure 4.12: Changes in cortical size tuning due to optical manipulation of pulvinar. Two examples of size tuned cells in rat V2, one with decreased firing rate at optimal size (20°) due to pulvinar inactivation and increase firing rate at the maximally suppressed size (80°) due to pulvinar inactivation (a), and one with increased firing rate at optimal size due to pulvinar excitation (b). Population medians and quartiles of percent change at the optimal diameter (c) show that inactivation of pulvinar consistently decreased firing rate.

4.6 Discussion

Here we demonstrated bi-directional optical control over populations of cortical and thalamic neurons using a modified rabies virus. To our knowledge it is the first use of two channelrhodopsins delivered in a single virus, and also the first use of the fluorescent protein mScarlet in a rabies virus vector. Using this virus we showed that pulvinar neurons suppress activity in higher visual cortex in the rat during flash stimulus presentation, and that pulvinar has influence over cortical size tuning. The virus was also very bright and filled whole cells in histology (see Figure 4.4), giving it potential use for neuron tracing experiments.

Overall, our method of dual opsin delivery is extremely efficient, utilizing the best currently available light-sensitive ion channels, fluorescent protein, and optimized rabies virus vector. Previous attempts to deliver bimodal opsins *in vivo* using separate lentiviral vectors (Zhang et al., 2007), or transgenic animals (Yizhar et al., 2011) have not been able to target the same population of cells with both transgenes. Our method using a rabies virus vector, however, is capable not only of simultaneous expression of both opsins in all infected cells, but also of selectively infecting populations of projection neurons to the injection site without the need for transgenic animals (Ghanem & Conzelmann, 2016). An alternative approach is to perform separate experiments using two or more optogenetic approaches, but again this limits analysis to separate populations of neurons and slows research due to the increased requirement for animals and surgical procedures.

Several improvements to the virus could be beneficial. First, the relationship between laser power and change in firing rate has not fully been quantified. We simply used the maximum available yellow laser power and 25% maximum available blue laser power after our initial tests showed that this was a suitable combination in most cases. However, we are uncertain whether interactions between the opsins could be diminishing the potential efficiency of either protein. Further testing, preferably in vitro using patch clamped cells and direct

laser activation and inactivation, may be needed to maximize the performance of the virus. Second, although useful for filling whole cells and visualizing cells *in vivo*, the fluorescence in axons is so bright that finding cell bodies can be challenging (see Figure 4.4). One potential solution is to fuse the fluorescent protein mScarlet to one or both of the channelrhodopsins, limiting fluorescence to the cell soma at the membrane. This is currently being pursued in our lab for applications that require precise cell counts but do not need bright *in vivo* fluorescence.

Pulvinar inactivation has been studied in the past by methods other than what we described here. For example, superior colliculus lesions in mice cause changes to speed tuning across multiple cortical areas (Tohmi et al., 2014). However these changes are hard to attribute to the pulvinar since superior colliculus projects to the lateral geniculate nucleus and other thalamic nuclei (Partlow, et al., 1977; Pasquier & Villar, 1982). Pulvinar inactivation by GABA receptor agonist injections drastically lowered cortical firing rates in monkeys (Purushothaman et al., 2012; Zhou et al., 2016), but such injections cause major changes to thalamic physiology, as well as potentially causing damage to cortex (Lomber, 1999; Majchrzak & Di Scala, 2000). Other nondestructive methods have also been used to correlate task-dependent activity in the pulvinar to activity in cortical areas (Saalmann et al., 2012), but these lack causal inference. Our method of optically manipulating smaller, targeted networks of cells shows that pulvinar can both increase and decrease firing rates in response to visual stimuli.

Pulvinar activation and inactivation had different effects on different systems, further illustrating the need for bi-directional control of membrane potentials. During flash stimulus presentation, activation of pulvinocortical projections caused decreased evoked potential amplitudes and firing rates, yet size tuned cells were facilitated at large diameters by pulvinar activation. Pulvinar projections to cortex do synapse with multiple cortical layers in rats (Nakamura et al., 2015), so perhaps the effects we saw are mediated by different laminar

networks in the cortex, one inhibitory and one excitatory.

We did observe laminar specificity of flash modulation, as the effect of pulvinar manipulation was greatest in superficial layer cortical cells (see Figure 4.10g and 4.11f), suggesting that the pulvinar modulates feedforward projections (Felleman & Van Essen, 1991; D'Souza & Burkhalter, 2017). At least for simple flash stimuli, pulvinar neurons might be amplifying responses traveling through hierarchical cortical areas to stimuli inside their receptive fields. It would be interesting to see if layer-specific modulation occurs for more complex stimuli, or during behavioral tasks in awake animals; neurons in the dorsomedial primate pulvinar that are enhanced during covert attention (Petersen et al., 1985) might modulate responses in cortex without the need for optogenetic manipulation.

The experiments here targeted mainly the lateral portion of LP, because in our initial injections most of the projections to V2 originated from the lateral subdivision (see Figure 4.4d). However, all of the three rodent pulvinar subdivisions send projections to visual cortex, although each has a distinct pattern of connectivity (Nakamura et al., 2015). These anatomical differences between the subdivisions could lead to functional differences as well. For example, the caudal portion of the pulvinar receives superior colliculus input while the rostromedial portion does not (Takahashi, 1985), and activity in the caudal pulvinar in mice is dependent on superior colliculus while activity in rostral pulvinar is dependent on cortex (Bennett et al., 2019). To test whether or not neurons each subdivision have similar effects on visual cortex, future experiments could simply place the optic fiber carefully in each subdivision otherwise using the same experimental paradigms shown here.

Cortical areas may also receive differential projections from the pulvinar. We made injections into both medial and lateral portions of V2, expecting differences in projection strength or cortical modulation by pulvinar neurons. However, in our tests, roughly the same number of neurons were found to project to both V2 areas, consistent with previous work (Nakamura et al., 2015), and the effects of optical control over pulvinar neurons were consistent across

V2M and V2L (see Figure 4.10g and 4.11f). Specializations within rodent V2 (Tohmi et al., 2014; Nishio et al., 2018) and of projections between pulvinar and V2 (Juavinett et al., 2019) suggest that the pulvinar supports multiple channels of transthalamic computation; further research in this area is warranted.

4.7 References

Adesnik, H., Bruns, W., Taniguchi, H., Huang, Z. J., and Scanziani, M. (2012). A neural circuit for spatial summation in visual cortex. *Nature*.

Allen, A. E., Procyk, C. A., Howarth, M., Walmsley, L., and Brown, T. M. (2016). Visual input to the mouse lateral posterior and posterior thalamic nuclei: photoreceptive origins and retinotopic order. *The Journal of Physiology*, 594(7):1911–1929.

Benevento, L. A. and Standage, G. P. (1983). The organization of projections of the retinorecipient and nonretinorecipient nuclei of the pretectal complex and layers of the superior colliculus to the lateral pulvinar and medial pulvinar in the macaque monkey. *Journal of Comparative Neurology*, 217(3):307–336.

Bennett, C., Gale, S. D., Garrett, M. E., Newton, M. L., Callaway, E. M., Murphy, G. J., and Olsen, S. R. (2019). Higher-Order Thalamic Circuits Channel Parallel Streams of Visual Information in Mice. *Neuron*, pages 1–16.

Bernstein, J. G., Garrity, P. A., and Boyden, E. S. (2012). Optogenetics and thermogenetics: technologies for controlling the activity of targeted cells within intact neural circuits. *Current Opinion in Neurobiology*, 22(1):61–71.

Bickford, M. E. (2015). Thalamic circuit diversity: Modulation of the driver/modulator framework. *Frontiers in Neural Circuits*, 9(JAN2016):1–8.

Bindels, D. S., Haarbosch, L., Van Weeren, L., Postma, M., Wiese, K. E., Mastop, M., Aumonier, S., Gotthard, G., Royant, A., Hink, M. A., and Gadella, T. W. (2016). mScarlet: A bright monomeric red fluorescent protein for cellular imaging. *Nature Methods*.

Bruno, R. M. and Sakmann, B. (2006). Cortex is driven by weak but synchronously active thalamocortical synapses. *Science*, 312(5780):1622–1627.

Callaway, E. M. and Luo, L. (2015). Monosynaptic circuit tracing with glycoprotein-deleted rabies viruses. *Journal of Neuroscience*, 35(24):8979–8985.

Ciabatti, E., González-Rueda, A., Mariotti, L., Morgese, F., and Tripodi, M. (2017). Life-Long Genetic and Functional Access to Neural Circuits Using Self-Inactivating Rabies Virus. *Cell*, 170(2):382–392.e14.

Clay Reid, R. and Alonso, J.-M. (1995). Specificity of monosynaptic connections from thalamus to visual cortex. *Nature*, 378(6554):281–284.

Connolly, J. D., Hashemi-Nezhad, M., and Lyon, D. C. (2012). Parallel feedback pathways in visual cortex of cats revealed through a modified rabies virus. *Journal of Comparative Neurology*.

Cowey, A., Smith, B., and Butter, C. (1984). Effects of damage to superior colliculi and pre-tectum on movement discrimination in rhesus monkeys. *Experimental Brain Research*, 56(1).

Cruikshank, S. J., Lewis, T. J., and Connors, B. W. (2007). Synaptic basis for intense thalamocortical activation of feedforward inhibitory cells in neocortex. *Nature Neuroscience*, 10(4):462–468.

Deisseroth, K. (2010). Optogenetics. *Nature methods*, 8(1):1–4.

Fabre-Thorpe, M., Viévard, A., and Buser, P. (1986). Role of the extra-geniculate pathway in visual guidance - II. Effects of lesioning the pulvinar-lateral posterior thalamic complex in the cat. *Experimental Brain Research*.

Finke, S., Cox, J. H., and Conzelmann, K.-K. (2000). Differential Transcription Attenuation of Rabies Virus Genes by Intergenic Regions: Generation of Recombinant Viruses Overexpressing the Polymerase Gene. *Journal of Virology*, 74(16):7261–7269.

Foik, A. T., Scholl, L. R., Lean, G. A., Aramant, R. B., McLelland, B. T., Seiler, M. J., Mathur, A., and Lyon, D. C. (2018). Detailed Visual Cortical Responses Generated by Retinal Sheet Transplants in Rats with Severe Retinal Degeneration. *The Journal of Neuroscience*, 38(50):10709–10724.

Ghanem, A. and Conzelmann, K. K. (2016). G gene-deficient single-round rabies viruses for neuronal circuit analysis. *Virus Research*, 216:41–54.

Gil, Z., Connors, B. W., and Amitai, Y. (1999). Efficacy of Thalamocortical and Intracortical Synaptic Connections. *Neuron*, 23(2):385–397.

Govorunova, E. G., Sineshchekov, O. A., Janz, R., Liu, X., and Spudich, J. L. (2015). Natural light-gated anion channels: A family of microbial rhodopsins for advanced optogenetics. *Science*, 349(6248):647–650.

Han, X. and Boyden, E. S. (2007). Multiple-color optical activation, silencing, and desynchronization of neural activity, with single-spike temporal resolution. *PloS one*, 2(3):e299.

Juavinett, A. L., Kim, E. J., Collins, H. C., and Callaway, E. M. (2019). A systematic topographical relationship between mouse lateral posterior thalamic neurons and their visual cortical projection targets. *Journal of Comparative Neurology*, (July):cne.24737.

Kaas, J. H. and Lyon, D. C. (2007). Pulvinar contributions to the dorsal and ventral streams of visual processing in primates. *Brain Research Reviews*, 55(2 SPEC. ISS.):285–296.

Kamishina, H., Conte, W. L., Patel, S. S., Tai, R. J., Corwin, J. V., and Reep, R. L. (2009). Cortical connections of the rat lateral posterior thalamic nucleus. *Brain Research*, 1264:39–56.

Katzner, S., Nauhaus, I., Benucci, A., Bonin, V., Ringach, D. L., and Carandini, M. (2009). Local Origin of Field Potentials in Visual Cortex. *Neuron*, 61(1):35–41.

Kim, E. J., Jacobs, M. W., Ito-Cole, T., and Callaway, E. M. (2016). Improved Monosynaptic Neural Circuit Tracing Using Engineered Rabies Virus Glycoproteins. *Cell Reports*.

Kim, E. J., Juavinett, A. L., Kyubwa, E. M., Jacobs, M. W., and Callaway, E. M. (2015). Three Types of Cortical Layer 5 Neurons That Differ in Brain-wide Connectivity and Function. *Neuron*.

Klapoetke, N. C., Murata, Y., Kim, S. S., Pulver, S. R., Birdsey-Benson, A., Cho, Y. K., Morimoto, T. K., Chuong, A. S., Carpenter, E. J., Tian, Z., Wang, J., Xie, Y., Yan, Z., Zhang, Y., Chow, B. Y., Surek, B., Melkonian, M., Jayaraman, V., Constantine-Paton, M., Wong, G. K. S., and Boyden, E. S. (2014). Independent optical excitation of distinct neural populations. *Nature Methods*, 11(3):338–346.

Lean, G. A., Liu, Y.-J., and Lyon, D. C. (2019). Cell type specific tracing of the subcortical input to primary visual cortex from the basal forebrain. *Journal of Comparative Neurology*, 527(3):589–599.

Lee, S. H., Kwan, A. C., Zhang, S., Phoumthipphavong, V., Flannery, J. G., Masmanidis, S. C., Taniguchi, H., Huang, Z. J., Zhang, F., Boyden, E. S., Deisseroth, K., and Dan, Y. (2012). Activation of specific interneurons improves V1 feature selectivity and visual perception. *Nature*.

Lignani, G., Ferrea, E., Difato, F., Amarù, J., Ferroni, E., Lugarà, E., Espinoza, S., Gainetdinov, R. R., Baldelli, P., and Benfenati, F. (2013). Long-term optical stimulation of channelrhodopsin-expressing neurons to study network plasticity. *Frontiers in Molecular Neuroscience*, 6(August):1–9.

Lim, S. T., Antonucci, D. E., Scannevin, R. H., and Trimmer, J. S. (2000). A novel targeting signal for proximal clustering of the Kv2.1 K + channel in hippocampal neurons. *Neuron*, 25(2):385–397.

Liu, Y. J., Ehrengruber, M. U., Negwer, M., Shao, H. J., Cetin, A. H., and Lyon, D. C. (2013). Tracing inputs to inhibitory or excitatory neurons of mouse and cat visual cortex with a targeted rabies virus. *Current Biology*, 23(18):1746–1755.

Lomber, S. G. (1999). The advantages and limitations of permanent or reversible deactivation techniques in the assessment of neural function. *Journal of Neuroscience Methods*, 86(2):109–117.

Lyon, D. C., Jain, N., and Kaas, J. H. (2003). The visual pulvinar in tree shrews II. Projections of four nuclei to areas of visual cortex. *The Journal of Comparative Neurology*, 467(4):607–627.

Mahn, M., Gibor, L., Patil, P., Cohen-Kashi Malina, K., Oring, S., Printz, Y., Levy, R., Lampl, I., and Yizhar, O. (2018). High-efficiency optogenetic silencing with soma-targeted anion-conducting channelrhodopsins. *Nature Communications*, 9(1).

Majchrzak, M. and Di Scala, G. (2000). GABA and muscimol as reversible inactivation tools in learning and memory. *Neural Plasticity*, 7(1-2):19–29.

Marshel, J. H., Mori, T., Nielsen, K. J., and Callaway, E. M. (2010). Targeting single neuronal networks for gene expression and cell labeling in vivo. *Neuron*.

Miyamichi, K., Amat, F., Moussavi, F., Wang, C., Wickersham, I., Wall, N. R., Taniguchi, H., Tasic, B., Huang, Z. J., He, Z., Callaway, E. M., Horowitz, M. A., and Luo, L. (2011). Cortical representations of olfactory input by trans-synaptic tracing. *Nature*.

Nakamura, H., Hioki, H., Furuta, T., and Kaneko, T. (2015). Different cortical projections from three subdivisions of the rat lateral posterior thalamic nucleus: A single-neuron tracing study with viral vectors. *European Journal of Neuroscience*, 41(10):1294–1310.

Nathanson, J. L., Jappelli, R., Scheeff, E. D., Manning, G., Obata, K., Brenner, S., and Callaway, E. M. (2009). Short promoters in viral vectors drive selective expression in mammalian inhibitory neurons, but do not restrict activity to specific inhibitory cell-types. *Frontiers in Neural Circuits*.

Negwer, M., Liu, Y. J., Schubert, D., and Lyon, D. C. (2017). V1 connections reveal a series of elongated higher visual areas in the California ground squirrel, Otospermophilus beecheyi. *Journal of Comparative Neurology*.

Nishio, N., Tsukano, H., Hishida, R., Abe, M., Nakai, J., Kawamura, M., Aiba, A., Sakimura, K., and Shibuki, K. (2018). Higher visual responses in the temporal cortex of mice. *Scientific Reports*, 8(1):1–12.

Oda, K., Vierock, J., Oishi, S., Rodriguez-Rozada, S., Taniguchi, R., Yamashita, K., Wiegert, J. S., Nishizawa, T., Hegemann, P., and Nureki, O. (2018). Crystal structure of the red light-activated channelrhodopsin Chrimson. *Nature Communications*, 9(1):1–11.

Olsen, S. R., Bortone, D. S., Adesnik, H., and Scanziani, M. (2012). Gain control by layer six in cortical circuits of vision. *Nature*.

Osakada, F. and Callaway, E. E. M. (2013). Design and generation of recombinant rabies virus vectors. *Nature protocols*, 8(8):1583–1601.

Osakada, F., Mori, T., Cetin, A. H. A., Marshel, J. H. J., Virgen, B., and Callaway, E. M. (2011). New rabies virus variants for monitoring and manipulating activity and gene expression in defined neural circuits. *Neuron*, 71(4):617–631.

Partlow, G. D., Colonnier, M., and Szabo, J. (1977). Thalamic projections of the superior colliculus in the rhesus monkey,Macaca mulatta. A light and electron microscopic study. *The Journal of Comparative Neurology*, 171(3):285–317.

Pasquier, D. A. and Villar, M. J. (1982). Subcortical projections to the lateral geniculate body in the rat. *Experimental Brain Research*, 48(3):409–419.

Paxinos, G. and Watson, C. (2013). The rat brain in stereotaxic coordinates. *London: Academic press*.

Prigge, M., Schneider, F., Tsunoda, S. P., Shilyansky, C., Wietek, J., Deisseroth, K., and Hegemann, P. (2012). Color-tuned channelrhodopsins for multiwavelength optogenetics. *Journal of Biological Chemistry*, 287(38):31804–31812.

Pula, J. H. and Yuen, C. A. (2017). Eyes and stroke: The visual aspects of cerebrovascular disease.

Purushothaman, G., Marion, R., Li, K., and Casagrande, V. a. (2012). Gating and control of primary visual cortex by pulvinar. *Nature neuroscience*, 15(6):905–12.

Purves, D., Augustine, G., Fitzpatrick, D., Katz, L., LaMantia, A.-S., McNamara, J., and Williams, M. (2001). Visual Field Deficits. In *Neuroscience (2nd ed.). Sunderland (MA): Sinauer Associates*.

Rancz, E. A., Franks, K. M., Schwarz, M. K., Pichler, B., Schaefer, A. T., and Margrie, T. W. (2011). Transfection via whole-cell recording in vivo: Bridging single-cell physiology, genetics and connectomics. *Nature Neuroscience*.

Romanski, L. M., Giguere, M., Bates, J. F., and Goldman-Rakic, P. S. (1997). Topographic organization of medial pulvinar connections with the prefrontal cortex in the rhesus monkey. *Journal of Comparative Neurology*, 379(3):313–332.

Roth, M. M., Dahmen, J. C., Muir, D. R., Imhof, F., Martini, F. J., and Hofer, S. B. (2015). Thalamic nuclei convey diverse contextual information to layer 1 of visual cortex. *Nature Neuroscience*, 19(2):299–307.

Saalmann, Y. B., Pinsk, M. a., Wang, L., Li, X., and Kastner, S. (2012). The Pulvinar Regulates Information Transmission Between Cortical Areas Based on Attention Demands. *Science*, 337(6095):753–756.

Schnell, M. J., McGettigan, J. P., Wirblich, C., and Papaneri, A. (2010). The cell biology of rabies virus: Using stealth to reach the brain. *Nature Reviews Microbiology*, 8(1):51–61.

Sherman, S. M. and Guillery, R. W. (1998). On the actions that one nerve cell can have on another: Distinguishing "drivers" from "modulators". *Proceedings of the National Academy of Sciences of the United States of America*, 95(12):7121–7126.

Shetht, B. R. and Young, R. (2016). Two visual pathways in primates based on sampling of space: Exploitation and exploration of visual information. *Frontiers in Integrative Neuroscience*, 10(NOV2016).

Snow, J. C., Allen, H. A., Rafal, R. D., and Humphreys, G. W. (2009). Impaired attentional selection following lesions to human pulvinar: Evidence for homology between human and monkey. *Proceedings of the National Academy of Sciences of the United States of America*, 106(10):4054–4059.

Sprague, J. M. and Meikle, T. H. (1965). The role of the superior colliculus in visually guided behavior. *Experimental Neurology*, 11(1):115–146.

Takahashi, T. (1985). The organization of the lateral thalamus of the hooded rat. *The Journal of comparative neurology*, 231(3):281–309.

Tohmi, M., Meguro, R., Tsukano, H., Hishida, R., and Shibuki, K. (2014). The extrageniculate visual pathway generates distinct response properties in the higher visual areas of mice. *Current biology : CB*, 24(6):587–97.

Van Vreeswijk, C. and Sompolinsky, H. (1996). Chaos in neuronal networks with balanced excitatory and inhibitory activity. *Science*.

Vermaercke, B., Gerich, F. J., Ytebrouck, E., Arckens, L., Op de Beeck, H. P., and Van den Bergh, G. (2014). Functional specialization in rat occipital and temporal visual cortex. *Journal of Neurophysiology*, 112(8):1963–1983.

Wall, N. R., de la Parra, M., Sorokin, J. M., Taniguchi, H., Huang, Z. J., and Callaway, E. M. (2016). Brain-wide maps of synaptic input to cortical interneurons. *Journal of Neuroscience*.

Wall, N. R., Wickersham, I. R., Cetin, A., De La Parra, M., and Callaway, E. M. (2010). Monosynaptic circuit tracing in vivo through Cre-dependent targeting and complementation of modified rabies virus. *Proceedings of the National Academy of Sciences of the United States of America*.

Wertz, A., Trenholm, S., Yonehara, K., Hillier, D., Raics, Z., Leinweber, M., Szalay, G., Ghanem, A., Keller, G., Rózsa, B., Conzelmann, K. K., and Roska, B. (2015). Single-cell-initiated monosynaptic tracing reveals layer-specific cortical network modules. *Science*.

Wickersham, I. R. I., Finke, S., Conzelmann, K. K., and Callaway, E. M. (2006). Retrograde neuronal tracing with a deletion-mutant rabies virus. *Nature ...*, 4(1):47–49.

Wickersham, I. R. I., Lyon, D. C. D., Barnard, R. J. R., Mori, T., Finke, S., Conzelmann, K. K., Young, J. A., and Callaway, E. M. (2007). Monosynaptic restriction of transsynaptic tracing from single, genetically targeted neurons. *Neuron*, 53(5):639–647.

Wilke, M., Mueller, K.-M., and Leopold, D. A. (2009). Neural activity in the visual thalamus reflects perceptual suppression. *Proceedings of the National Academy of Sciences*, 106(23):9465–9470.

Wilson, N. R., Runyan, C. A., Wang, F. L., and Sur, M. (2012). Division and subtraction by distinct cortical inhibitory networks in vivo. *Nature*.

Xue, M., Atallah, B. V., and Scanziani, M. (2014). Equalizing excitation-inhibition ratios across visual cortical neurons. *Nature*.

Yizhar, O., Fenno, L. E., Prigge, M., Schneider, F., Davidson, T. J., Ogshea, D. J., Sohal, V. S., Goshen, I., Finkelstein, J., Paz, J. T., Stehfest, K., Fudim, R., Ramakrishnan, C., Huguenard, J. R., Hegemann, P., and Deisseroth, K. (2011). Neocortical excitation/inhibition balance in information processing and social dysfunction. *Nature*, 477(7363):171–178.

Zhang, F., Wang, L.-P. P., Brauner, M., Liewald, J. F., Kay, K., Watzke, N., Wood, P. G., Bamberg, E., Nagel, G., Gottschalk, A., and Deisseroth, K. (2007). Multimodal fast optical interrogation of neural circuitry. *Nature*, 446(7136):633–9.

Zhou, H., Schafer, R. J., and Desimone, R. (2016). Pulvinar-Cortex Interactions in Vision and Attention. *Neuron*, 89(1):209–220.

Zhou, N., Masterson, S., Damron, J., Guido, W., and Bickford, M. (2017). The mouse pulvinar nucleus links the lateral extrastriate cortex, striatum, and amygdala. *The Journal of Neuroscience*, pages 1279–17.

5. Summary and conclusions

5.1 Final summary

Although the cortex is responsible for much of the computation involved in conscious vision, the thalamus, in particular the pulvinar nucleus, is a centralized hub that links together the primary visual cortex (V1), superior colliculus (SC), and higher order visual cortex (V2). In the previous three chapters, we developed a foundational understanding of the role of the pulvinar nucleus in rodents, illustrating how pulvinar integrates spatiotemporal information from visual cortex and the SC, and regulates firing rates in rodent V2. In chapter 2, we undertook a large scale analysis of neural responses to sinusoidal grating stimuli in the rat pulvinar, aiming to understand the functional sources of visual input to the thalamic nucleus. We found receptive fields that were consistent with previous research in other species (Gattass et al., 1979; Petersen et al., 1985; Casanova et al., 1989), and also distinguished two distinct roles for the rostromedial and lateral portions of LP. The lateral part, having more cells with high temporal frequency selectivity, is more likely involved in temporal frequency and speed processing, whereas the rostromedial portion has stronger direction processing. To address whether this difference could be due in part to differences in collicular input or connectivity with higher visual cortex, in chapter 3 we quantitatively measured the strength of inputs and outputs of the rat pulvinar subdivisions. Data from previous studies in rats and other species (Robson & Hall, 1977; Lyon et al., 2003; Kaas & Lyon, 2007; Nakamura et al., 2015; Juavinett et al., 2019) suggested that the projection from pulvinar to V1 was weak, but this had never been formally tested. We used rabies virus to retrogradely infect projections from pulvinar to V1 and showed that this projection is indeed much weaker than the lateral geniculate nucleus projection to V1 or the pulvinar projection to V2. In addition, we showed

that the anatomically-defined lateral subdivision has more numerous connections with cortex than the medial subdivision in rats. The new rabies virus variant described in chapter 4 was used to directly manipulate these projections from pulvinar to V2 using two independent light-activated ion channels. We tested whether the pulvinar has a direct influence over activity in V2 but found that evoked responses were unchanged during laser manipulation without any visual stimulus. Instead, pulvinar activation and inactivation had modulatory effects on size tuning and responses to flash stimuli.

5.2 Insights

The number and structure of subdivisions within the rodent pulvinar has not fully been resolved. Initially, four subdivisions were reported by Takahashi (1985), rostromedial (LPrm), caudomedial (LPcm), and lateral (LPl), which was further divided into rostral and caudal subnuclei. More recent anatomical analysis (Nakamura et al., 2015) found no distinction between the rostral and caudal parts of LPl, thus defining the three subdivisions we used in the previous chapters. Until recently, however, no studies had identified functional differences between portions of the rodent LP. Bennett et al. (2019) showed that silencing input from the superior colliculus in mice affects activity in the caudal pulvinar, whereas silencing input from the primary visual cortex (V1) affects activity in the rostral pulvinar. They made no functional distinction between LPrm and LPl, nor LPcm and LPl, although the authors agreed that there is a third, medial subdivision defined by anatomy. Our results presented in chapter 2 and chapter 3 illustrated functional differences between the LPl and LPrm of the pulvinar in rats, both anatomically in terms of the number of inputs and outputs to visual cortex, and physiologically in terms of the speed and direction preferences of neurons in each subdivision. Together, we take these findings to imply three functional subdivisions as well as three anatomical subdivisions, but an argument could be made that our medial-lateral

axis distinction may overlap with the anterior-posterior axis distinction made by Bennett and colleagues. Future experiments could test whether activity along the medial-lateral axis depends on input from higher visual cortex, which we showed sends more projections to LPl than to LPrm.

In chapter 3, our analysis of pulvinocortical projections showed a large population of projections from pulvinar to rat V2. Since the new virus described in chapter 4 uses an optimized glycoprotein to increase uptake efficiency into axon terminals (Kim et al. 2016), we expected to find an even larger number of retrogradely labeled neurons in the pulvinar following injections into V2. Compared to injections using non-optimized rabies virus we performed in chapter 3, these new injections did increase the number of labeled cells by around two to three times. Furthermore, an increase was not seen in the number of LP cells labeled following injections into primary visual cortex (data not shown), strengthening our position on the lack of a direct projection from pulvinar to V1.

In previous studies in galago, pulvinar inactivation has been observed to almost entirely shut off activity in V1 (Purushothaman et al., 2012). The lack of direct projections we found from pulvinar to V1 makes such a drastic effect seem unbelievable, but it is possible that sparse projections to V1 are strongly connected to inhibitory networks in the cortex, or that feedback from higher visual cortex is important for normal activity in V1. Zhou et al. (2016) performed a similar experiment but recorded activity in V4 instead of V1, and found a similar general enabling role of the pulvinar, indicating that the pulvinar is necessary for normal cortical activity.

However, the approach taken by these labs is not physiologically plausible; the whole pulvinar would never be entirely inactivated in a normal animal. Using targeted retrograde virus injections, we showed that physiological activation and inactivation of pulvinar, via 20 Hz channelrhodopsin excitation, did not directly affect firing rates in visual cortex. Rather, stimulus evoked responses were subtly modulated in ways that need further exploration to be

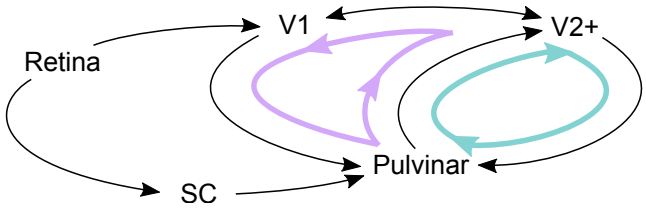

Figure 5.1: Summary of pulvinar circuitry. Multiple corticothalamic loops (colored) exist due to feedforward and feedback connections within visual cortex. Pulvinar may have a stronger influence over feedforward (blue) connections as discussed in chapter 4. SC superior colliculus, V1 primary visual cortex, V2+ higher visual cortex.

fully understood. For example, we expected pulvinar inactivation might reduce suppression at large stimulus sizes in cortex, but it instead lowered firing rates at optimal stimulus sizes, whereas activation of pulvinar reduced suppression at large sizes. Future experiments could explore these questions with the same techniques outlined here; the virus we developed in chapter 4 is well suited to test theories of pulvinar function in non-transgenic animals such as cats or non-human primates, where models of pulvinar are already well developed.

Many critical cognitive functions could be supported by the unique circuitry of the pulvinar. Due to the recurrent nature of the connections between pulvinar and visual cortex (see Figure 5.1), and additional layers of inhibitory input from the thalamic reticular nucleus (FitzGibbon, 1994; Guillery et al., 1998; Sherman & Guillery, 2001), the pulvinar is strongly positioned to perform computations that contextualize perceptual processing in the visual cortical hierarchy (Kanai et al., 2015; Jaramillo et al., 2019). As an example, in chapter 4 we demonstrated the capability of the pulvinar to alter size tuning in the visual cortex; we think the pulvinar is integrating input from cortex, then feeding back these large receptive fields, providing context about information outside a cell's classical receptive field. Researchers seeking neural correlates of this kind of contextual modulation should look to the pulvinar.

5.3 Conclusion

Together, the results presented here illustrate that the pulvinar and visual cortex are structurally and functionally intertwined. In addition to collicular and other cortical sources of input, projections to the pulvinar from visual cortex areas V1 and V2 drive receptive field properties in LPrm and LPl, which in turn strongly modulate responses to stimuli in V2, and only weakly project to V1. The tools we developed, including a new modified rabies virus for bi-directional control over retrogradely labeled neurons, should also be widely useful and scientifically productive.

5.4 References

Bennett, C., Gale, S. D., Garrett, M. E., Newton, M. L., Callaway, E. M., Murphy, G. J., and Olsen, S. R. (2019). Higher-Order Thalamic Circuits Channel Parallel Streams of Visual Information in Mice. *Neuron*, pages 1–16.

Casanova, C., Freeman, R. D., and Nordmann, J. P. (1989). Monocular and binocular response properties of cells in the striate-recipient zone of the cat's lateral posterior-pulvinar complex. *J Neurophysiol*, 62(2):544–557.

FitzGibbon, T. (1994). Rostral Reticular Nucleus of the Thalamus Sends a Patchy Projection to the Pulvinar Lateralis-Posterior Complex of the Cat. *Experimental Neurology*, 129(2):266–278.

Gattass, R., Oswaldo-Cruz, E., and Sousa, A. P. (1979). Visual receptive fields of units in the pulvinar of cebus monkey. *Brain Research*, 160(3):413–429.

Guillery, R., Feig, S., and Lozsádi, D. (1998). Paying attention to the thalamic reticular nucleus. *Trends in Neurosciences*, 21(1):28–32.

Jaramillo, J., Mejias, J. F., and Wang, X. J. (2019). Engagement of Pulvino-cortical Feedforward and Feedback Pathways in Cognitive Computations. *Neuron*, 101(2):321–336.e9.

Juavinett, A. L., Kim, E. J., Collins, H. C., and Callaway, E. M. (2019). A systematic topographical relationship between mouse lateral posterior thalamic neurons and their visual cortical projection targets. *Journal of Comparative Neurology*, (July):cne.24737.

Kaas, J. H. and Lyon, D. C. (2007). Pulvinar contributions to the dorsal and ventral streams of visual processing in primates. *Brain Research Reviews*, 55(2 SPEC. ISS.):285–296.

Kanai, R., Komura, Y., Shipp, S., and Friston, K. (2015). Cerebral hierarchies: Predictive processing, precision and the pulvinar. *Philosophical Transactions of the Royal Society B: Biological Sciences*, 370(1668).

Kim, E. J., Jacobs, M. W., Ito-Cole, T., and Callaway, E. M. (2016). Improved Monosynaptic Neural Circuit Tracing Using Engineered Rabies Virus Glycoproteins. *Cell Reports*.

Lyon, D. C., Jain, N., and Kaas, J. H. (2003). The visual pulvinar in tree shrews II. Projections of four nuclei to areas of visual cortex. *The Journal of Comparative Neurology*, 467(4):607–627.

Nakamura, H., Hioki, H., Furuta, T., and Kaneko, T. (2015). Different cortical projections from three subdivisions of the rat lateral posterior thalamic nucleus: A single-neuron tracing study with viral vectors. *European Journal of Neuroscience*, 41(10):1294–1310.

Petersen, S. E., Robinson, D. L., and Keys, W. (1985). Pulvinar nuclei of the behaving rhesus monkey: Visual responses and their modulation. *Journal of Neurophysiology*, 54(4):867–886.

Purushothaman, G., Marion, R., Li, K., and Casagrande, V. a. (2012). Gating and control of primary visual cortex by pulvinar. *Nature neuroscience*, 15(6):905–12.

Robson, J. A. and Hall, W. C. (1977). The organization of the pulvinar in the grey squirrel (Sciurus carolinensis). I. Cytoarchitecture and connections. *Journal of Comparative Neurology*, 173(2):355–388.

Sherman, S. M. and Guillery, R. W. (2001). *Exploring the Thalamus*.

Takahashi, T. (1985). The organization of the lateral thalamus of the hooded rat. *The Journal of comparative neurology*, 231(3):281–309.

Zhou, H., Schafer, R. J., and Desimone, R. (2016). Pulvinar-Cortex Interactions in Vision and Attention. *Neuron*, 89(1):209–220.